

UNIVERSITY OF BELGRADE
FACULTY OF TECHNOLOGY AND METALLURGY

Salah Salem Musbah

**OPTICAL AND MECHANICAL
PROPERTIES OF HYBRID
NANOCOMPOSITE LIGHT GUIDE
FIBERS**

Doctoral Dissertation

Belgrade, 2013

UNIVERZITET U BEOGRADU
TEHNOLOŠKO-METALURŠKI FAKULTET

Salah Salem Musbah

**OPTIČKA I MEHANIČKA SVOJSTVA
HIBRIDNIH KOMPOZITNIH
SVETLOVODNIH VLAKANA**

Doktorska Disertacija

Beograd, 2013

Supervisor

Dr Radoslav Aleksić, full professor, University Of Belgrade
Faculty Of Technology And Metallurgy

Member of Committee

Dr Petar Uskoković, full professor, University Of Belgrade
Faculty Of Technology And Metallurgy

Dr Vesna Radojević, associate professor, University Of Belgrade
Faculty Of Technology And Metallurgy

Dr Ljilana Brajović, assistant professor, University Of Belgrade
Faculty Of Civil Engineering

Date: _____

ACKNOWLEDGEMENTS

It is a great pleasure for me to express my sincere gratitude to the people whose generous assistance and support this research.

First and foremost, I would like to express my sincere thanks and appreciation to my project supervisor Dr. Radoslav Aleksic, for his patient guidance. His intellectual insight, work discipline and personal strengths have had a positive influence on my research life, for which I am grateful.

I would like to acknowledge Dr. Petar Uskokovic, Dr. Vesna Radojevic and Dr. Ljiljana Brajovicc my thesis examiners for their insightful suggestions and comments on my thesis.

Special thanks to Dr. Dusica Stojanovic for her encouragements in my research life and technical support in experiments.

DEDICATION

I would like to dedicate this thesis to my deceased father “SALEM MUSBAH” who valued education above all. His words of inspiration and encouragement in pursuit of excellence still linger on, You worked so hard for us and we owe everything to you. You longed to live the day and see your children hold the highest level of education, unfortunately you are not here with us to be happy for me, but you are never forgotten. I will always value your insight, effort, motivation, advices and all that you thought me since i was a child, i hope i will do the same with my children May god bless your soul.

I would also like to express my sincere thanks to my mother, sisters my wife and my children. Their prayers, unending tolerance, and words of encouragement were valuable to me immensely.

Optička i mehanička svojstva hibridnih kompozitnih svetlovodnih vlakana

Rezime

U uvodu istaknut je značaj istraživanja u oblasti nanokompozitnih materijali na bazi oksida aktiviranih jonima lantanida koji imaju veoma značajnu primenu za izradu lasera, laserskih i LED dioda, luminescentnih lampi, displeja, optičkih vlakana, biomedicinskih markera itd. Za primenu posebno su od interesa emisije uskog energetskog opsega, dugo vreme života pobuđenih elektronskih stanja (fosforescencija) i fotohemijaska stabilnost. U zavisnosti od načina pobuđivanja, luminescencija se može podeliti na: a) fotoluminescenciju (PL) – posledica apsorpcije elektromagnetnog zračenja, b) elektroluminescencija – posledica apsorpcije električnog polja, c) radioluminescencija – posledica jonizujućeg zračenja, d) katodoluminescencija – posledica interakcije snopa elektrona velike brzine sa tankim slojem fluorescentne supstance, e) hemiluminescencija – posledica pretvaranja hemijske energije u svetlosnu, f) bioluminescencija. Predmet ove doktorske disertacije su luminiscentni materijali. Kada se fosforescentna čestica izloži dejstvu eksitacionog izvora, kao što je ultraljubičasta (UV) ili vacuum-UV (VUV) svetlost, ona prolazi kroz proces apsorpcije, relaksacije i emisije. Svetlost se apsorbuje od strane materijala domaćina i apsorbovana energija se prenosi sa materijala domaćina na aktivator (luminescentni centar). Aktivator na kraju emituje vidljivu svetlost preko mehanizma prenosa energije. Fotoekscitacija na određenoj talasnoj dužini u bliskoj infracrvenoj oblasti koja je praćena luminiscencijom na kraćim talasnim dužinama u vidljivoj svetlosti se naziva prelaz iz bliske infracrvene u vidljivu oblast. To je veoma neobična pojava jer se fotoni niže energije „pretvaraju“ u fotone sa višom energijom. Najmanje dva fotona u infracrvenoj oblasti su potrebna za generisanje jednog fotona u vidljivoj oblasti. Upkonverzija se uglavnom dešava u materijalima u kojima procesi relaksacije više fotona ne dominiraju, što omogućava više od jednog metastabilnog stanja. U jedinjenjima retkih zemalja, elektroni 4f i 5f su efikasno zaštićeni i samim tim nisu značajnije vezani- metal-ligand. Kao posledica toga, spoj elektron-fonon na f-f prelazima se smanjuje, a proces otpuštanja više fonona je manje konkurentan. Fenomen upkonverzije je zbog toga najčešće proučavan na materijalima koji sadrže jone lantanida. Kada neki medijum (na primer laser) emituje fosforescenciju kao posledicu ekscitacije sa upadnom svetlošću, talasna dužina je duža od ekscitovane svetlosti. To znači da se smanjuje energija fotona. Međutim, pod izvesnim okolnostima može doći do upkonverzije fluorescencije gde je talasna dužina emitovane svetlosti kraća. To je moguće putem ekscitacionih mehanizama koji uključuju više od jednog apsorbovanog fotona. Upkonverzija fluorescencije se može potisnuti kada imamo mnogo prelaza fotona, jer oni mogu smanjiti život metastabilnih nivoa. Vlakna sa niskom maksimalnom energijom fotona, kao što su neka fluoridna vlakna, imaju mnogo slabije, više fononske procese, pa stoga i jači upkonverziju.

U drugom poglavlju dat je prikaz luminiscentnih materijala. Luminescentni materijali, zvani fosfori konvertuju neki tip energije u elektromagnetno zračenje, najčešće u vidljivoj oblasti, mada se može javiti i u ultraljubičastoj i infracrvenoj oblasti. Ovi materijali su uglavnom neorganska jedinjenja u formi prahova ili tankih filmova, koji sadrže odgovarajuće jone, odnosno aktivatore. Aktivator apsorbuje pobuđujuće zračenje, prelazi u pobuđeno stanje, nakon čega se vraća u osnovno stanje

na dva konkurentna načina: radijativnom emisijom ili neradijativnim procesima. Da bi fosfor bio efikasan potrebno je neradijativne procese svesti na minimum. Ponekad se u matricu fosfora dodaju i joni koji poboljšavaju luminescenciju na taj način što apsorbuju zračenje, zatim ga u procesu transfera energije predaju jonu aktivatora koji dalje vrši emisiju. Bitne karakteristike fosfora su spektralna distribucija energije emisije (emisioni spektar) i pobuđivanja (ekscitacioni spektar), kao i odnos brzina radijativnih i neradijativnih prelaza u osnovno stanje. Tipični aktivatori fosfornih materijala su joni retkih zemalja i prelaznih metala, kao i molekularni anjoni, kao što su volframatne i vanadatne grupe. Joni retkih zemalja i prelaznih metala se dodaju u veoma maloj količini, reda veličine nekoliko atomskih procenata, pa je samim tim međusobna interakcija tih jona zanemarljiva. Joni prelaznih metala se formiraju kada se uklone elektroni iz spoljašnjih $4s$ orbitala neutralnih atoma. Na taj način se formiraju joni $3d$ konfiguracije, gde su $3d$ orbitale velikih radijusa i izložene su uticaju okolnih atoma matrice. Joni retkih zemalja se formiraju uklanjanjem $6s$ elektrona, ostavljajući optički aktivne $4f$ orbitale unutar popunjenih $5s$ i $5p$ ljuski. To znači da su one malog radijusa i da su delom zaštićene od spoljašnjeg uticaja matrice. Zato se može reći da optičke karakteristike jona prelaznih metala umnogome zavise od kristalne strukture matričnog materijala i značajno se razlikuju u odnosu na slobodne jone. Nasuprot tome, joni retkih zemalja zadržavaju slične optičke karakteristike i u kristalnoj rešetki različitih matričnih materijala. Zbog svega navedenog emisioni spektri fosfora dopiranih jonima retkih zemalja se sastoje od uskih, oštih traka, dok fosfori dopirani jonima prelaznih metala daju spektre širokih traka. Itrijum-oksidi su jedan od najznačajnijih materijala u koji se ugrađuju joni retkih zemalja radi dobijanja efikasnih svetlosnih izvora. Poseduju hemijsku i visokotemperaturnu stabilnost (temperatura topljenja $2430\text{ }^{\circ}\text{C}$), veliki energetski procep ($E_g=5,8\text{ eV}$) u koji se lako smeštaju osnovni i pobuđeni elektronski nivoi jona retkih zemalja, transparentan je u opsegu talasnih dužina od 280 nm do $8\text{ }\mu\text{m}$ i poseduje veliku toplotnu provodnost. Kada je dopiran trovalentnim jonima Eu i Tb efikasno emituje crvenu i zelenu svetlost pod pobudom visokoenergetskog zračenja (gama, X ili ultraljubičasti zraci), dok dopiran dvovalentnim jonima Eu emituje plavu svetlost. U slučaju dopiranja trovalentnim jonima Er, Ho, Nd i Tm moguće je ostvariti emisiju u bliskoj infracrvenoj oblasti. Sa istim jonima moguće je i dobiti emisiju u ultraljubičastoj, plavoj, zelenoj i crvenoj oblasti spektra nakon pobude u bliskom infracrvenom delu spektra. Ova „up-converted“ emisija, odnosno emisija fotona veće energije od energije pobudnih fotona, ima danas primene za izgradnju lasera i detektora zračenja.

U trećem poglavlju dat je literaturni pregled stanja luminiscentnih nanokompozitnih materijala. Mnoge aplikacije luminescentnih materijala zahtevaju visoku čvrstoću i homogenost raspodele aktivatora, kao i čestice nanometarskih dimenzija. Primena nanostrukturnih materijala se zasniva na veoma velikoj specifičnoj površini i činjenici da male čestice nude dodatne mogućnosti za manipulaciju i prostor za dopiranje aktivatorima. Izazovi u vezi sa sintezom luminescentnih nanomaterijala potiču najpre od zahteva za malom veličinom čestica, zatim za uniformnom raspodelom čestica, identičnim oblikom i morfologijom, istim hemijskim sastavom i kristalnom strukturom. Dalje, od izvanredne je važnosti uniformno i homogeno distribuirati aktivne primese u materijalu. Svi ovi zahtevi vode do toga da se traže nove metode sinteze u cilju poboljšanja karakteristika i performansi fosfora. Usled brzog napretka u nanotehnologijama, a posebno zbog razvoja novih metoda za sintezu nanomaterijala, raste interes za istraživanje svojstava i primenu nanostrukturnih materijala dopiranih

jonima retkih zemalja. Poseban značaj istraživanjima daje moguća primena za izgradnju visokorezolucioničkih displeja i bioloških markera. Nanomaterijali imaju mnoga svojstva koja uzrokuju da joni retkih zemalja ugrađeni u njih imaju drugačiju emisiju svetlosti u poređenju sa istim materijalom mikrometarskih dimenzija. Na primer, odnos površine prema zapremini nanočestica je značajno veći nego kod mikrometarskih čestica, pa se veliki broj dopantskih jona nalazi blizu površine. U takvom asimetričnom kristalnom okruženju njihova emisija se razlikuje od emisije iz regularnih kristalografskih položaja. Kvantizirajući efekat se javlja kada su dimenzije čestica iste veličine ili manje od nekih „karakterističnih dužina“ kao što su talasna dužina fonona. Efekti kvantnog konfiniranja menjaju preklapanja talasnih funkcija dopantskih jona i jona materijala u koje su ugrađeni, što često dovodi do mnogo efikasnijih interakcija između tih jona. Na primer, u nanokristalnom Gd_2O_3 (Eu^{3+}) efikasnost emisije raste proporcionalno sa kvadratom smanjenja čestice. Nanokristalni monoklinični Y_2O_3 ima duže vreme emisije nego što je primećeno u makro kristalu. Ustanovljeno je da nanočestice imaju veću kvantnu efikasnost emisije, kao i drugačiji odnos boja emitovane svetlosti pri upkonverziji. Osim toga, nove metode sinteze omogućavaju dobijanje specifičnih morfologija čestica (nanocevi, nanodiskovi), kao i „core-shell“ čestica sa unapređenim optičkim svojstvima.

U četvrtom poglavlju dat je literaturni pregled najnovijih modifikacija kod polimernih optičkih vlakana (POV) koji se koriste za izradu svetlovoda. Ključne prednosti POV tehnologije u odnosu na druga kablovska rešenja mreža za pristup sastoji se u jednostavnosti izrade instalacije, kabl ima mali prečnik, malu gustinu, fleksibilan je, potpuno je imun na EMI, otporan je na vlagu, koroziju i prašinu. Rad sa POV vlaknima je potpuno bezbedan, za prenos se može koristiti svetlosni signal u vidljivom spektru koji je bezopasan za vid, a provera veza je izuzetno jednostavna pošto je signal vidljiv i golim okom. Međutim, da bi POV vlakna zauzela svoje mesto u mrežama za pristup najnovije generacije potreban je dalji rad na: usavršavanje optoelektronskih komponenti primopredajnika za rad pri brzinama od nekoliko Gb/s uz poboljšanje linearnosti, propusnog opsega i pouzdanosti; razvoj lasera i fotodioda za montažu na štampanim pločicama, pogodnih za višezilne POV kablove; razvoj višezilnih (*ribbon*) POV kablova; razvoj za rukovanje i instalisanje veoma jednostavnih konektora i kablova, čime bi se obezbedila niska cena instalisanja i pružila mogućnost za izradu instalacije po principu uradi sam; proširenje propusnog opsega primenom novih tehnologija i usavršenih modulacionih postupaka. U novije vreme za izradu jezgra POV vlakna koriste se deuterirani PMMA i perfluorirani polimeri, kojima se značajno smanjuje slabljenje i povećava propusni opseg vlakana. Slabljenje deuteriranih polimera povezano je sa samom tehnologijom izrade vlakna, ali je tipično za red veličine manje od slabljenja kod PMMA polimera. Do sada su najbolji rezultati po pitanju slabljenja vlakna postignuti sa materijalom CYTOP (Cyclic Transparent Optical Polymer) sa kojim je ostvareno slabljenje reda 10 dB/km na talasnim dužinama od 1300 nm. Može se očekivati da će vlakna izrađena korišćenjem CYTOP materijala imati slabljenje manje od 1 dB/km. S obzirom da se kod vlakana od perfluoriranih polimera prenos vrši unutar spektra od 650 nm do 1300 nm, sa ovim vlaknima se mogu koristiti komponente razvijene za staklena vlakna koje rade na talasnim dužinama od 850 nm do 1300 nm. Na osnovu izvršenih analiza i prikazanih rezultata može se zaključiti da nova polimerna

optička vlakna, pružaju značajne prednosti u odnosu na druge kablovske strukture. Na ovom mestu je potrebno istaći da šira primena optičkih vlakana u realizaciji mreža za pristup i kućnih lokalnih mreža ne isključuje buduću primenu bežičnih tehnologija u ovim segmentima komunikacionog sistema. Bežični prenos, koji se odvija pri brzinama reda 100 Mb/s, ostaje prisutan unutar objekata korisnika, ali se podrazumeva da kičmu ovog sistema čini optička kablovska struktura koja dozvoljava prenos pri brzinama od nekoliko Gb/s.

U petom poglavlju dat je prikaz mogućnosti dinamičko-mehaničke analize (DMA) kod polimernih materijala. DMA je opšti naziv metode za dinamičko-mehaničko deformisanje uzorka i merenje odziva materijala. Deformacija može imati sinusoidnu, stepenastu, konstantnu vremensku zavisnost ili da raste unapred zadatom brzinom. Odziv materijala na deformaciju se može pratiti kao funkcija temperature, ili vremena. Dinamičkom- mehaničkom analizom dobijaju se informacije o: a) mehaničkim svojstvima materijala (moduli absorbovane i izgubljene energije viskoelastičnih materijala tokom vremena i pri različitim temperaturama), b) pomeranja na molekularnom nivou i c) zavisnosti svojstvo-struktura ili morfologija. Mehanička svojstva polimera proističu iz hemijskog sastava polimera (diktira koja od mehaničkih svojstava će se promeniti) i molekularne strukture polimera (diktira način na koji će se promeniti mehanička svojstva). Kod amorfnog polimera imamo nasumičnu rasporelu polimernih lanaca kroz matricu, bez prisustva pravilnih struktura koje srećemo kod kristaliničnih i delimično kristaliničnih polimera. Zbog ove činjenice imamo kretanje molekula amorfnog polimera ispod tačke topljenja takvog kristalita. Sa povećanjem kretanja molekula u amorfnom polimeru, uzorak prolazi od staklaste, kroz gumoliku do tečne faze. Polimer prolazeći kroz različite faze, menja fizička svojstva pa samim tim može se analizirati mogućnost njegove primene. Zbog toga bitno je ispitati na koji način kretanje molekula amorfnog polimera, utiče na njegova fizička svojstva. Ova kretanja molekula zovu se relaksacija. Dinamičko-mehanička analiza daje karakterizaciju sledećih svojstava polimernih materijala: staklasti prelaz, sekundarni prelaz, kristaliničnost, nadmolekulsko strukturalno-poprečno povezivanje, fazno razdvajanje (polimerne smeše, kopolimeri), kompoziti, starenje (fizičko i hemijsko), vulkanizacija mreža, orijentacija kao i efekte aditiva. Dinamičko-mehanička analiza (DMA) je jedna od najefikasnijih metoda za proučavanje ponašanja plastičnih i polimernih kompozitnih materijala i potencijalno može biti veoma korisna za simulaciju ponašanja polimernih optičkih vlakana (POV) u realnim primenama.

U šestom poglavlju dati su eksperimentalni rezultati istraživanja ponašanja optičkih vlakana pod dinamičkim neizotermnim uslovima odnosno simultano merenje optičkih i dinamičko-mehaničkih svojstava polimernih optičkih vlakana. Mogućnost istovremenog merenja nekih optičkih svojstava za vreme DMA može značajno da unapredi proučavanje POV, samih ili ugrađenih u neki materijal. U ovom radu je opisano i diskutovano merenje mehaničkih svojstava POV pomoću 'single cantilever' DMA koje je izvršeno istovremeno sa merenjem intenziteta propuštene svetlosti kroz

POV. Kako bi se uporedili rezultati DMA koji su dobijeni za pravougaone i cilindrične uzorke od istog materijala, ista vrsta ispitivanja vršena je i na pravougaonim pločicama dobijenim topljenjem POV. U radu je pokazano da promene intenziteta optičkih signala odgovaraju promenama modula sačuvane energije POV za vreme DMA, a da dobijene maksimalne vrednosti optičkih signala označavaju početak procesa prelaza u staklasto stanje u materijalu od koga je napravljeno optičko vlakno.

U sedmom poglavlju dati su rezultati eksperimentalnih istraživanja optičkih i mehaničkih svojstava PMMA-Y₂O₃ (Eu³⁺) nanokompozita. U okviru ovog rada prezentirano je istraživanje procesiranja i karakterizacije nanokompozitnog materijala PMMA-Y₂O₃ (Eu³⁺). Uzorci sa različitim sadržajem nanofosfora Y₂O₃ dopiranog sa Eu-jonima procesirani su u laboratorijskom uređaju za umešavanje termoplastičnih polimera. Ispitivan je uticaj udela nanočestica na optička i dinamičko-mehanička svojstva kompozita. Intenzitet luminiscentnog emisionog spektra kompozita raste sa udelom nanofosfora. Rezultati DMA pokazuju da modul absorbovane energije, modul gubitaka i temperatura transformacije rastu sa povećanjem udela nanočestica. Mikrotvrdoća kompozita takođe raste sa povećanjem udela nanočestica u kompozitu i pokazuje skoro linearnu zavisnost sa temperaturom transformacije (T_g).

U osmom poglavlju dati su rezultati istraživanja optičkih i mehaničkih svojstava PMMA-Gd₂O₃ (Eu³⁺) nanokompozita. U okviru ovog rada prezentirano je istraživanje procesiranja i karakterizacije nanokompozitnog materijala PMMA-Gd₂O₃ (Eu³⁺). Poseban značaj ovih istraživanja je u tome što je za dobijanje nanokompozita korišćena metoda elektropredenja što prema detaljnom literaturnom pregledu do sada nije objavljeno u literaturi.

U devetom poglavlju dati su zaključci postignutih rezultata istraživanja koji odgovaraju zadatim ciljevima disertacije. Na kraju je dat spisak korišćene literature.

Ključne reči: Polimerna optička vlakna, Dinamičko mehanička analiza, Nanokompoziti, Luminiscencija, Mehanička svojstva, Mikrotvrdoća, nanofosfori, Elektropredenje, Nanoindentacija

Naučna oblast: Hemija i hemijska tehnologija

Uža naučna oblast: Nauka o materijalima i inženjerstvo materijala

UDK: 66..017

OPTICAL AND MECHANICAL PROPERTIES OF HYBRID NANOCOMPOSITE LIGHT GUIDE FIBERS

Abstract

Dynamic Mechanical Analysis (DMA) is one of the most powerful tools to study the behavior of plastic and polymer composite materials and it is potentially very useful tool to simulate behavior of plastic optic fibers (POF) in real applications. Possibility of simultaneous measurements of some optical properties during DMA would significantly upgrade investigations of POF alone or embedded in some materials. In this work, single cantilever DMA of the POFs that was done simultaneously with measuring the transmitted optical signal intensity is described and discussed. In order to compare mechanical results of the same material for cylindrical and rectangular specimens, rectangular plates were prepared by melting POFs and the same kind of tests were performed. It is shown that changing the optical signal intensity corresponds to the changes of storage modulus of the POF during DMA, and the maximums in optical signals intensity indicate the beginning of glass transition processes in the POF material.

The results of a study related to the processing and characterization of PMMA-Y₂O₃ (Eu³⁺) nanocomposites are presented herein. The nanocomposite samples were prepared using a laboratory mixing molder with different contents of Eu-ion doped Y₂O₃ nanophosphor powder. The influence of particle content on the optical and dynamic mechanical properties of the nanocomposites was investigated. The intensity of the luminescence emission spectra increased as the nanophosphor content in the composite increased. The results of dynamic mechanical analysis revealed that the storage modulus, loss modulus and glass transition temperature (T_g) of the polymer composites increased with increasing content of the nanophosphor powder. The microhardness data also confirmed that the hardness number increased with nanoparticles concentration in the PMMA nanocomposites. The obtained results revealed a relatively linear relationship between T_g and the Vickers hardness.

This study reports research related to different preparation methods and characterization of polymer nanocomposites for optical applications. The Eu-ion doped Gd₂O₃ nanophosphor powder with different nanoparticle content was embedded in the matrix of PMMA. Preparation was carried out by mixing molding (bulk), electrospinning

(nanofibers) and solution casting (thin films) with neat particles and particles coated with AMEO silane. Among the pros and cons for proposed methods, the mixing molding enables to avoid solvent use while the best deagglomeration and nanoparticle distribution is gained using the electrospinning method. The results of dynamic mechanical analysis (DMA) and nanoindentation revealed that the storage modulus of the composites was higher than that of pure PMMA and increased with nanophosphor content. Surface modification of particles improved the mechanical properties of nanocomposites.

Keywords: Plastic optical fibers, Dynamic Mechanical Analysis, Nanocomposites, Luminescence, Mechanical properties, Microhardness., Nanophosphors, Electrospinning, Nanoindentation

Academic Expertise: Chemistry and Chemical Technology

Field of Academic Expertise: Materials Science and Engineering

UDK: 66.017

TABLE OF CONTENTS

1. INTRODUCTION	14
2. LUMINESCENT MATERIALS	21
2.1 PHOSPHOR QUANTUM DOTS	21
2.2 NANOSTRUCTURED MATERIALS	24
2.3 QUANTUM DOTS	26
2.4 RARE EARTH IONS AS OPTICAL DOPANTS	27
2.5 THE Eu^{3+} - Gd_2O_3 SYSTEM	32
3. POLYMER NANOCOMPOSITES FOR OPTICAL APPLICATIONS	39
4. PLASTIC OPTICAL FIBER	42
4.1 THE STRUCTURE OF THE POF	43
4.2 THE FACTORS AFFECTING THE ATTENUATION LOSS LEVEL OF THE POF	44
5. DYNAMIC MECHANICAL ANALYSIS (DMA)	49
5.1 INSTRUMENTAL CONSIDERATIONS	50
5.2 APPLICATIONS	51
5.2.1 MATERIAL SELECTION FOR SPECIFIC END-USE APPLICATIONS	51
5.2.2 PROJECTION OF MATERIAL BEHAVIOR USING SUPERPOSITIONING	53
5.2.3 DETERMINATION OF CURING BEHAVIOR	55
5.2.4 FILM AND FIBER STRESS/STRAIN MEASUREMENTS	55
6. OPTICAL AND DYNAMIC MECHANICAL PROPERTIES OF PLASTIC OPTICAL FIBERS	57
6.1 INTRODUCTION	57
6.2 EXPERIMENTAL	58
6.3 RESULTS AND DISCUSSION	60
6.3.1 MEASUREMENTS WITH POF-SINGLE CANTILEVER TESTS	60
6.3.2 DYNAMIC TEMPERATURE SCAN TEST	66
6.3.3 MEASUREMENTS ON RECTANGULAR SPECIMENS	69
7. OPTICAL AND MECHANICAL PROPERTIES PMMA-Y_2O_3 (Eu^{3+}) NANOCOMPOSITES	72
7.1 INTRODUCTION	72
7.2 EXPERIMENTAL	74
7.3 RESULTS AND DISCUSSION	75
8. OPTICAL AND MECHANICAL PROPERTIES PMMA- Gd_2O_3 (Eu^{3+}) NANOCOMPOSITES	82
8.1 INTRODUCTION	82

<i>8.2 EXPERIMENTAL</i>	83
<i>8.3 RESULTS AND DISCUSSION</i>	85
9. CONCLUSIONS	93
REFERENCES	96
APENDIX I/III	104

1. INTRODUCTION

Nanostructure science and technology is a broad area of research and development activity that has been growing explosively worldwide in the past decades. It has the potential for revolutionizing the ways in which materials and products are synthesized and the range and nature of functionalities that can be accessed. It is already having a significant commercial effect, which will assuredly increase in the future.

Of particular interest to materials scientists is the fact that nanostructure materials have higher surface areas than do normal materials. The effect of nanostructure on the properties of high surface area materials is an area of increasing importance to understanding, synthesizing, and improving materials for wide applications.

Nanocomposites are a distinct form of composite materials, which involve embedding nano- or molecular domain-sized particles into organic polymer, metal or ceramic matrix materials.^{1,2} The intimate inclusion of nanoparticles in these matrices can greatly change the mechanical, electrical, optical or magnetic properties of these materials. The reason for this is that with such small inclusions, a large amount of interfacial phase material exists in the bulk of these nanocomposites.

This thesis is related to the processing and characterization of polymer–nanophosphor composites, as promising materials for the production of nanocomposite fibers. Plastic optical fibers (POF) can be used for a number of applications, such as light transmission for signs and illumination, sensors and data communication^{3,4,5}. Signal attenuation of commercial polymer fibers is much higher than that of glass fibers. In order to improve POF optical efficiency, research and processing are being developed in the direction of nanocomposite POF doped with dyes, and fluorescent or phosphorescent nanopowder⁶.

The optical properties of nano-sized phosphors are significantly improved in comparison to bulk materials (stronger luminescence emission and modified radiative lifetime)^{7,8,9,10}. Poly(methyl methacrylate), PMMA, nanocomposites containing Y_2O_3 and Gd_2O_3 doped with rare earths (RE) ions have been investigated^{11,12} and it was suggested that doped Y_2O_3 nanocrystals embedded in PMMA would have potential for

various photonic applications, including laser systems and optical communication devices¹³. Nanocomposites PMMA-Y₂O₃:RE were successfully prepared by mixing Y₂O₃:Er³⁺, Yb³⁺ or Y₂O₃:Er³⁺ with PMMA for infrared cards¹⁴. The Eu-ion doped nanophosphor is useful for nanocomposite POF light guides because the luminescence wavelength of the Eu-ion (611 nm) is in the visible range of spectrum. It is very important to preserve their optical properties for a synergetic effect in functional nanocomposites.

Nanotechnologies are now poised to revolutionize the electronic, chemical and biotechnology industries and biomedical fields. There are many interesting areas in nanotechnology. One of the most important aspects of this field is the preparation and development of nanomaterials, such as nanoparticles. There have been a variety of techniques for preparing different types of nanoparticles.

The perception of everyday world around us is generally biased. Most people never give a thought to size dependence of the fundamental properties of a material and, if they do, they tend to think that they are size independent.

Size effect is already known for a decades. The pioneer was none other than the great Faraday who, in 1856, first started to study the size dependence of the physical properties of material. He used gold, which he started with very small pieces of gold (nanocrystalline gold) in solution and, by pressing them together, made bigger pieces of gold. Faraday distinguished that the colour of a metal can become size dependent below a certain critical size. What this critical size was, and why it was different for the different metals that he investigated, was something that Faraday did not understand, and could not have understood.

Many years later, the first experiments were published that proved that this size dependence of material properties also applied to semiconductors. It was found that both the absorption and the emission of CdS shifted to shorter wavelengths for smaller crystal sizes. Again, a qualitative explanation was sought in terms of the reduced size of the CdS crystal. So, it had been experimentally proven that the fundamental properties of a material can become strongly dependent on the size of the material below a certain threshold size. It would take understanding of the structure of metals, the discovery of

the electron and the advent of quantum mechanics before, in the second half of the 20th century, a quantitative explanation was found.

The explanation is: When a semiconductor crystal is illuminated with photons of sufficiently high energy then the light can be absorbed by the material. The absorption of light by the semiconductor usually results in the promotion of an electron from the valence band to the conduction band. Another way to describe this process, is to say that the absorption of light by the semiconductor results in the excitation of the semiconductor and the formation of an electron (in the conduction band) - hole (in the valence band) pair. Such an electron-hole pair is usually denoted by the term ‘exciton’ (Figure 1.1).

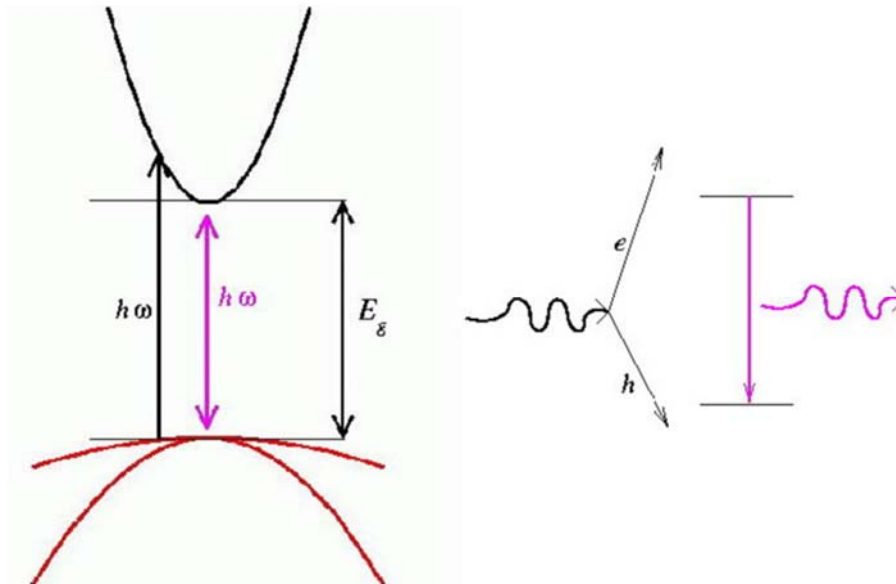


Figure 1.1. Schematic presentation of excitation of semiconductor structure and creation of electron-hole pair (exciton)⁶.

However, because of the potential step present at the surface of the crystal, the exciton wave function cannot extend beyond the edge of the crystal without a severe energetic ‘penalty’. As a result, the total exciton wave function will have to be squeezed to fit into the crystal. This results in an increase in the kinetic energy of the exciton, usually called the “confinement energy”. When this happens there will be a change in the band structure of the semiconductor. This change is quite significant and consists of effects, which often referred to as “quantum size effects”

Nanoparticles are made out of metallic, semiconductor or insulating materials that are much smaller than the wavelength of light. In the last decades there has been much interest on nanoparticles made out of semiconductor materials, especially on II-VI semiconductor types, e.g. CdSe, CdTe, CdS, ZnS, etc., and III-V, e.g. GaAs^{15,16,17}.

That was the first time that researcher became aware of the quantum confinement effects produced by the change of bulk semiconductor electronic properties with decreasing size. This effect occurs when the nanostructures themselves become smaller than a fundamental scale intrinsic to the substance. It was later proven that the exciton Bohr radius could determine this intrinsic scale. Since this effect is determined by hydrogen atom model of the exciton Bohr radius they were named ‘quantum dots’ or ‘artificial atoms’. Quantum dots belong to the category of zero dimensional structures. They are made of few thousand atoms that keep the structural features of the bulk solid but particularly different electronic properties as a function of their size.

With the advent of modern synthesis techniques, scientists have acquired the ability to create structures with dimensions on the nanometre scale. One major point in these developments has been the reduction of the dimension of particles from three-dimensional bulk systems to two-dimensional, to one-dimensional, and finally to zero-dimensional systems. When the size of all these particles becomes comparable with the de Broglie wavelength, a consequence of the wave nature of electrons, electrons confined in these particles shows quantum effects.

The new electronic and optical properties of these reduced-dimensional particles, which can be controlled to a certain extent, make these particles promising candidates for a variety of future applications that include improved semiconductor lasers and microelectronics. Quantum dots represent the ultimate reduction in the dimensionality of a semiconductor system. In these systems, electrons are confined in all directions. Therefore they have no kinetic energy (except the ubiquitous zero-point energy) and as a result they occupy spectrally sharp energy levels like those found in atoms.

These zero-dimensional quantum confined particles are useful for considering the fundamental concepts of nanostructures as well as for its potential to act at the level of a single electron, certainly the ultimate limit for an electronic device. With a good

knowledge of their electrical and optical properties, scientists have now focused their attention on devices based on quantum dots. Some of the best examples are QD photodetectors, QD lasers and QD memory devices. Quantum dots have also found applications in fluorescence markers, exciton storage, a step toward smart pixels, quantum computing and quantum cryptography^{18,19,20}.

Quantum size effects that are very well known by the box model can be also observed in absorption spectroscopy. The absorption bands shift to higher energies with decreasing quantum dot sizes, “blue shift”. It was proved that the optical band gap is blue shifting dramatically from the bulk size amount to the quantum sizes. Below exciton Bohr radius the absorption spectra shows a fine structure. Appearance of a fine absorption spectrum is due to the presence of discrete energy levels. Since the exciton levels become delocalized over the whole quantum dot the absorption spectra of this quantum dots will be affected by the exciton transitions²¹.

The emission spectra of most of the quantum dots consists of a single-broad emission band, which is symmetric and comes from states that fall in the quantum dot’s band gap. These states are not clear in absorption spectra. Photoluminescence spectroscopy may help distinguish the sub-structures that are present in the absorption spectra. However, the explanation of the emission spectra is more difficult to interpret than for the absorption spectra. The emission in CdSe quantum dots has an unusual long recombination lifetime of around 1 μ s compared to that in the bulk of few nanoseconds. Moreover trapping of an exciton by the surface state defects may lead to nonradiative recombination pathways and therefore fluorescence quenching. Coating the quantum dot with a higher band gap material has been shown to improve the photoluminescence quantum yields by passivating the nonradiative recombination sites, e.g. CdSe/ZnS core-shell quantum dots. Quantum yield of the photoluminescence increased from about 5% to 30-50% for this particular case. In very homogenous high quality QDs samples it has been observed that the fluorescence band exhibits a blue shift with decreasing size and they can be tuned from 470 to 625 nm, covering most of the visible spectra. This is a very important property for application of the quantum dots in biological application²².

Nanosize materials have become the focus of intensive fundamental and applied research. The strong interest on these materials arises from the viability on designing and building structures that exhibit outstanding electrical, mechanical, chemical, optical and magnetic properties compared to the bulk materials. This feature of nanosize materials allows the achievement of unique properties enabling them to be considered for a wide range of markets, including medicine, plastics, energy, electronics, and aerospace. In addition, nanocrystals are increasingly used in various medical systems, such as drug targeting, magnetic fluid hyperthermia, and magnetic resonance imaging (MRI), among others. In this regard, nanosize rare earth (RE)-doped phosphors become a very promising type of material in terms of both their fundamental and potential applications including solid state lasers, lighting and luminescence systems. In RE-doped nanoparticles, emission lifetime, luminescence quantum efficiency, and concentration quenching can be affected by particle size²³.

Hybrid nanocomposites. In this thesis, the organic/inorganic optical nanocomposite is defined as a composite which consists of an organic host material and inorganic inclusions with a diameter of nanometer range (nano-inclusions). The essence of the research can be concisely described as follows: The important prerequisite is that the inorganic nano-inclusions are randomly dispersed in the organic host material without aggregation to form a heterogeneous composite structure as schematically drawn in [Figure-1.2](#)

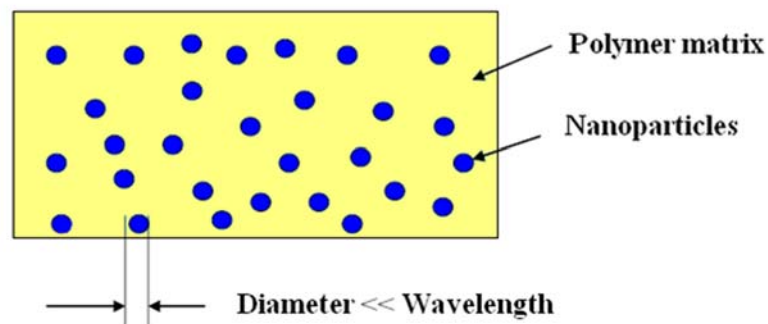


Figure 1.2. Schematic drawing of heterogeneous nanocomposite structure.

When the nano-inclusions are randomly dispersed, the scattering arisen from the interaction between propagating light and nano-inclusions is substantially expressed by

the Rayleigh scattering theory. For this reason, high transparency could be maintained when the diameter of the nano-inclusion is optimized by taking into account the ratio of the refractive index of the nano-inclusion to that of the host material. The dielectric property of the nano-inclusions, as that of molecular assembly reflecting its structural characteristics such as molecular symmetry, chemical bonding property and electron distribution, appear in the effective dielectric property of the nanocomposite. This suggests that it would be possible to design and control the optical property of the nanocomposite by designing and controlling the nano-inclusion, which will finally appear in the average optical property of the nanocomposite. When amplifying this consideration, it is expected that one could create a novel material exhibiting an optical property, which cannot be exhibited by organic materials alone, while maintaining preferable transparency²⁴.

From an optical property control of view, the group of rare earth (RE) is a bonanza of optical phenomena, so to speak, for investigating on the development of a novel nanocomposite. During more than a hundred years of history, REs have occupied the attention of a huge variety of photonic applications; for example, phosphors for a variety of photonic devices such as lighting devices, color TVs, lasers, fiber optical amplifiers, and scintillators. Versatile optical processes in terms of light-matter interaction peculiar to REs are generally ascribed to the local-environmental characteristics of RE ions.

In the past few decades significant interest has been shown in polymer-based sensing materials, which exhibit a change of their absorption and/or fluorescence characteristics in response to an external stimulus. Some examples of these stimuli include heat^{25,26}, deformation^{27,28}, chemicals^{29,30} light^{31,32}, and others^{33,34}, which make the sensors useful for a wide range of technologies^{35,36}.

2. LUMINESCENT MATERIALS

2.1 PHOSPHOR QUANTUM DOTS

The word ‘phosphor’ comes from the Greek language. It means ‘light bearer’, to describe light-emitting or luminescent materials; barium sulfide is one of the earlier known naturally occurring phosphors³⁷. A phosphor is luminescent, that is, it emits energy from an excited electron as light. The excitation of the electron is caused by absorption of energy from an external source such as another electron, a photon or an electric field. An excited electron occupies a quantum state whose energy is above the minimum energy ground state. In semiconductors and insulators, the electronic ground state is commonly referred to electrons in the valence band, which is completely filled with these electrons. The excited quantum state often lies in the conduction band, which is empty and is separated from the valence band by an energy gap called the band gap, ΔE_g (Figure 2.1).

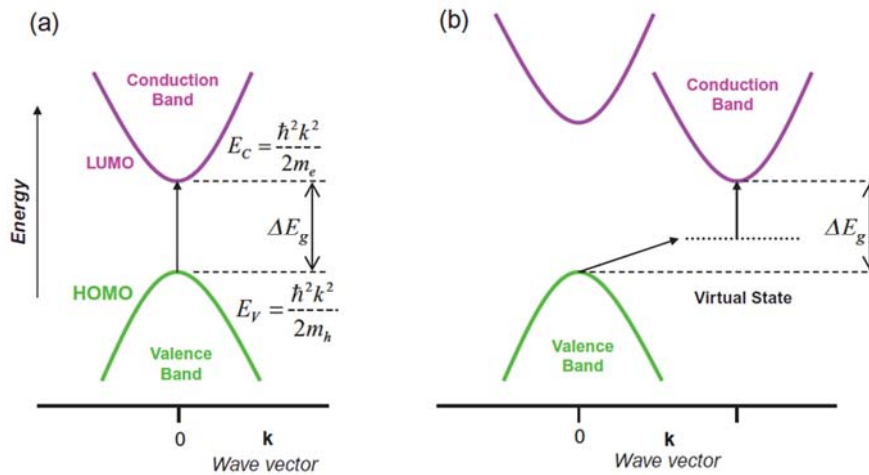


Figure 2.1 Schematic band-energy diagrams for: (a) direct band gap; and (b) indirect band gap semiconductors³⁸

Therefore, unlike metallic materials, small continuous changes in electron energy within the band are not possible. Instead a minimum energy equal to the band gap is necessary to excite an electron in a semiconductor or insulator, and the energy released by deexcitation is often nearly equal to the band gap. The band gap of a semiconductor

material is such that at room temperature very few electrons are promoted from the valence band to the conduction band leaving holes in the valence band.

Figure 2.1 (a) shows an energy band diagram (plot of allowed quantum state energy vs. wave vector magnitude k) for a direct band gap semiconductor. In the direct band gap semi-conductors, the positions of the highest energy state of the valence band (HOMO-highest occupied molecular orbital) and the lowest energy state of the largely unoccupied conduction band (LUMO-lowest unoccupied molecular orbital) are at the same k resulting in a high probability of emitting light. The case of an indirect band gap semiconductor is shown in Figure 2.1 (b), and has the valence band maximum and conduction band minimum at different values of k . Therefore, electrons need to undergo a change of k -value followed by a change in energy. Therefore, the transition requires a change in both energy and momentum. In other words, an indirect transition requires energy excitation of an electron simultaneous with an electron-phonon interaction to give the required momentum change. Therefore, the absorption and recombination efficiency of direct band gap materials is about four orders of magnitude larger than that of indirect material. Zinc sulfoselenide ($\text{ZnS}_{1-x}\text{Se}_x$) and gallium phosphide (GaP) are examples of direct and indirect band gap compound semiconductors, respectively. As discussed above, luminescence from phosphors can be observed by exciting the electrons to higher energy states, for example, into the conduction band. There are several approaches that provide this excitation, such as:

- photoluminescence (PL)
- electroluminescence (EL)
- cathodoluminescence (CL)
- mechanoluminescence
- chemiluminescence
- thermoluminescence.

In this chapter, only PL, EL and CL (Figure 2.2) will be discussed, with most emphasis on PL and EL.

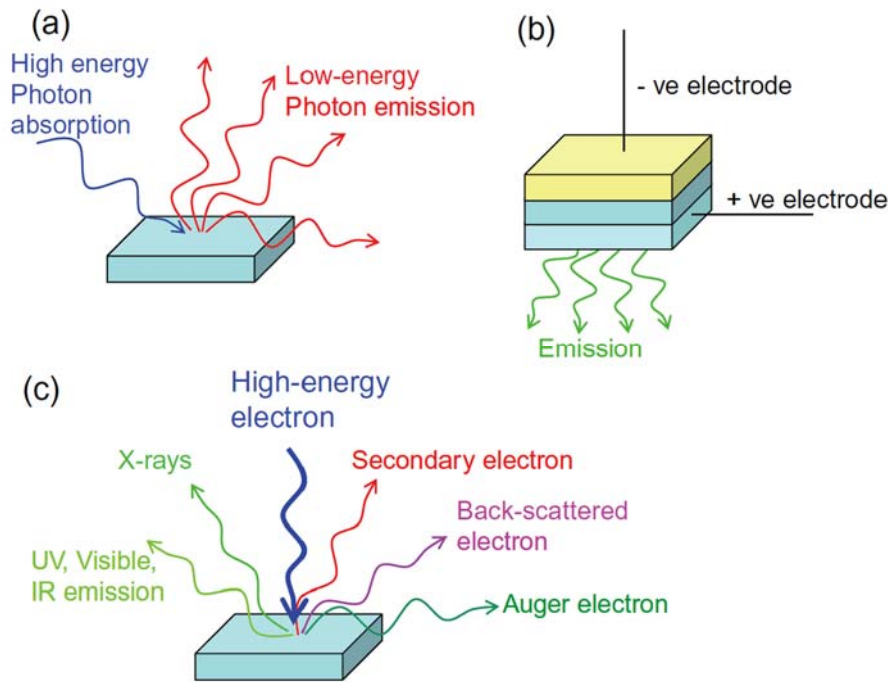


Figure 2.2 Schematic illustrations of: (a) photoluminescence; (b) electroluminescence; and (c) cathodoluminescence³⁸

When an insulator or semiconductor absorbs electromagnetic radiation (i.e. a photon) an electron may be excited to a higher energy quantum state. If the excited electron returns (relaxes) to a lower energy quantum state by radiating a photon, the process is called photoluminescence (PL). Some of the quantum state relaxation transitions are not allowed, based on the spin and Laporte selection rules³⁹. The PL intensity depends on the measured temperature and the energy of the exciting light (known as photoluminescence excitation or PLE spectrum). In general, peaks in the PLE spectrum are higher in energy than those in the PL spectrum. Figure 2.2 (a) schematically illustrates the excitation and emission processes of PL.

When a material emits electromagnetic radiation as a result of the application of an electric field, the process is called electroluminescence (EL). The photon emitted results from radiative recombination of electrons and holes created in the phosphor by the voltage between the two electrodes (Figure 2.2 (b)). One of the electrodes is transparent to the wavelength of the light emitted by the device. The first report of an EL device was in 1907⁴⁰, when Henry Joseph Round observed that light was emitted from silicon carbide under application of a high voltage. As discussed below, there is significant

interest in inorganic nanophosphors combined with conducting organic materials to produce EL devices, because of their potentially high efficiencies. Other advantages for EL devices in comparison to conventional lighting systems also include small to large size, flexible substrates and shapes, high brightness, long device lifetimes, lower operating temperatures, non-directionality and antiglare lighting. Depending on the applied bias, thin-film electroluminescence (TFEL) device can be categorized as either DC or AC (ACTFEL) devices.

Cathodoluminescence (CL) is emission of light from a material that is excited by energetic electrons. The exciting primary electrons can be focused into a beam and scanned across the surface (as in a scanning electron microscope), resulting in high spatial resolution CL. The CL process is shown schematically in [Figure 2.2 \(c\)](#), along with other phenomena that result from primary electron–material interactions, for example, X-ray and various electron emissions.

2.2 NANOSTRUCTURED MATERIALS

Nanostructured materials, by definition, can exist as individual particles or clusters of nanoparticles of various shapes and sizes⁴¹. Research has shown that nanostructured materials generally exhibit geometries that reflect the atomistic bonding analogous to the bulk structure. The nanomaterials are of interest because they can bridge the gap between the bulk and molecular levels and lead to entirely new avenues for application. Nanostructured materials have a high surface-to-volume ratio compared to their bulk counterparts. Therefore, a large fraction of atoms is present on the surface, which makes them possess different thermodynamic properties. During the last two decades, a great deal of attention has been focused on the optoelectronic properties of nanostructured semiconductors with an emphasis on fabrication of the smallest possible particles. The research has revealed that many fundamental properties are size-dependent in the nanometer range. For example, the density of states (DOS), that is the number of quantum states vs. energy for periodic materials with three, two or one dimension, is shown in [Figure 2.3⁴²](#). If the extent of the material is on the order of one to ten nanometers in all three directions, the material is said to be a quantum dots (Qdots). A Qdot is zero-dimensional relative to the bulk, and the DOS depends upon whether or not

the Qdots have aggregated (Figure 2.3). The DOS for a molecule and an atom are also shown in Figure 2.3.

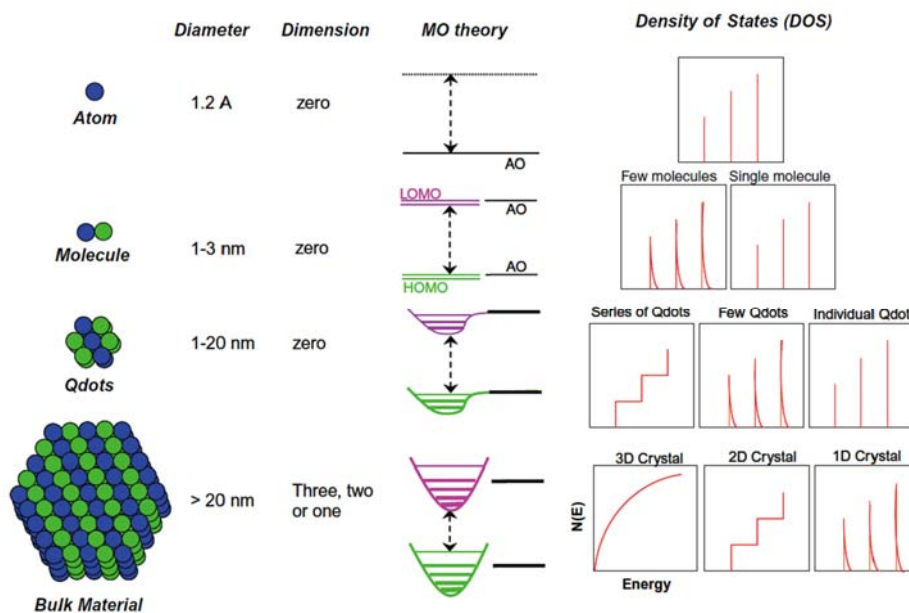


Figure 2.3 Schematic illustration of the changes of the density of quantum states (DOS) with changes in the number of atoms in materials (see text for detailed explanation).

AO: atomic orbital, MO: molecular orbital³⁸

The density of electrons in a three-dimensional bulk crystal is so large that the energy of the quantum states becomes nearly continuous (Figure 2.3). However, the limited number of electrons results in discrete quantized energies in the DOS for two, one and zero-dimensional structures (Figure 2.3). The presence of one electronic charge in the Qdots repels the addition of another charge and leads to a staircase-like I-V curve and DOS. The step size of the staircase is proportional to the reciprocal of the radius of the Qdots. The boundaries as to when a material has the properties of bulk, Qdot or atoms, are dependent upon the composition and crystal structure of the compound or elemental solid. When a solid exhibits a distinct variation of optical and electronic properties with a variation of size, it can be called a nanostructure, and is categorized as:

- two-dimensional, e.g. thin films or quantum wells;
- one-dimensional, e.g. quantum wires; or
- zero-dimensional, e.g. Qdots.

Although each of these categories shows interesting optical properties, our discussion will be focused on quantum dots, or Qdots. An enormous range of fundamental properties can be realized by changing the size at a constant composition. In the following sections, we will discuss the history, structure and properties relationships, and the optical properties of Qdots.

2.3 QUANTUM DOTS

Nanostructured semiconductors or insulators have dimensions and numbers of atoms between the atomic-molecular level and bulk material with a band gap that depends in a complicated fashion upon a number of factors, including the bond type and strength with the nearest neighbors. For isolated atoms, there is no nearest-neighbor interaction. Therefore, sharp and narrow luminescent emission peaks are observed. A molecule consists of only a few atoms and therefore exhibits emission similar to that of an atom. However, a nanoparticle is composed of approximately 100–10000 atoms, and has optical properties distinct from its bulk counterpart. Nanoparticles with dimensions in the range of 1–30 nm are called quantum dots (Qdots). Zero-dimensional Qdots are often described as artificial atoms due to their d-function-like density of states, which can lead to narrow optical line spectra.

A significant amount of current research is aimed at using the unique optical properties of Qdots in devices, such as light-emitting diodes (LEDs), solar cells and biological markers. Qdots are of interest in biology for several reasons:

- higher extinction coefficients;
- higher quantum yields;
- less photobleaching;
- absorbance and emissions can be tuned with size;
- generally broad excitation window but narrow emission peaks;
- multiple Qdots can be used in the same assay with minimal interference with each other;
- toxicity may be less than conventional organic dyes; and
- the Qdots may be functionalized with different bio-active agents^{43,44}.

The inorganic Qdots are more photostable under ultraviolet excitation than organic molecules, and their fluorescence is more saturated. The ability to synthesize Qdots with narrow size distributions with high quantum yields has made them an attractive alternative to organic molecules in hybrid light-emitting devices and solar cells.

2.4 RARE EARTH IONS AS OPTICAL DOPANTS

Due to their very distinct chemical and optical properties, RE-bearing compounds are extensively used in a large number of applications, such as superconductors, optical fibers, data storage, nuclear technology, high-power laser systems, magnetostrictive alloys, magnetic refrigeration, paint and coatings, permanent magnets, catalysts, etc. As explained before, because of the identical configuration of the outermost (6s) shell, all RE elements are chemically very similar. This strong chemical affinity makes any selective separation process between RE species a very difficult task; therefore, rare-earth compounds usually containing minor proportions of other RE species. Since the 4f electrons of the RE are shielded from perturbations with the lattice by the outer 5s and 5p electrons, the 4f orbitals retain their hydrogenic character, resulting in sharp transitions between the 4f levels. Consequently, RE species will exhibit temperature stable and sharp spectroscopic emission lines largely independently of the type of the host material⁴⁵. This is a major advantage since the wavelength required for a specific application can be matched with the energy of transitions in the 4f-shell of the RE atoms to effectively select an appropriate emitter.

Rare earths (RE) form a group of chemically similar elements which have in common an open 4f shell. In neutral state, these elements possess the electron configuration $4f^n 6s^2$, except for Gadolinium, which shows the configuration $4f^7 5d^1 6s^2$, where the number of f electrons 'n' ranges from 2 for Cerium to 14 for Ytterbium. Unlike the corresponding 3d transition series, the 4f electrons of the RE generally remain highly localized in the solid, and they have almost no contribution to the chemical valence, therefore the atom can easily lose the 6s and 5d electrons and also one electron from the 4f shell, so they are most stable as trivalent ions, although 2+ or 4+ are frequently found in some compounds. The series is conveniently divided at the point of a half-filled 4f shell into light (La-Eu) and heavy (Gd-Lu) groups.

The filling of the of the 4f shell can be explained by Hund's rules, which predict that the term with the highest quantum number S has the lowest energy and if there are several terms with the same S, the one with the highest angular momentum quantum number L has the lowest energy. Furthermore, due to spin-orbit coupling, the terms $2S+L$ are split into levels $J=L+S, L+S-1, \dots, |L-S|$, where for less than half-filled shells, the term with the smallest J has the lowest energy. The optical and magnetic properties of the RE ions are determined by the 4f electrons, which are well shielded from the environment by the outer 5s and 5p electrons.

On the other hand, the general tendency toward trivalent state is clearly related to the increasing localization of the f electrons with atomic number. The highly directional f orbitals are only partially able to screen each other from the attractive force of the nucleus, which leads to the well-known lanthanide contraction. This interesting property of the lanthanide series consist in the decrease in both the ionic and covalent radii (Figure 2.4) and the increase in Pauling's electronegativity by increasing nuclear charge. This effect is the main reason for differences found in compounds throughout the lanthanide series.

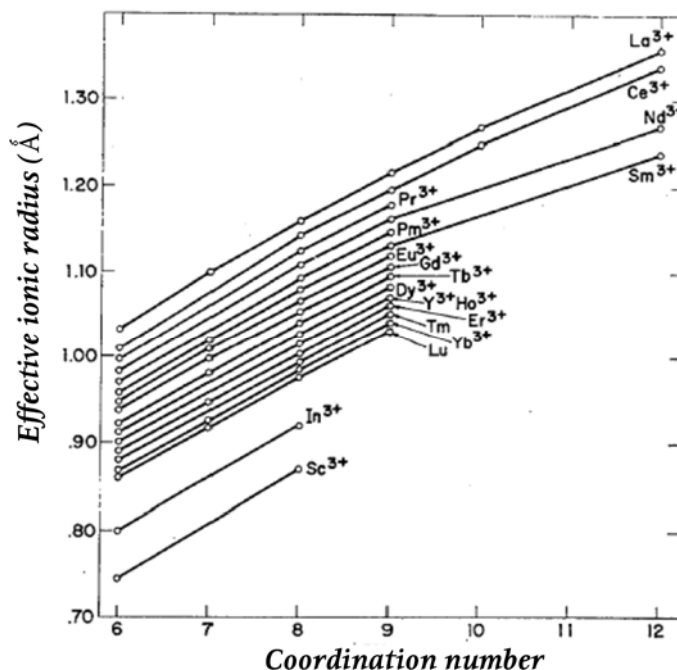


Figure 2.4 Effective ionic radius (\AA) for some common cations (CN: coordination number)⁴⁶.

As was before indicated, Rare earths species exist as 3+, or occasionally 2+ ions when incorporated in a solid host. The trivalent ions exhibit intense narrow-band intra-4f luminescence in a wide variety of hosts, whereas the shielding provided by the 5s² and 5p⁶ electrons causes that rare-earth radiative transitions in solid hosts resemble those of the free ions and, as a consequence, the electron–phonon coupling becomes weak.

In principle the rare earth ions can be classified in three groups^{47,48} according to their strength of luminescence:

a) Tb³⁺, Dy³⁺, Eu³⁺ and Sm³⁺ are the strongest emitters, which all have fluorescence in the visible region. (Tb³⁺: 545nm, 5D₄→7F₄; Dy³⁺: 573nm, 4F_{9/2}→6H_{13/2}; Eu³⁺: 611nm, 5D₀→7F₂; Sm³⁺: 643nm, 4G_{5/2}→6H_{11/2}).

b) Er³⁺, Pr³⁺, Nd³⁺, Ho³⁺, Tm³⁺ and Yb³⁺ are weak emitters in the near infrared region. The weakness of their luminescence is based on the fact that these ions have closely spaced energy levels, making the non-radiative transition easy. For the erbium ion there are, besides some other very weak spin forbidden lines (e.g. 4fⁿ-15d → 4fⁿ), two characteristic transitions: one in the visible region at about 550 nm (4S_{3/2}→4I_{15/2}) and the other, the most important one for commercial use, at 1.55μm (4I_{13/2}→4I_{15/2}).

c) La³⁺, Gd³⁺ and Lu³⁺ exhibit no ion fluorescence because the lowest-lying resonance level lies far above the triplet level of any of the commonly used ligands.

Like other RE-ions, the luminescence attributed to trivalent Eu is characterized by sharp peaks attributed to the intra-4f shell transitions 5D₀→7F_j (see [Figure 2.5](#))⁴⁹. After excitation with energy of at least 2.18 eV the energy state 5D₀ is populated and, by recombination to the 7F_j states, red light is emitted. The spectral positions are independent of the embedding matrix but their intensities may vary⁵⁰. Moreover, due to crystal field, the individual j-levels (except j = 0) are splitted up, and the crystal-field splitting appears as fine structure and provides information about the symmetry of the rare-earth site and the shape of the coordination polyhedron. The intensities of spectral transitions reflect also the interaction between the RE ion and its environment.

A number of excitation pathways are available for rare-earth luminescence in solid hosts, which can be broadly classified as either direct or indirect excitation mechanisms. For instance, in the Eu^{3+} -doped Gd_2O_3 system the different sensitization processes of Eu^{3+} are the following: the host Gd_2O_3 absorption, O-Eu charge transfer, the Gd^{3+} ion absorption and the Eu^{3+} ion self-excitation. After Ch. Liu, et al⁴⁹ the excitations from the host band and charge transfer band for the $5\text{D}_0 \rightarrow 5\text{F}_2$ transition of Eu^{3+} ions, in nanocrystalline, are almost equal for the bulk Gd_2O_3 .

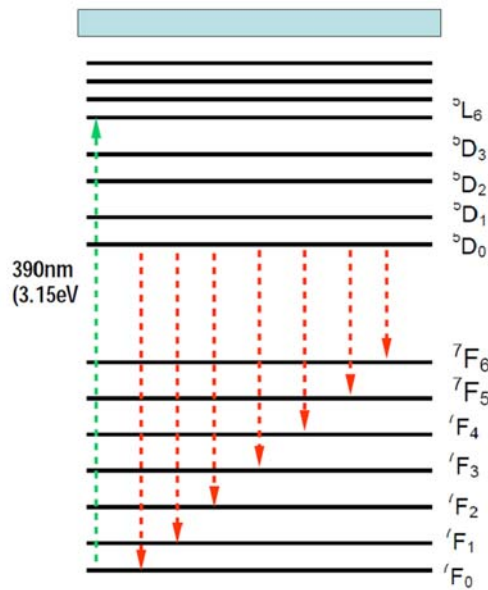


Figure 2.5 Energy level diagram of the optical transitions within Eu^{3+} ions⁵¹.

The excitation residing in an ion can migrate to another of the same species in the ground state as a result of resonant energy transfer promoted by the shortening of the inter-ionic distance. Energy migration processes increase the probability to optical excitation be trapped at defects or impurity sites, enhancing non-radiative relaxation. This non-radiative relaxation will be enhanced by increasing the concentration of the RE species leading to concentration quenching. Also, the energy transfer between different ion species can take place when they have closely matched energy levels. Then, the energy transfer from the host crystal to luminescent dopants leads to host-excited luminescence. Therefore, the energy transfer process will result either in the enhancement or in the quenching of emission. In order to demonstrate the occurrence of energy transfer, various methods have been proposed⁵¹. One of them is based on the measurement of the excitation spectrum of the emission from the luminescent dopant. If

the excitation spectrum of the dopant emission shows the excitation band of the host in addition to those of dopant, this indicates energy transfer from the host to luminescent dopant. This fact would indicate that the actual incorporation of dopant in the host structure was accomplishment, and therefore a phosphor material is obtained.

In general, functional doping of a nanomaterial requires that the dopant ions substitute metal ions of the host lattice, i.e., that they occupy lattice sites of the host metal ions. Similar to electrical doping, the term optical doping is used to describe the incorporation of centers in a host material to enhance and/or tailor its optical properties. A well known example of optical doping is the phosphor technology that is used in a large number of lighting and display applications. Optical doping is also very important in optoelectronics, a technology that forms the basis for components such as semiconductor lasers, optical discs, image sensors, or optical fibers. With optical doping it is possible to enhance both the emission and absorption characteristics of a material.

As was above mentioned, in cubic Eu^{3+} -doped Gd_2O_3 , Eu^{3+} ions occupy two kinds of lattice sites after substituting the Gd^{3+} ions (Figure 2.6).

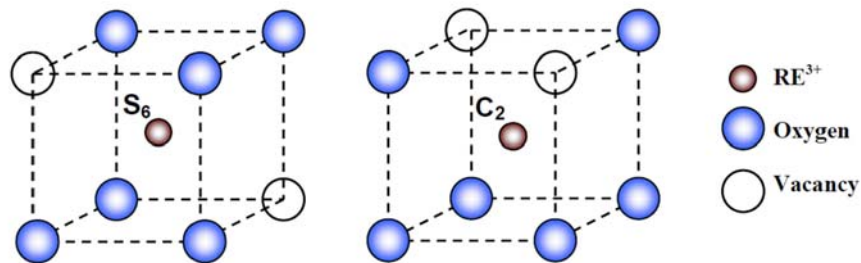


Figure 2.6 Schematic presentation of the RE^{3+} coordination in the S_6 and C_2 sites of cubic (C-type) sesquioxide.

These sites are sixfold coordinated distinctly non equivalent with C_2 and S_6 point symmetry, and which differ from each other in the position of RE^{3+} ion relative to the vacancy oxygen, as was described above. It has been established⁵² that the presence of inversion symmetry in the RE^{3+} site drastically affects the luminescence spectra of the RE^{3+} -doped materials

On the other hand, due to nearly identical radii ions, 0.94\AA for Gd^{3+} and 0.95\AA for Eu^{3+} , the lattice distortion in Eu^{3+} -doped Gd_2O_3 is insignificant⁵³ and, unlike in Y_2O_3 , where

pairs of neighboring Eu^{3+} ions leads to slight distortions in crystal field, in Gd_2O_3 the mutual proximity of the Eu^{3+} ions has no effect⁵⁴, since Eu^{3+} and Gd^{3+} have nearly the same size, which allows an unambiguous analysis of the transfer process.

In this chapter, some previous works on properties of Eu^{3+} - Gd_2O_3 nanostructures, which are matter of study in this thesis, are briefly reviewed.

2.5 THE Eu^{3+} - Gd_2O_3 SYSTEM

Using the sol-gel method, Lin et al.⁵⁵ prepared nanocrystalline powders of Eu-doped Gd_2O_3 with concentrations of Eu in the 3-15 mol% range. From GdCl_3 and EuCl_3 , as precursor salts, while water D.I. and NH_4OH were used as solvent and chelating agent, respectively. The mixture of Gd and Eu hydroxides obtained was calcinated between 800°C and 1100°C for 2h. In this work, the effect of Eu/Gd composition ratio and calcination temperature on the structure and luminescent properties were investigated. From their XRD measurements the authors report that pure crystalline phase Gd_2O_3 can be formed at temperatures above 900°C , while at 800°C both phases GdO_2 and Gd_2O_3 coexisted. The crystallite sizes were 12, 21, 34 and 24nm for calcinations temperatures of 800, 900, 1000 and 1100°C , respectively. TEM analyses revealed the following particle size distributions for different calcinations temperatures: 50-120nm (800°C), 80-140nm (900°C), 80-180nm (1000°C) and 90-200nm (1100°C). The discrepancy between estimated XRD crystallite sizes and TEM size was attributed to aggregation of particles. Regarding the luminescent properties, the authors found that, monitoring the emission at 612nm, and after calcining the intermediates at temperatures above 800°C the excitation spectra exhibited a wide band about 254nm, assigned to $\text{O}^{2+} \rightarrow \text{Eu}^{3+}$ Charge Transfer Band (CTB). The intensity of the excitation peak was increased by increasing the calcination temperature up to 1000°C . A further increase in the temperature was conducive to the drop in the corresponding peak intensity. This fact was not discussed by the authors. Also, a weak and broad peak at 312nm, related to Gd^{3+} transitions, was observed. These transitions were caused by the $\text{Gd}^{3+} \rightarrow \text{Eu}^{3+}$ energy

transfer mechanism. In the emission spectra, the maximum intensity was shown in those samples treated at 1000°C and was attributed to the enhanced crystallinity achieved at such temperature. The effect of the concentration of Eu^{3+} ion was investigated in powders calcined at 1000°C; the optimum doping level was determined as 7% w/w. The decreasing in the PL emission intensity, for higher concentrations, was attributed to the concentration quenching phenomena, which was described in the earlier section of this thesis.

M. Pires et al.⁵⁶ produced Eu-doped Gadolinium oxide by the precipitation method. The influence of Eu^{3+} concentration on optical and morphological properties was investigated. Non crystalline monohydrate gadolinium basic carbonate bare and doped with 1 to 5 at.% of europium were obtained as precursor. The precursors were annealed at 750°C for 4h, under argon continuous flow. Although the authors claimed the cubic phase was obtained, no evidence on crystallinity quality and lattice parameter values were discussed within the paper. SEM analyses revealed the presence of particles with an average diameter in the 110-150nm range, irrespective of the concentration of the dopant species. The same reference proposed that doping species should have been located on the particle surface inhibiting particle growth after nucleation. Luminescence spectroscopy measurements showed a pronounced CTB centered around 250nm was observed. The intensity of this CTB was found to increase by rising the Eu^{3+} concentration. It was also observed weak peaks up to 330nm, related to internal Gd^{3+} f-f transitions. These peaks became noticeable because of the $\text{Gd}^{3+} \rightarrow \text{Eu}^{3+}$ energy transfer. Similar trend on the luminescence intensity was observed at higher fractions of Eu, indicating the absence of concentration quenching at least for the considered interval of concentrations, which was explained for the authors, considering that the doping ion distribution in the surface of oxide samples does not achieved the minimum distance necessary to cause energy transfer between emission centers.

G. Liu, et al.⁵⁷, prepared spherical and submicrometer-sized hollow Gd_2O_3 (Eu^{3+}) phosphors by homogeneous precipitation and hydrothermal crystallization techniques. The report considered the variation of dopant concentration and modification of the synthesis conditions as follows: in the precipitation step, spherical nucleus were formed and allowed to grow. In the subsequent hydrothermal step, large particles were

crystallized. $\text{Gd}_2\text{O}_3(\text{Eu}^{3+})$ phosphors were obtained by annealing those products from the hydrothermal stage at different temperatures (550-850°C) for 2h in air. It was found that the crystals morphology was strongly dependent on the reactants concentration and aging time. Depending on those conditions, rods and solid or hollow spheres were obtained. The XRD pattern for the precursor showed the presence of sharp peaks that were attributed to $\text{Gd}_2(\text{CO}_3)_3 \cdot x \text{H}_2\text{O}$. Moreover, the authors claimed that the samples annealed at 600°C exhibited the pure cubic phase. The diffraction peaks became sharper when the solids were produced at higher annealing temperatures. However, from their FT-IR results, in addition to Gd-O bond peak (553cm^{-1}), the presence of -OH group (3410cm^{-1}) and CO_3^{2-} anion (1508 and 1429cm^{-1}) bands were evident, which suggested an incomplete conversion of the precursors into the anhydrous oxide phase. The corresponding luminescence measurements (the excitation spectra were monitored by using the 610nm line) revealed an intense band at 260nm that was attributed to the CTB and whose intensity increases as the annealing temperature increases. Furthermore, the weak lines observed at 279nm and 310nm were related to internal Gd^{3+} f-f transitions ($^8\text{S}-^6\text{I}$) and ($^8\text{S}-^6\text{P}$) indicating an effective energy transfer from Gd^{3+} to Eu^{3+} . The authors reported that the obtained spherical $\text{Gd}_2\text{O}_3(\text{Eu}^{3+})$ phosphors had better red luminescence properties, and that the relative luminescence intensity and the lifetime increased with increasing annealing temperatures (Figure 2.7). Moreover, they considered that, because with the increasing the annealing temperature, the crystallinity becomes better, and the impurities such as -OH, CO_3^{2-} decrease, the quenching of the luminescence of Eu^{3+} by the vibrations of these impurities decreases, resulting in the increase of the lifetime of Eu^{3+} .

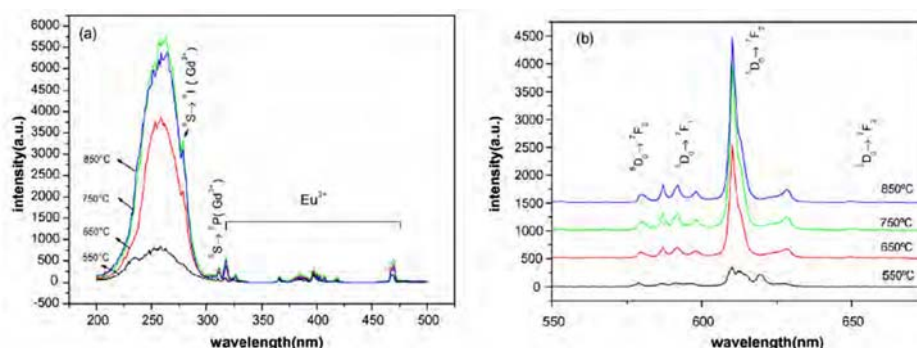


Figure 2.7 Excitation (a) and emission (b) spectra of samples calcined at different temperatures⁵⁷.

In the same work, the excitation spectra shown in [Figure 2.7-b](#), for 611nm emission, consisted of a large band with a maximum at 254nm. This band was assigned to CTB. In these spectra, the maximum intensity was observed for the 10wt% Eu-doped Gd₂O₃. The CTB was shifted towards longer wavelengths (265nm) for the 15wt% Eu-doped Gd₂O₃ phosphor. Typical peaks for internal Gd³⁺ f-f transitions were no mentioned within the

Ch.S. Park, et al.⁵⁸, synthesized nanoparticles of Gd₂O₃ (Eu³⁺) by a liquid-phase reaction method using hydrated acetate as the precursor salts. They investigated the influence of Eu³⁺ content (in the range of 5-15wt%,) on the optical properties of phosphors. After synthesized, the precursors were treated at 600°C for one hour and under oxygen atmosphere (2l/min). The XRD analyses reported that, regardless of the europium content, all solids crystallized in the cubic Gd₂O₃ structure even at a temperature as low as 600°C. The average crystallite size was estimated in the range 21-41 nm. The largest sizes corresponded to the phosphor with 10wt% Eu³⁺. The apparent relationship between composition and average crystallite size was not discussed by the authors.

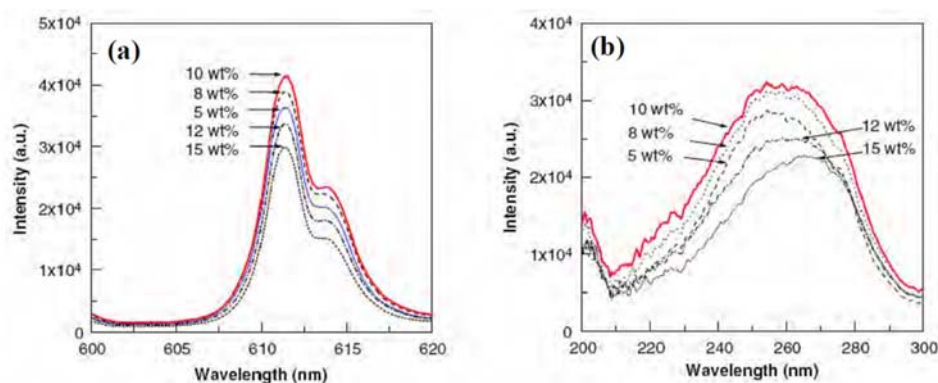


Figure 2.8 (a) Emission (excitation at 254nm) and (b) excitation (monitoring 611nm) spectra of Gd₂O₃ (Eu³⁺)⁺ phosphors having different concentrations⁵⁸

In the same work, the excitation spectra shown in [figure 2.8](#), for 611nm emission, consisted of a large band with a maximum at 254nm. This band was assigned to CTB. In these spectra, the maximum intensity was observed for the 10wt% Eu-doped Gd₂O₃. The CTB was shifted towards longer wavelengths (265nm) for the 15wt% Eu-doped

Gd₂O₃ phosphor. Typical peaks for internal Gd³⁺ f-f transitions were not mentioned within the manuscript. Similarly, when the phosphors were excited by UV light of 254nm (CTB), only the main emission peak (detected at 611nm) was reported. The authors found that the phosphors showed an initial increase in luminescence and then a subsequent decrease with further doping (above 10wt%), which was attributed to the previously discussed concentration quenching effect.

Phosphor particles of Eu-Gd₂O₃ were synthesized by Y.C. Kang, et al.⁵⁹, by a continuous spray pyrolysis method. The effects of process temperature (800-1600°C) and Eu content (2-12at.%) on PL, morphology and crystallinity of the products, were investigated. Unlike normal spray pyrolysis methods, no milling was applied to powders. The mean size of the particles increased from 0.35 to 1.2 μm when the solution concentration was increased from 0.02 to 1M. The particles prepared at 800°C exhibited sharp XRD peaks corresponding to cubic Gd₂O₃. The crystallinity of the cubic phase was increased by rising the process temperature up to 1400°C. A transition from highly crystalline cubic to poorly crystalline monoclinic phase was observed at 1600°C, which was higher than the 1250°C previously reported for Gd₂O₃⁶⁰. This discrepancy with expected transition temperature was explained in terms of the short residence time of the particles inside the hot wall reactor. The average size of the particles increased from 0.35 to 1.2μm when the solution concentration was increased from 0.02 to 1M; nevertheless, the effect of process temperature on crystal nor particle size was not reported. The Eu-Gd₂O₃ particles absorbed excitation energy in the range between 220 nm and 300 nm, with a maximum excitation wavelength around 255nm. The optimum brightness was obtained at a doping concentration of 10at.%, while the maximum PL intensity was observed in the sample annealed at 1400°C, (the main peak emission was at 612nm in both cases.) In turn, the particles prepared at 1600°C, showed two main emission peaks at 615 and 624nm and much lower intensity than for other samples synthesized at lower temperatures (between 1000 and 1400°C), as shown [figure 2.9](#).

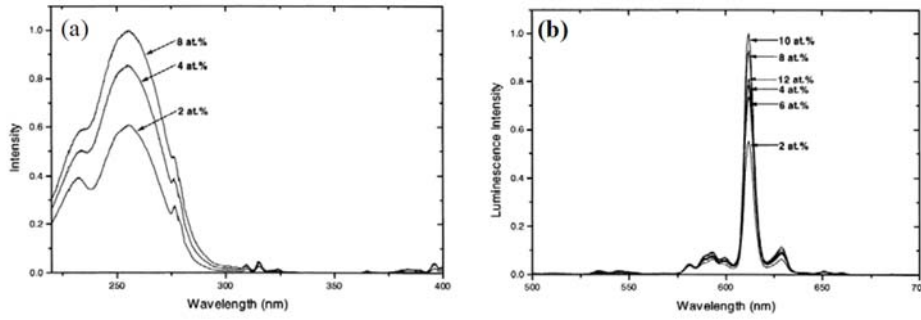


Figure 2.9 Excitation (a) and emission (b) spectra of Gd_2O_3 (Eu^{3+}) particles at different doping concentrations, prepared at $900^\circ C$ ⁵⁹.

On the other hand, A. Garcia-Murillo, et al.⁶¹ synthesized Eu^{3+} -doped Gd_2O_3 thin films by sol-gel method. In this work, used Gd (III) isopropoxide and Eu (III) nitrate pentahydrate were used as precursors. The solution was prepared under argon flux and deposited on pure silica substrate by di-coating in a glove box under argon controlled atmosphere. The authors found that films present waveguiding properties and the crystallization in the cubic phase occurs at $700^\circ C$, but no preferential orientation was observed. Also, after annealing at $1000^\circ C$ very dense films were obtained with a refractive index of 1.88 at 632.8nm. Their PL studies revealed that the thin films synthesized have the same sharp emission bands as Eu^{3+} -doped Gd_2O_3 powders produced by solid state reaction method, corresponding to the ${}^5D_0 \rightarrow {}^7F_J$ ($J=0$ to 4). After the authors, these bands of cubic phase appear at $700^\circ C$ by sol-gel process although with conventional method they become visible only after $900^\circ C$, but explain this fact.

It is evident from the reviewed literature that, due to the potential applications in various fields, the study of Eu^{3+} -doped Gd_2O_3 nanostructured is matter of intense research, in order to search up its better properties. However, nevertheless the actual incorporation of Eu ions into Gd_2O_3 structure has been demonstrated, phenomena like the concentration quenching are strongly dependent of the methods and conditions of synthesis. In addition, it is clear that the luminescent properties of this material are strongly dependent on method and condition synthesis. Therefore, in this work, the effect of Eu^{3+} content and annealing temperature on the structural, luminescent and

magnetic properties of Gd_2O_3 nanoparticles; and the effect of Eu^{3+} on structural, optical and luminescent properties of Gd_2O_3 thin films are studied.

3. POLYMER NANOCOMPOSITES FOR OPTICAL APPLICATIONS

Composite materials are well known, and generally comprise two or more materials each offering its own set of properties or characteristics. The two or more materials may be joined together to form a system that exhibits properties derived from each of the materials. A common form of a composite is one with a body of a first material (a host matrix) with a second material distributed in the host matrix.

One class of composite materials includes nanoparticles distributed within a host matrix material. Nanoparticles are particles of a material that have a size measured on a nanometer scale. Generally, nanoparticles are larger than a cluster (which might be only a few hundred atoms in some cases), but with a relatively large surface area-to-bulk volume ratio. While most nanoparticles have a size from about 10 nm to about 500 nm, the term nanoparticles can cover particles having sizes that fall outside of this range. For example, particles having a size as small as about 1 nm and as large as about 1×10^3 nm could still be considered nanoparticles. Nanoparticles can be made from a wide array of materials. Among these materials examples include, transition metals, rare-earth metals, group VA elements, polymers, dyes, semiconductors, alkaline earth metals, alkali metals, group IIIA elements, and group IVA elements.

Further, nanoparticles themselves may be considered a nanoparticle composite, which may comprise a wide array of materials, single elements, mixtures of elements, stoichiometric or non-stoichiometric compounds. The materials may be crystalline, amorphous, or mixtures, or combinations of such structures.

The host matrix may comprise a random glassy matrix such an amorphous organic polymer. Organic polymers may include typical hydrocarbon polymers and halogenated polymers. It is generally desirable that in an optical component, such as a planar optical waveguide, an optical fiber, an optical film, or a bulk optical component, e.g., an optical lens or prism, the total optical loss be kept at a minimum. For example, in the case of a planar optical waveguide, the total loss should be approximately equal to, or less than, 0.5 dB/cm in magnitude, and such as less than 0.2 dB/cm. For a highly transparent

optical medium to be used as the optical material, a fundamental requirement is that the medium exhibits little, or no, absorption and scattering losses.

Intrinsic absorption losses commonly result from the presence of fundamental excitations that are electronic, vibrational, or coupled electronic-vibrational modes in origin. Further, the device operating wavelength of the optical component should remain largely different from the fundamental, or overtone, wavelengths for these excitations, especially in the case of the telecommunication wavelengths of 850, 1310, and 1550 nm located in the low loss optical window of a standard silica glass optical fiber, or waveguide. Further, these absorptive overtones can cause the hydrocarbon polymers to physically or chemically degrade, thereby leading to additional and often times permanent increase in signal attenuation in the optical fibers or waveguides

Material scattering losses occur when the signal wave encounters abrupt changes in refractive index of the otherwise homogeneous uniform optical medium. These discontinuities can result from the presence of composition inhomogeneities, crystallites, nanoporous structures, voids, fractures, stresses, faults, or even foreign impurities such as dust or other particulates.

Among the various mechanisms of optical scattering loss, an important factor is the porosity of the optical material. As a result of the interplay between various material characteristics, e.g., surface energy, solubility, glass transition temperature, entropy, etc., and processing conditions, e.g. temperature, pressure, atmosphere, etc., optical materials, such as amorphous perfluoropolymers can exhibit a large amount of nanoporous structures under normal processing conditions. Such nanoporous structures can cause optical scattering loss and should be eliminated, or converted to smaller sizes, in order to satisfy a certain low optical loss device performance requirement. The smaller sized pores are called nanopores. Nanopores are pores in a material that have a size measured on a nanometer scale. Generally, nanopores are larger than the size of an atom but smaller than 1000 nm. While most nanopores have a size from about 1 nm to about 500 nm, the term nanopores can cover pores having sizes that fall outside of this range. For example, pores having a size as small as about 0.5 nm and as large as about 1×10^3 nm could still be considered nanopores. By introducing nanoparticles into

optically transparent host matrix , the absorption and scattering losses due to the nanoparticles may add to the optical loss. In order to keep the optical loss to a minimum, in addition to controlling the loss contribution from the host matrix, it is essential to control the absorption and scattering loss from the nanoparticles doped into the host matrix for optical applications.

For discrete nanoparticles that are approximately spherical in shape and doped into the host matrix, the scattering loss α , in dB per unit length, resulting from the presence of the particles is dependent on the particle diameter d , the refractive index ratio of the nanoparticles and the waveguide core $m=n_{\text{par}}/n_{\text{core}}$, and the volume fraction of the nanoparticles in the host waveguide core V_p . The nanoparticle induced scattering loss can be calculated by:

$$\alpha = 1.692 \times 10^3 \left(\frac{m^2 - 1}{m^2 + 2} \right)^2 \frac{d^3 V_p}{\lambda^4} \quad (1)$$

where λ is the vacuum propagation wavelength of the light guided inside the waveguide. As an example, when $m=2$, $V_p=10\%$, $\lambda=1550\text{nm}$, $d=10\text{ nm}$, the calculated scattering loss α is 0.07dB/cm . To fabricate a certain waveguide device with a set loss specification, and therefore a nanoparticle induced waveguide loss budget of α , the nanoparticle diameter d must satisfy the following equation relationships:

$$d < \left(\alpha \frac{1}{1.692 \times 10^3} \left(\frac{m^2 + 2}{m^2 - 1} \right)^2 \frac{\lambda^4}{V_p} \right)^{1/3} \quad (2)$$

where λ is the vacuum propagation wavelength of the light guided inside the waveguide, $m=n_{\text{pa}}/n_{\text{core}}$ the refractive index ratio of the nanoparticles and the core, and V_p the volume fraction of the nanoparticles in the host waveguide core. For example, following Equation 2, with a nanoparticle loss budget of $\alpha = 0.5\text{dB/cm}$, when $m=2$, $V_p=10\%$, $\lambda=1550\text{nm}$, the nanoparticle diameter d must be smaller than 19 nm . In general, the diameter of the nanoparticles must be smaller than about 50nm , and more preferably, 20nm .

The description for nanoparticle loss also can be applied to nanopore contributions to propagation loss by representing the nanopores as equivalent nanoparticles with refractive index of 1.

Composite materials including nanoparticles distributed within a host matrix material have been used in optical applications. The nanoparticles increase the index of refraction of the host matrix material to create a packaging material that is more compatible with the relatively high refractive index of the LED chip disposed within the packaging material. Because the nanoparticles do not interact with light passing through the packaging material, the packaging material remains substantially transparent to the light emitted from the LED.

4. PLASTIC OPTICAL FIBER

Specifically, the well-known plastic optical fibers with PMMA core were introduced in the 1960s, although the first optical fibers that were used as a communications channel were made of glass. In the past several decades, concurrent with the successive improvements in glass fibers, POFs have become increasingly popular, owing to their growing utility.

Table 4.1 The historical evolutions of the important landmark

Year	Organization	Development
1968	Du Pont	First report of PMMA-core SI POF
1982	Keio Univ. NTT	First report of GI POF (1070dB/km at 670nm) Perdeuterated PMMA-core SI POF (20dB/km at 650nm)
1983	Mitsubishi Rayon	PMMA-core SI POF "ESKA"
1990	Keio Univ.	First report of high speed transmission by PMMA GI POF(300MHz.km)
1994	USA Japan Keio, NEC Asahi Chemical	High speed POF network(HSPN) consortium POF consortium Japan 2.5Gbps-100m transmission at 650nm by PMMA GI POF Multi core SI POF
1996	Keio	First perfluorinated(PF) polymer base GI POF for 1.3 μ m
1997	POF Consortium Keio, Asahi Glass	Standardization of ATM LAN & IEEE1394 (156Mbps 50 SI POF) 2.5 Gbps · 200m transmission at 1.3 μ m by PF GI POF
1999	Lucent tech.	11 Gbps · 100m transmission at 1.3 μ m by PF GI POF
2000	Mitsubishi Rayon	500 Mbps · 50m transmission at 650nm by PMMA Multi SI POF

The historical evolutions of the important landmark are listed in Table I-4⁶². The first POF was manufactured by Dupont at the late sixties. Due to the incomplete purification of the source materials used, attenuation was still in the vicinity of 1,000 dB/km. During the seventies it became possible to reduce losses nearly to the theoretical

limit of approximate 125 dB/km at a wavelength of 650 nm. At that point in time glass fibers with losses significantly below 1 dB/km at 1,300 nm / 1,550 nm were already available in large quantities and at low prices. Digital transmission systems with a high bit rate were then almost exclusively used in telecommunications for long-range transmissions. The field of local computer networks was dominated by copper cables (either twisted-pair or coaxial) that were completely satisfactory for the typical data rates of up to 10 Mbit/s commonly used then. There was hardly any demand for an optical medium for high data rates and small distances so that the development of the polymer optical fiber was slowed down for many years. A significant indicator for this development is the history of the International Conference for Polymer Fibers and Applications which has been taking place annually since 1992 and represents the most significant scientific event in this specialized field. Nowadays, with the PMMA-core optical fibers, transmissions at 156 Mbit/s over distances up to 100 m can be carried out⁶³, and transmission speeds of 500 Mbit/s over 50 m can be reached⁶⁴. To achieve higher transmission speeds graded index POFs can be used⁶⁵. In addition, a special type of POF made from an amorphous fluorinated polymer called CYTOP and developed by Koike and Asahi Glass is available in the market⁶⁶. This new fiber presents a considerably lower attenuation than the common POFs (30 dB/km), which allows the transmission distance to be increased up to 1 km for a transmission speed of 1.2 Gbit/s·km. Today, a multitude of different variants are available for widely differing areas of application. There is a choice of parameters such as diameter, bandwidth and temperature range as well as mechanical properties and the coating material⁶⁷.

All of these examples demonstrate that completely new markets for digital transmission systems are being developed for short-range applications. Polymer optical fibers can meet many of these requirements to an optimum degree and are therefore and are therefore increasingly of interest.

4.1 THE STRUCTURE OF THE POF

POFs used for optical communications are highly flexible waveguides composed of nearly transparent dielectric materials. The cross-section of these fibers is circular and, generally, divisible into three layers called the core, cladding, and jacket (a protective cover) which carries out a function of mechanical protection for the optical

fiber, providing robustness made of polyethylene, polyvinylchloride, and chlorinated polyethylene. Within the core, the refractive-index profile can be uniform (step-index fibers, SI) or graded (graded-index fibers, GI), while the cladding index is typically uniform. As shown in Figure 4.1, the GI-POF which has high transmission speed without modal dispersion can be used for the large data transmission, while SI-one can be used only in image guide and small data transmission⁶⁸.

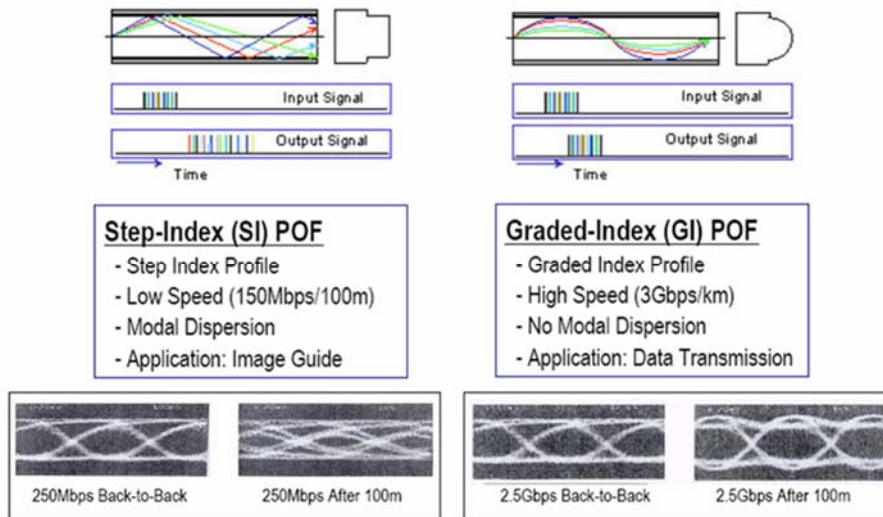


Figure 4.1 Comparison of the SI-POF and GI-POF⁶⁸.

4.2 THE FACTORS AFFECTING THE ATTENUATION LOSS LEVEL OF THE POF

The factors affecting the attenuation loss level of the POF are listed in Table 4.2. There are inherent and external factors. Inherent factors could be divided in an absorption term and a scattering term of light passing through the fiber which stem from the intrinsic chemical nature of POF materials. In most cases, the external factors might come from impurities which are not fully removed during purification process and bubbles or imperfections which are created during manufacturing and drawing process.

Table 4.2. Factors affecting attenuation loss of the POF

	Inherent Factor	External Factor
Absorption	<ul style="list-style-type: none"> ▪ Higher harmonic of C-H vibration ▪ Electronic transition 	<ul style="list-style-type: none"> ▪ Transition metals ▪ Organic contaminants <ul style="list-style-type: none"> ▪ OH group
Scattering	<ul style="list-style-type: none"> ▪ Rayleigh Scattering 	<ul style="list-style-type: none"> ▪ Dust & Micro-void <ul style="list-style-type: none"> ▪ Disturbance at core/cladding interface ▪ Fluctuation of core diameter <ul style="list-style-type: none"> ▪ Micro-bending/Birefringence due to orientation

The basic attenuation mechanisms in a POF can be classified into two main groups: intrinsic and extrinsic. Among the intrinsic losses, we have the absorption of the constituent material and the Rayleigh scattering. Both contributions depend on the composition of the optical fiber and, therefore, they cannot be eliminated. They represent the ultimate transmission loss limit. Basically, they are caused by the molecular vibrational absorption of the groups C-H, N-H, and O-H, by the absorption due to electronic transitions between different energy levels within molecular bonds and by the scattering arising from composition, orientation, and density fluctuations. Regarding the group of extrinsic losses, this is composed of those losses that would not appear in an ideal fiber. Among them, we find the absorption caused by both metallic and organic pollutants and the dispersion provoked by dust particles, microfractures, bubbles, and other structural imperfections in the POF. Besides, there are also radiation losses, originated by perturbations both microscopic and macroscopic in the fiber geometry. Whenever the POF is bent with a finite curvature radius, radiation losses occur, although they are not significant unless this radius is small enough, e.g., only ten times as long as the fiber diameter.

In a straight optical fiber, the power decreases exponentially with the distance z , as shown in the following expression:

$$P(z) = P(0)10^{-\alpha z/10} \quad (4.1)$$

The value of α is called the attenuation coefficient of the optical fiber, and it expresses the value of the attenuation as a function of the fiber length. The expression for the attenuation in decibels (dB/km) is given by:

$$\alpha = -\frac{1}{z}10 \log \frac{P(z)}{P(0)} \quad (4.2)$$

The spectral attenuation of two different materials used for the POF's core is shown in [Figure 4.2](#)⁶⁹. For the PMMA POF two absolute minima of attenuation can be observed, both of 70 dB/km, located at 522 and 570 nm green, although there is a relative minimum around 650 nm red. The polystyrene (PS) POF ($n=1.59$) has similar applications to those of the PMMA POF, but its minimum of attenuation is located in the red region. From a mechanical point of view, these fibers are better than those made of PMMA, although they have a higher attenuation. While their core is PS, their cladding is usually PMMA. Another fiber is the polycarbonate PC POF $n=1.5\sim 1.59$ which is a high-temperature-resistant fiber. Its minimum of attenuation is found to be 600 dB/km and it is located at 770 nm. This kind of fiber can be used in industrial applications where the temperature is an important parameter.

The large diameter and high numerical aperture of polymer optical fibers facilitate fiber coupling and interfacing to other components. Moreover, coupling requires optically smooth surfaces at both ends of the fiber, and polishing of the surfaces of POF's is relatively easy compared to inorganic optical fibers. Consequently, the installation and overall systems cost are low. POF's are, therefore, potentially an excellent alternative for inorganic optical fibers especially in short and medium range applications which require many junctions and connections.

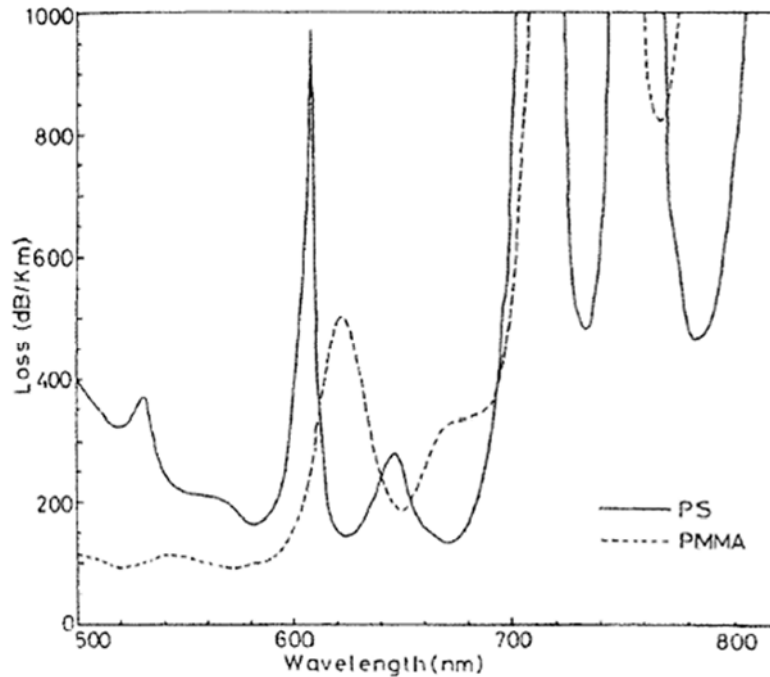


Figure 4.2 Attenuation loss spectra for POF with PMMA and PS core⁶⁹.

These attenuation loss values, however, cannot be achieved in real application due to extrinsic factors exist: Microbubbles and core-clad imperfection during POF drawing and scattering by density fluctuation and unreacted monomers in the glassy polymer matrix⁷⁰. The lowest attenuation loss of methacrylate polymers reported is about 120 dB/km in real application⁷¹.

Especially, future applications of polymer optical fibers in local area networks and fiber optics to and in the home as shown in Figure 4.3 have attracted attention recently. However, the step-index characteristics of commercial POF's result in modal dispersion and a bandwidth that is too low (<10 MHz.km) for these applications⁷². A large research and development effort was therefore devoted, especially in the Far East, to the production of graded-index polymer optical fibers with a strongly enhanced bandwidth⁷³ [13,14].

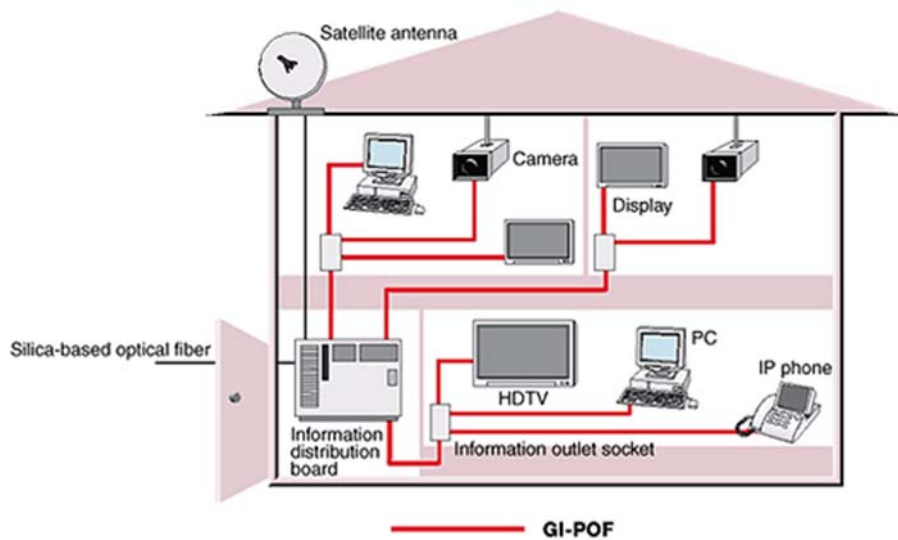


Figure 4.3 *Polymer Optical Fibers for Data Communication*

The large diameter and high numerical aperture of polymer optical fibers facilitate fiber coupling and interfacing to other components. Moreover, coupling requires optically smooth surfaces at both ends of the fiber, and polishing of the surfaces of POF's is relatively easy compared to inorganic optical fibers. Consequently, the installation and overall systems cost are low. POF's are, therefore, potentially an excellent alternative for inorganic optical fibers especially in short and medium range applications which require many junctions and connections.

5. DYNAMIC MECHANICAL ANALYSIS (DMA)

Dynamic mechanical analysis (DMA)-is a thermal analysis technique that measures the properties of materials as they are deformed under periodic stress. Specifically, in DMA a variable sinusoidal stress is applied, and the resultant sinusoidal strain is measured. If the material being evaluated is purely elastic, the phase difference between the stress and strain sine waves is 0° (i.e., they are in phase). If the material is purely viscous, the phase difference is 90° . However, most real-world materials including polymers are viscoelastic and exhibit a phase difference between those extremes. This phase difference, together with the amplitudes of the stress and strain waves, is used to determine a variety of fundamental material parameters, including storage and loss modulus, $\tan \delta$, complex and dynamic viscosity, storage and loss compliance, transition temperatures, creep, and stress relaxation, as well as related performance attributes such as rate and degree of cure, sound absorption and impact resistance, and morphology. The diagram in [Figure 5.1](#) shows the relationship between several of these parameters.

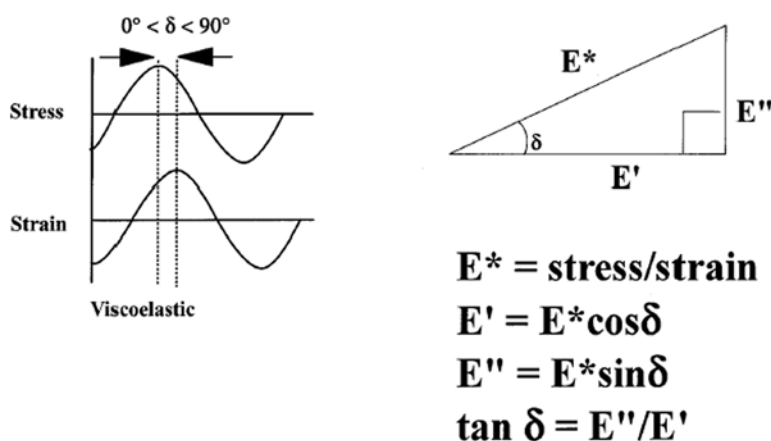


Figure 5.1 Viscoelasticity and complex modulus

Most DMA measurements are made using a single frequency and constant deformation (strain) amplitude while varying temperature. Measurements, where the amplitude of deformation is varied or where multiple frequencies are used, provide

further information.

5.1 INSTRUMENTAL CONSIDERATIONS

There are several components that are critical to the design and resultant performance of a dynamic mechanical analyzer. Those components are the drive motor (which supplies the sinusoidal deformation force to the sample material), the drive shaft support and guidance system (which transfers the force from the drive motor to the clamps that hold the sample), the displacement sensor (which measures the sample deformation that occurs under the applied force), the temperature control system (furnace), and the sample clamps. The DMA Q800 dynamic mechanical analyzer (TA Instruments, Inc., New Castle, DE) , [Figure 5.2](#) is based on a patentpending design that optimizes the combination of these critical components.

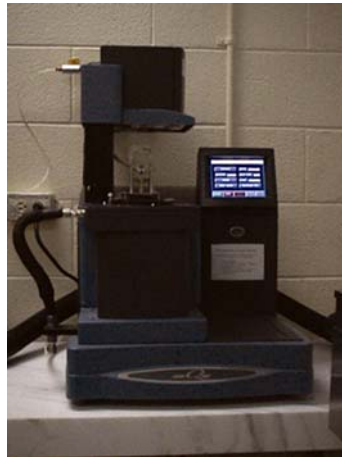


Figure 5.2 DMA Q800

Specifically, the analyzer incorporates a noncontact direct drive motor to deliver reproducible forces (stresses) over a wide dynamic range of 0.001–18 N; an air bearing shaft support and guidance system to provide frictionless continuous travel over 25 mm for evaluating large samples (e.g., fibers as long as 30 mm) or for evaluating polymers at large oscillation amplitudes (± 0.5 –10,000 mm); an optical encoder displacement sensor to provide high resolution (one part in 25 million) of oscillation amplitude, which results in excellent modulus precision ($\pm 1\%$) and $\tan \delta$ sensitivity (0.0001); and a bifilar-wound furnace complemented by a gas cooling accessory to allow a broad temperature range (-150 to 600 °C) to be covered. The DMA Q800 also features a

variety of clamping configurations to accommodate rigid bars, fibers, thin films, and viscous liquids (e.g., thermosets) in bending, compression, shear, and tension modes of deformation.

5.2 APPLICATIONS

5.2.1 MATERIAL SELECTION FOR SPECIFIC END-USE APPLICATIONS

The task of evaluating new materials and projecting their performance for specific applications is a challenging one for engineers and designers. Often, materials are supplied with short-term test information such as deflection temperature under load (DTUL), which is used to project long-term, high-temperature performance. However, because of factors such as polymer structure, filler loading and type, oxidative stability, part geometry, and molded-in stresses, the actual maximum long-term use temperatures may be as much as 150 °C below or above the DTUL. DMA, on the other hand, continuously monitors material modulus with temperature and, hence, provides a better indication of long-term, elevated temperature performance. *Figure 5.3* shows the DMA modulus curves for three resins with nearly identical DTULs but very different moduli at the DTUL and, more importantly, very different modulus trends beyond the DTUL.

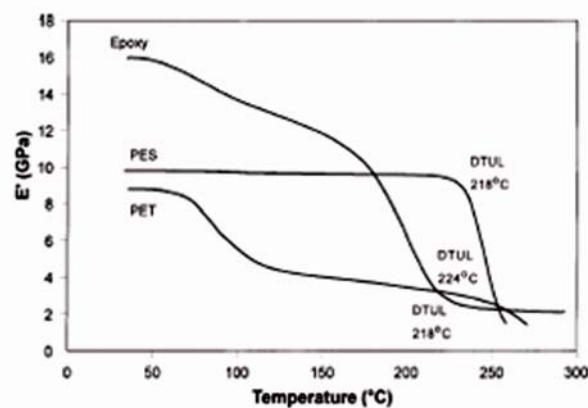


Figure 5.3 DMA comparison of materials with similar DTULs.

The polyethylene terephthalate (PET) in this example represents a semicrystalline material, and its modulus begins to decrease rapidly at 60 °C as the material enters its glass transition. The amorphous component in the polymer achieves an increased degree of freedom, and at the end of the glass transition, the modulus of the material has declined by about 50% from room temperature values. Because of its crystalline component, the material then exhibits a region of relative stability before the modulus again drops rapidly as the crystalline structure approaches the melting point. The actual modulus of a resin of this type at the DTUL is only 10–30% of the room temperature value. The DTULs of highly filled systems based on this resin are more closely related to the melting point than to the significant structural changes associated with the glass transition temperature (T_g).

The polyethersulfone (PES)-in [Figure 5.3](#) is a high-performance amorphous resin. Amorphous materials exhibit higher T_g s than their semicrystalline counterparts and maintain a high percentage of their room temperature properties up to that point. However, with the onset of the glass transition, the loss in properties is sudden and complete, even for highly reinforced grades.

The DTULs of these systems are closely associated with the T_g , but almost always fall on the steeply sloped part of the modulus curve. Thus, the DTUL occurs in a region of great structural instability, and the actual maximum temperature for reliable performance under load is 15–30 °C below the DTUL. Finally, the epoxy is a cross-linked system with a well-defined T_g . The temperature dependency of the modulus in such materials is related to the cross-link density. The relationship of the DTUL modulus is similar to that observed for PET. However, in this case, the crosslinked system provides an extended region of stability well beyond the T_g and the DTUL. Thus, while both thermoplastic systems are no longer solid above 250 °C, the epoxy has structural integrity and virtually the same modulus at 300 °C as it has at 250 °C. It is therefore still serviceable for short-term excursions above the DTUL and may prove useful for extended periods under reduced loads, providing that it possesses good thermal and oxidative stability.

5.2.2 PROJECTION OF MATERIAL BEHAVIOR USING SUPERPOSITIONING

Polymeric materials, because of their viscoelastic nature, exhibit behavior during deformation and flow that is both temperature and time (frequency) dependent. For example, if a polymer is subjected to a constant load, the deformation or strain (compliance) exhibited by the material will increase over a period of time. This occurs because the material under a load undergoes molecular rearrangement in an attempt to minimize localized stresses. Hence, compliance and modulus measurements performed over a short time span result in lower and higher values, respectively, than longer-term measurements. This time-dependent behavior would seem to imply that the only way to accurately evaluate material performance for a specific application is to test the material under the actual temperature and time conditions the material will see in the application. This implication, if true, would present real difficulties for the material scientist because the range of temperature and/or frequencies covered by a specific instrument might not be adequate or, at best, might result in extremely long and tedious experiments.

Fortunately, however, there is a treatment of the data, designated as the method of reduced variables or time-temperature superposition (TTS), which overcomes the difficulty of extrapolating limited laboratory tests at shorter times to longer-term, more real-world conditions. This TTS-treatment is well grounded in theory and can be applied to the data obtained from DMA multifrequency experiments. The underlying bases for TTS are that the processes involved in molecular relaxation or rearrangements in viscoelastic materials occur at accelerated rates at higher temperatures and that there is a direct equivalency between time (the frequency of measurement) and temperature. Hence, the time over which these processes occur can be reduced by conducting the measurement at elevated temperatures and transposing (shifting) the resultant data to lower temperatures.

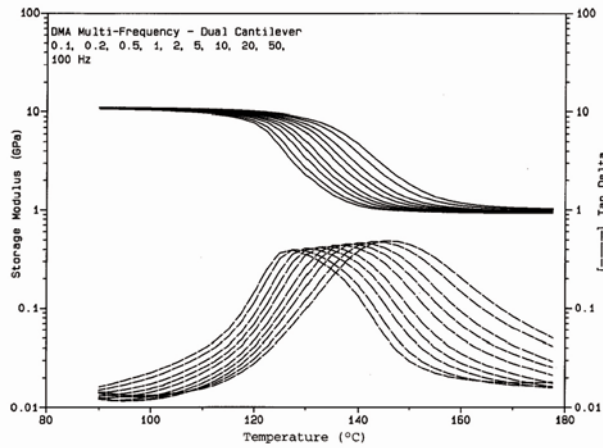


Figure 5.4 Epoxy fiberglass composite-stepwise isothermal frequency sweeps

The result of this shifting is a master curve where the material property of interest at a specific enduse temperature can be predicted over a broad time scale. Figures 5.4 and 5.5 show TTS results for an epoxy composite. Figure 5.4 shows the DMA multifrequency curves obtained over four decades (0.1–100-Hz). The ability of the DMA Q800 to obtain data at 100 Hz and above shortens the experimental time required to obtain the four decades of frequency required for good TTS extrapolations. Figure 5.5 shows the master curve obtained by combining the multifrequency experiments. Note that the behavior of the epoxy (at 148 °C) can be projected over 15 decades of frequency, which is well beyond the four decades used in the experiment. Further evaluation of the data indicates that the behavior of this material around the glass transition follows the William-Landel-Ferry (WLF) equation.

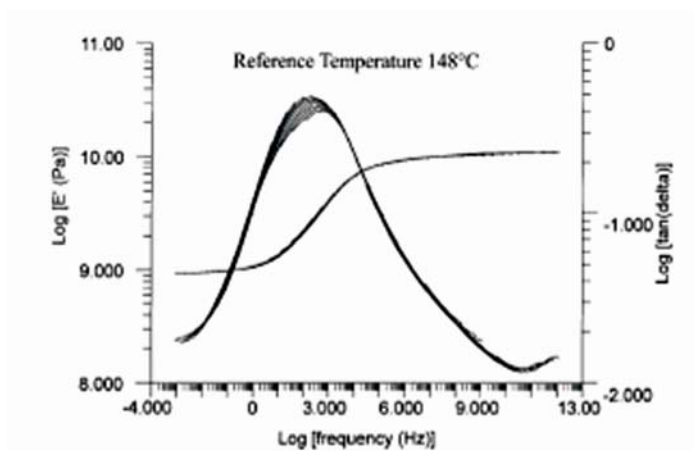


Figure 5.5 TTS of epoxy fiberglass results

5.2.3 DETERMINATION OF CURING BEHAVIOR

Thermosetting liquids such as prepregs, adhesives, and paints/coatings can be evaluated in DMA (dual-cantilever mode) using a supporting structure such as fiberglass braid. In these experiments, information about the curing properties (e.g., onset of cure, gel point, vitrification) can be obtained as the material progresses from a liquid to a rigid solid. *Figure 5.6* illustrates the results for a latex paint. The large change in modulus at about 12 min reflects the onset of drying and curing.

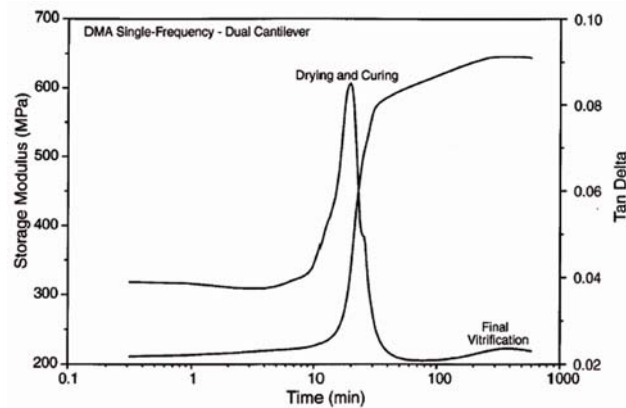


Figure 5.6 Latex curing on fiberglass braid

The use of log (time) as the x axis accentuates the weak $\tan \delta$ peak associated with final vitrification. Although not shown in this figure, a related plot of E' and E'' versus time is often used to detect gel point as the point where those curves intersect.

5.2.4 FILM AND FIBER STRESS/STRAIN MEASUREMENTS

Stress/strain measurements are widely used to characterize films and fibers over a broad range of viscoelastic behavior. Although conventional physical testing devices can accommodate thin films and singlefilament fibers, the results are difficult to obtain, and the accuracy is doubtful since the mass and inertia of the grips are much greater than the tensile strength of the material being evaluated. The clamping arrangements and force range of DMA are more suitable for examining these materials. Curves like that shown in *Figure 5.7* for a polyethylene film can be obtained by ramping the force (stress). In this case, the broad range of travel for the DMA Q800 (25 mm) allows the behavior of this 4-mm long film to be completely characterized through breaking.

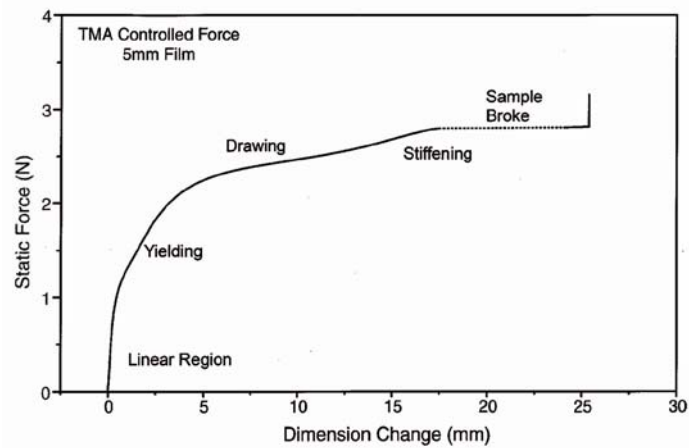


Figure 5.7 *Stress–strain evaluation of polyethylene film*

DMA is a versatile technique that complements the information provided by the more traditional thermal analysis techniques (DSC, TGA [thermogravimetric analysis], and TMA [thermomechanical analysis]). Hence, it is rapidly becoming a necessary component of a laboratory interested in characterizing the properties of polymers.

6. OPTICAL AND DYNAMIC MECHANICAL PROPERTIES OF PLASTIC OPTICAL FIBERS

6.1 INTRODUCTION

Plastic optical fibers (POF) have various applications: in home and local area networks (LAN), lighting technology, for fiberoptic sensors and sensors networks, for fiber light amplifiers and as scintillating fibers⁷⁴. They have some great advantages over glass multimode optical fibers such as: easy installation owing to large diameter, efficient light coupling owing to large numerical aperture (NA) (typically 0.5), high ductility or low modulus, resistance to impact and vibrations and low cost. The main disadvantage is higher optical loss⁷⁵. During their applications POF are exposed to different kinds of static and dynamic stresses and environmental conditions. It is of great importance that they keep their optical properties unchanged when they are exposed to different influences in LAN and lighting applications, but on other hand in sensors applications they should have significant, regular and repetitive change of some optical property.

The most important property of POF is the optical transmission which mainly depends on core materials, drawing process and the conditions employed in the manufacturing process. The poly(methyl methacrylate) (PMMA), polystyrene (PS) and polycarbonate (PC) are the most used polymers as core materials in commercially available multimode step and graded index POF. PMMA has the highest transparency among them⁷⁶. The major source of optical loss in POF are intrinsic factors such as absorption (higher harmonics of C-H absorption and electronic transitions absorption) and Rayleigh scattering. During their practical operations environmental factors and mechanical stresses bring both physical and chemical changes of core material and cause change in optical transmission^{77,78,79}.

Dynamic Mechanical Analysis (DMA) is one of the most powerful tools to study the behavior of plastic and polymer composite materials by applying an oscillating force to a sample and analyzing the material deformation response as a function of frequency,

time or temperature^{80,81}. It is potentially very useful tool to simulate behavior of POF in case of versatility of mechanical and environmental conditions, although DMA of cylindrical rods and fibers is up today not very common compared to other geometries⁸². Possibility of simultaneous measurements of some optical properties during DMA would significantly upgrade investigations of POF alone or embedded in some materials.

In this work, DMA of the POF that was done simultaneously with measuring the transmitted optical signal intensity is described. In order to compare mechanical results of the same material for cylindrical and rectangular specimens, rectangular specimens, with optimal dimensions for single cantilever DMA, were prepared by melting POFs and the same kind of tests were repeated with them.

6.2 EXPERIMENTAL

Two kinds of DMA were performed on POF: single cantilever tests with constant amplitude and frequency and on constant temperature and the dynamic temperature scan tests. During both tests the storage modulus (E') was determined. At the same time light was launched into the POF under test and the output light intensity (I) was measured in real time.

The experimental set up consisted of two parts, mechanical and optical. The DMA instrument (TA Instruments Q800) and its personal computer (PC) were used for mechanical measurements and data acquisition. The investigated POF (ESKATM GK-40) with output diameter 1mm (core diameter 0.98 mm) was clamped inside the DMA instrument between the movable and stationary fixtures and enclosed in the thermal chamber. The length of a fiber between clamps was 18.14 mm, but the whole length of a fiber was about 2.5 meters. The clamped parts of the optical fiber were protected with Teflon sleeves in order to prevent its damage during testing. The ends of the POF were carefully brought out from the temperature chamber of the DMA instrument through a hole on its top. Those two outlet ends were connected to light source and the photodetector (PD), the optical parts of the experimental set up. Light source was light emitting diode (LED), with peak wavelengths 840 nm or 650 nm. The PD was

phototransistor based circuit. The light from the LED was launched to the POF and the intensity of the propagated light was measured by PD. The output signal from the PD was connected to acquisition system (USB type A/D converter (A/D) and personal computer (PC)). The schematic view of the experimental set-up is presented in [Figure 6.1](#).

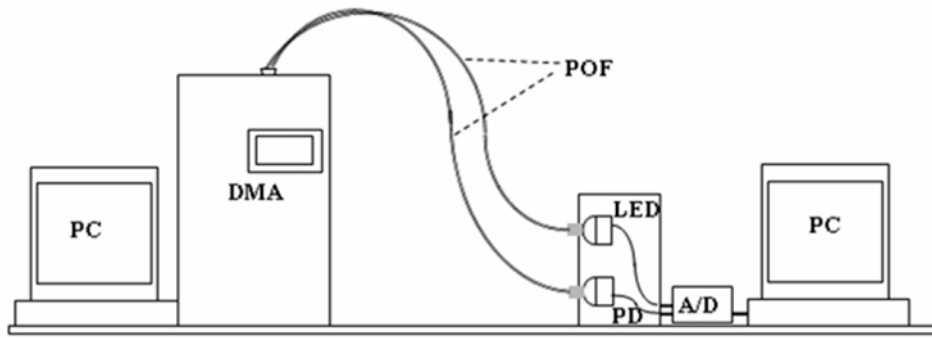


Figure 6.1. *The experimental set up*

Single cantilever test was performed at constant frequency of 3Hz, constant amplitude of 30 μm and at constant temperature. The number of the oscillation at one temperature was about 6400. Each test lasted from 35-40 min because the time for temperature stabilization was not the same at each temperature and that is why the net number of oscillation for the same biased parameters except temperature varied a little from one to another temperature. This kind of DMA was performed successively on 50, 60, 70, 80 and 90 $^{\circ}\text{C}$ on the same POF without opening the temperature chamber. So, set of five successive single cantilever tests on five temperatures could be considered as an accelerated fatigue test, and the POF is considered as fatigued after those tests.

The dynamic temperature scan test was performed approximately from 40-120 $^{\circ}\text{C}$ at one fixed POF. The experiment was done in standard single cantilever mode using a ramping rate of 3 $^{\circ}\text{C}/\text{min}$, with an oscillation frequency of 1 Hz and amplitude of 20 μm

A set of tests was performed with the launched light at one wavelength. First of them was dynamic temperature test at one POF considered as not fatigued. Than that POF was removed from the instrument and new POF of the same type was fixed. The five successive single cantilevered tests were performed at five constant temperatures, and

then the dynamic temperature test on the same POF, considered as fatigued, without opening the temperature chamber.

The performed single cantilever tests are originally provided for the rectangular specimens. In order to investigate their applicability to fibers the comparison of mechanical results on the same material for cylindrical and rectangular specimens was done. The rectangular plates dimensions 3x12x30mm were prepared by melting the POFs and the same set of mechanical measurements as for the POFs was performed on them with the DMA instrument.

6.3 RESULTS AND DISCUSSION

6.3.1 MEASUREMENTS WITH POF-SINGLE CANTILEVER TESTS

Before all mechanical tests, the transmission spectral characteristic of the investigated POF was measured with spectrometer (Carl Zeiss Jena 384824), and it is presented in [Figure 6.2](#). Two wavelengths 650 nm and 840 nm are chosen for further measurements. From the spectral characteristics, it is obvious that 650 nm is in the middle of the near constant part of spectral characteristics with maximum transmission and other chosen wavelength, 840 nm, is at the near infrared descending slope and transmission is about half compared to the maximum. Those both wavelengths are frequently used in fiber optic applications.

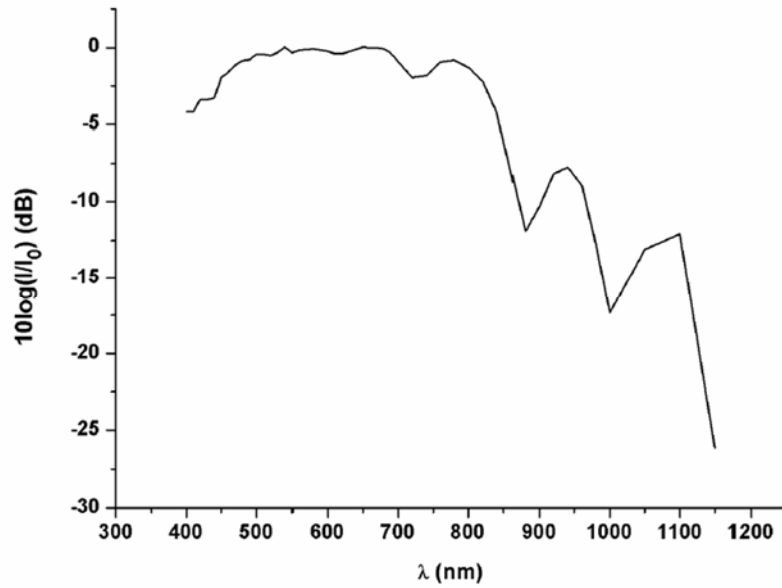


Figure 6.2. The transmission spectra of POF

The first set of measurements was at wavelength 840 nm, and the second at 650 nm. The number of performed oscillations on each temperature and at each wavelength is presented in Table 6.1.

Table 6.1. Number of performed oscillations, N , during single cantilever test on 5 different temperatures, and at two different wavelengths of launched light

t (°C)	N ($\lambda=840$ nm)	N ($\lambda=650$ nm)
50	6405	6409
60	6393	6583
70	6680	6391
80	6440	6409
90	6393	6294

The measured results for single cantilever tests with optical signal wavelength 840 nm are presented in Figure 6.3. and Figure 6.4.

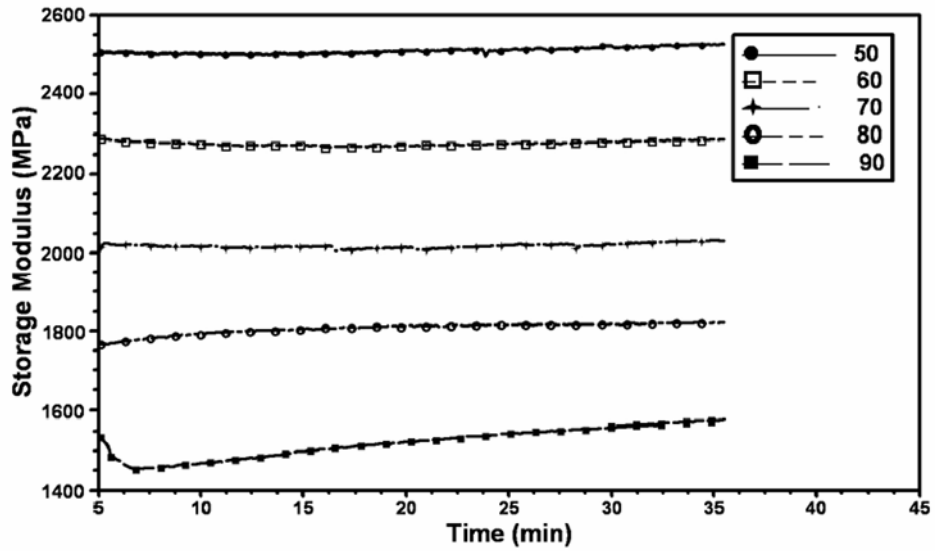


Figure 6. 3. The changes of E' versus time of POF during single cantilever tests (wavelength 840 nm)

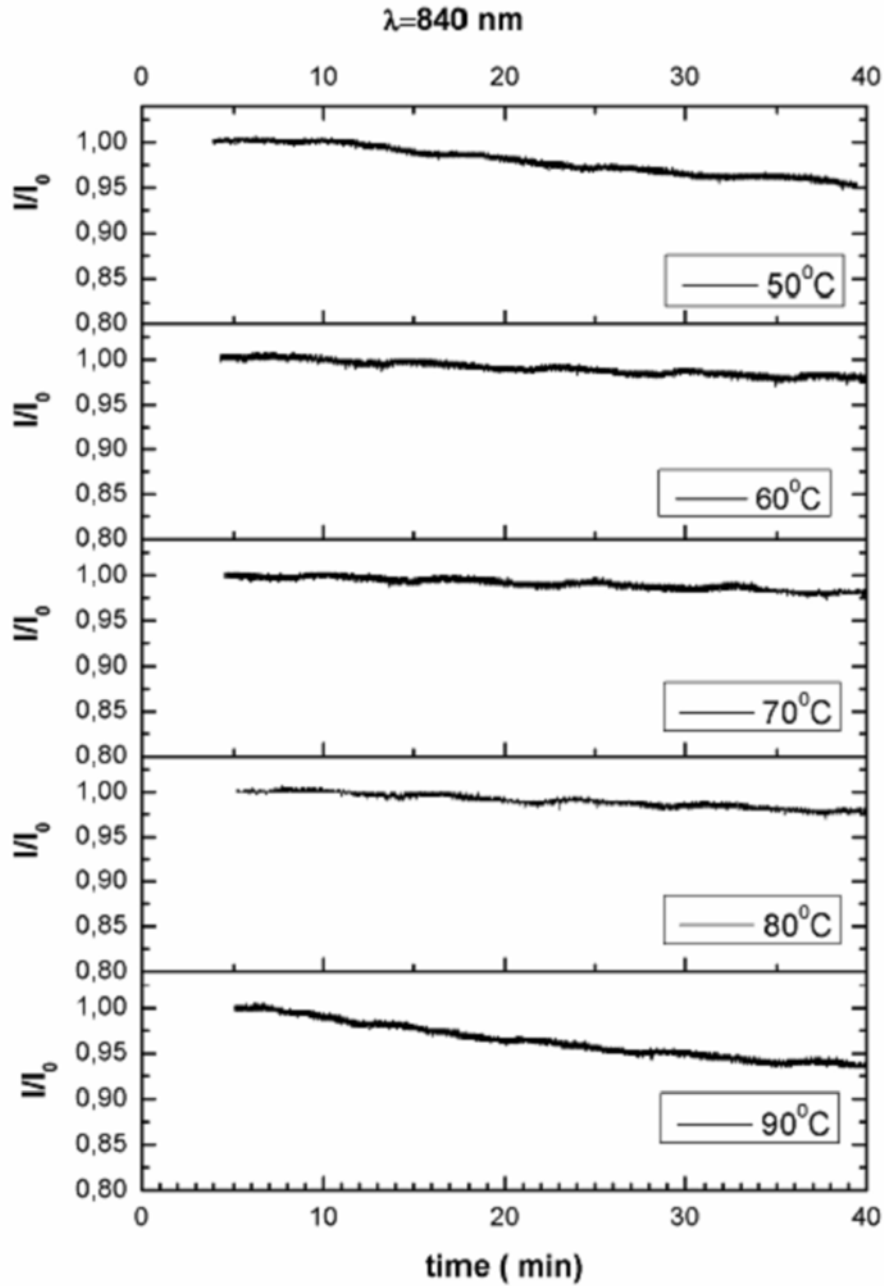


Figure 6.4. The change of I/I_0 of POE versus time during single cantilever tests (wavelength 840 nm)

The changes of E' of POE versus time are presented in Figure 6.3. for five constant temperatures. The measured changes in optical signal intensity during the same tests are presented by normalized signal intensities (I/I_0) versus time in Figure 6.4. Parameter I is the measured signal on the PD, and I_0 is the measured signal on the PD at the beginning of the single cantilever test at that measuring temperature. Comparing graphs in Figure

6. 3. and Figure 6.4. it is obvious that after some period of temperature stabilization the E' is slightly rising, while I/I_0 is descending during single cantilever tests. The most significant changes of E' and I/I_0 has occurred at 90 °C

In order to quantify and compare changes in E' , and I , their relative changes are calculated and presented in Table 6.2. The relative changes of E' denoted as $\Delta E'/E'$, and of optical normalized signal intensity denoted as $\Delta I/I_0$ are obtained from the values of E' and I/I_0 at $t_1=15$ min and $t_2=35$ min after temperature stabilization.

The similar graphs of E' and I/I_0 versus time, but for wavelength 650 nm are presented in Figure 6.5. and Figure 6.6. The calculated values of $\Delta E'/E'$ and $\Delta I/I_0$ for measurements on 650 nm are also presented in Table 6.2. During the tests at 80 °C and 90 °C the measurements were disturbed before $t=35$ min which could be seen from irregular changes of E' in Figure 6.5, as well as, from the change of slope of optical signals in Figure 6.6. So, the relative changes $\Delta E'/E'$, and $\Delta I/I_0$, for 80 °C were calculated from the values at $t_1^*=15$ min, and $t_2^*=32$ min, and for 90 °C at $t_1^{**}=5.65$ min, and $t_2^{**}=13.25$ min. That irregular behavior was emphasized in the Table 6.2. with values that have superscripts * and **.

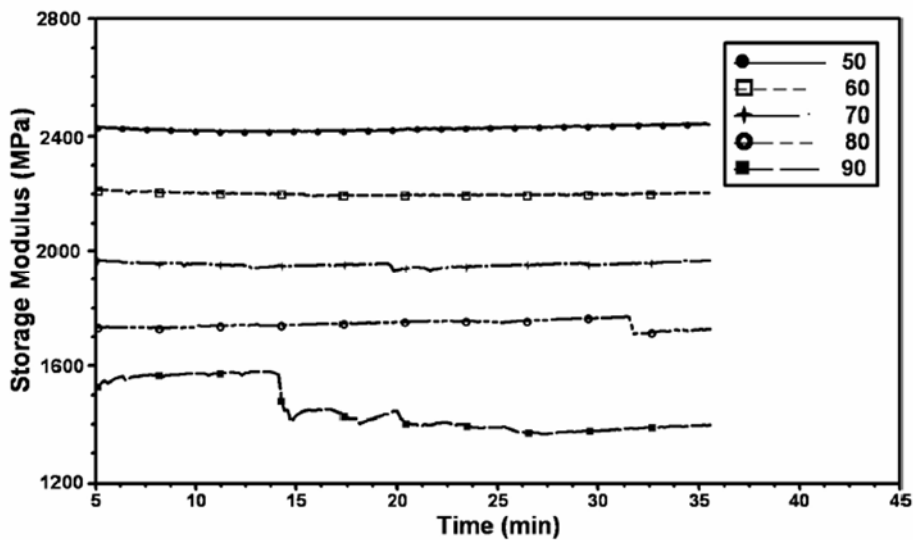


Figure 6.5. The changes of E' of POF versus time during single cantilever tests (wavelength 650 nm)

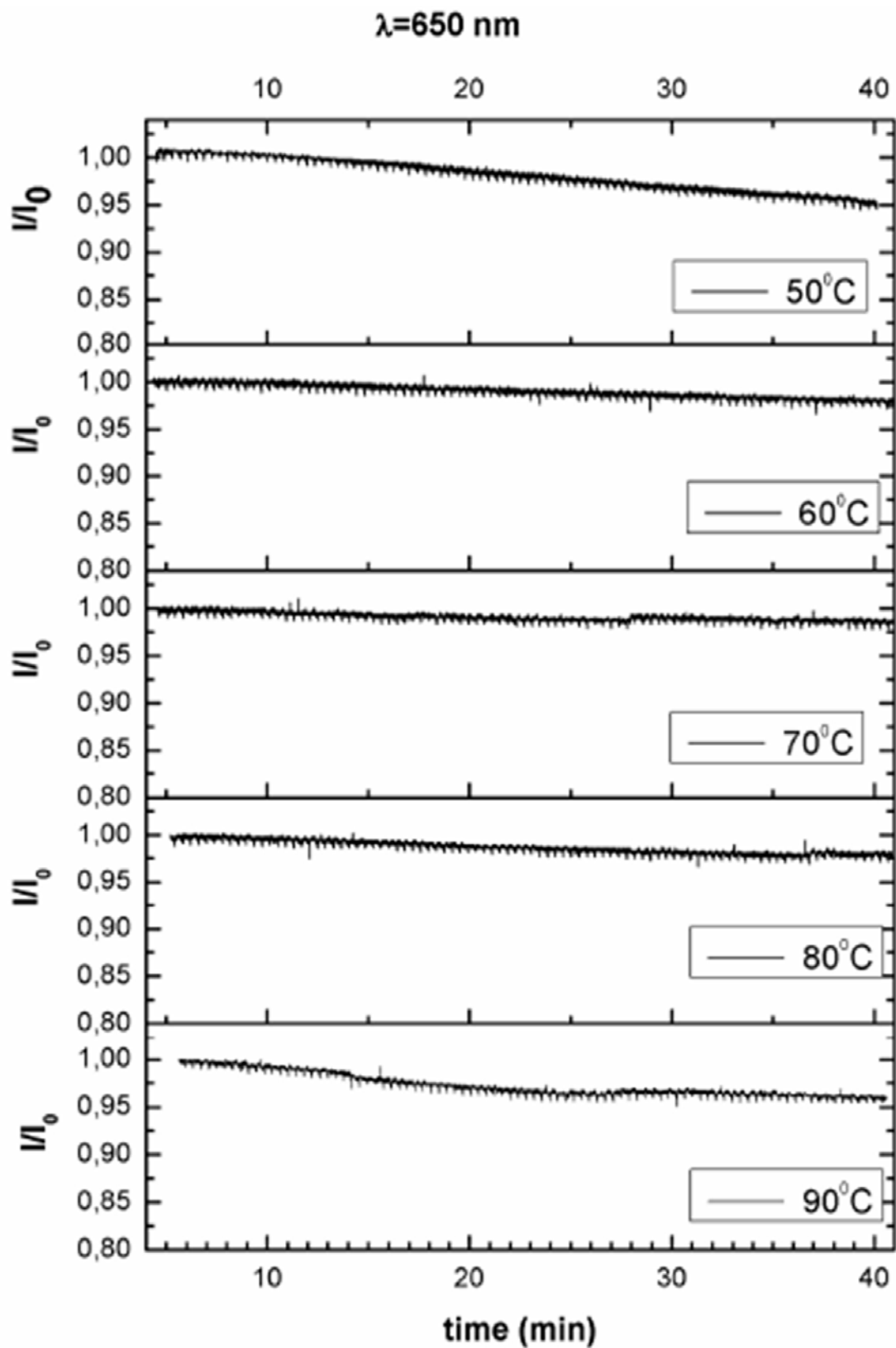


Figure 6.6. The change of I/I_0 of POF versus time during single cantilever tests (wavelength 650 nm)

Table 6.2. Relative changes $\Delta E'/E'$ and $\Delta I/I_0$ for POFs and $\Delta E'/E'$ for rectangular specimen after single cantilever tests at various temperatures

t(°C)	POF ($\lambda=840$ nm)		POF ($\lambda=650$ nm)		Rectangular specimen
	$\Delta I/I_0$ (%)	$\Delta E'/E'$ (%)	$\Delta I/I_0$ (%)	$\Delta E'/E'$ (%)	$\Delta E'/E'$ (%)
50	-2,39	0,94	-3,81	0,99	0,56
60	-1,74	0,88	-1,02	1,56	0,46
70	-1,01	0,81	-0,65	0,80	0,60
80	-1,53	0,82	-1,47*	1,51*	0,77
90	4,76	4,81	-1,35**	1,96**	1,00

The measurements at both wavelengths show similar relative changes of E' and I/I_0 and the most significant changes were at 90 °C.

6.3.2 DYNAMIC TEMPERATURE SCAN TEST

Two POFs were examined at each wavelength, one not fatigued and the other was fatigued. The changes of E' versus temperature of the both POFs with launched light wavelength 840 nm are presented in Figure 6. 7. The E' descended linearly from 40 °C to 80 °C for both fatigued and not fatigued POF. Nonlinear behavior started at temperatures higher than 80 °C. The values of I/I_0 for the not fatigued and fatigued POF at 840 nm are presented in Figure 6.8. The intensity of optical signal was almost constant from 40 °C to 50 °C, and ascended almost linearly from 50 to 80 °C. At temperatures higher than 80 °C the dependence of I/I_0 versus temperature had non linear behavior, reached their maximums and then constantly descended. The maximum I/I_0 for not fatigued POF was at 89 °C and for fatigued was at 104 °C

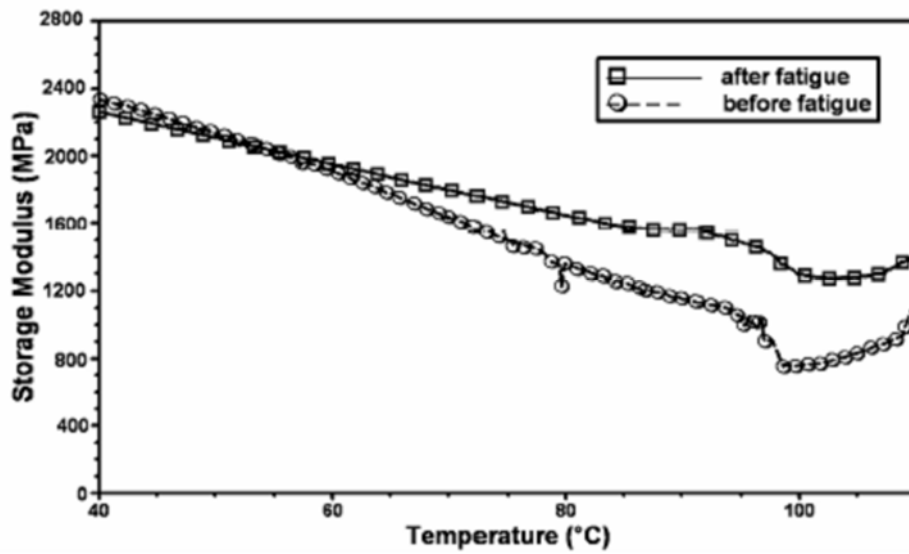


Figure 6.7. The changes of E' versus temperature for fatigued and not fatigued POF (wavelength 840 nm)

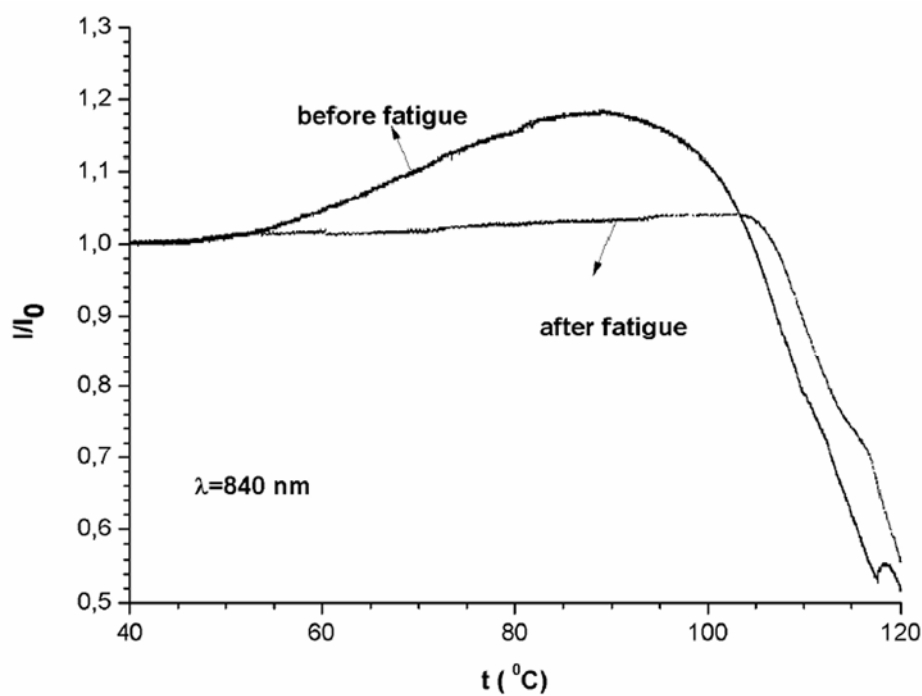


Figure 6.8. The changes of I/I_0 versus temperature for fatigued and not fatigued POF (wavelength 840 nm)

Similar changes in E' and I/I_0 had occurred during the measurements at wavelength 650 nm. The changes of E' versus temperature are presented at [Figure 6.9](#), and the changes of I/I_0 are presented at [Figure 6.10](#) both for fatigued and not fatigued POFs. The

maximum I/I_0 of not fatigued POF was at 88 °C. For fatigued POF the maximum I/I_0 was between 95 °C and 105 °C, The relative changes $\Delta E'/E'$ and $\Delta I/I_0$ at 650 nm are presented in Table 6.3.

The relative changes $\Delta E'/E'$ and $\Delta I/I_0$ for fatigued and not fatigued POFs at both wavelengths are presented in Table 6.3. Two kinds of relative changes were calculated: one for the temperature range from 40-80 °C, and the other from 40 °C to the temperatures at which I/I_0 was maximum.

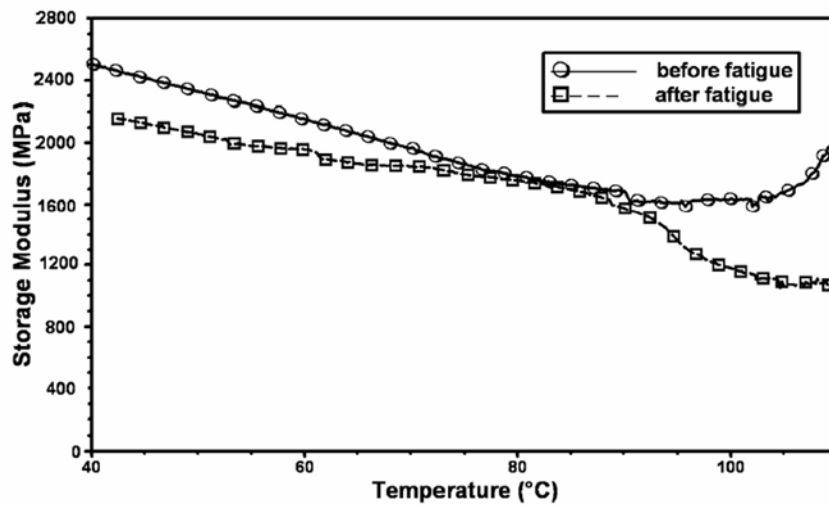


Figure 6.9. The changes of E' versus temperature for fatigued and not fatigued POE (wavelength 650 nm)

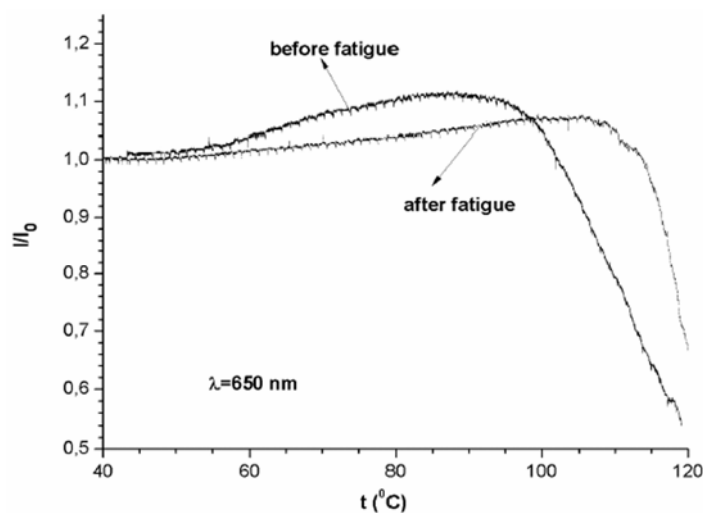


Figure 6.10. The changes of I/I_0 versus temperature for fatigued and not fatigued POE (wavelength 650 nm)

Table 6. 3. Relative change of I/I_0 and E' of POFs and $\Delta E'/E'$ of rectangular specimens in dynamic temperature scan tests

	POF ($\lambda=840$ nm)				POF ($\lambda=650$ nm)				Rectangular specimen	
	Not fatigued POF		Fatigued POF		Not fatigued POF		Fatigued POF		before fatigue	after fatigue
	$\Delta E'/E'$ (%)	$\Delta I/I_0$ (%)	$\Delta E'/E'$ (%)	$\Delta I/I_0$ (%)	$\Delta E'/E'$ (%)	$\Delta I/I_0$ (%)	$\Delta E'/E'$ (%)	$\Delta I/I_0$ (%)	$\Delta E'/E'$ (%)	$\Delta E'/E'$ (%)
40-80	-41,9	15,4	-27,4	2,4	-28,7	9,9	-18,7	3,5	-28,9	-26,9
40-89	-50,4	18,3	-31,2	3,0	-34,1	10,6	-25,8	5,4	-36,3	-34,1
40-104	/	/	-43,7	3,6	/	/	-50,8	7,9	-49,7	-47,8

The changes of I/I_0 versus temperature for not fatigued POFs are bigger than for not fatigued. This is more significant for signals at 840 nm. Maximums of I/I_0 for not fatigued POF are almost at the same temperature (88-89 °C) for both wavelengths as well as for the fatigued pof (104 °C).

6.3.3 MEASUREMENTS ON RECTANGULAR SPECIMENS

Single cantilever test mode used for described measurements is originally provided for rectangular specimens. The calculated values of E' obtained by DMA are based on expressions for rectangular specimens divided by π . In order to compare results of mechanical characteristics on the same material for cylindrical and rectangular specimens, two rectangular specimens, are prepared by melting POFs. The dynamic temperature scan test was performed on the first one in order to compare E' of not fatigued POF with it. Then, the single cantilever tests on five temperatures and the dynamic temperature test were performed on the second rectangular one.

The single cantilever test . The curves representing storage modulus versus time at five constant temperatures are presented in Figure 6.11. The $\Delta E'/E'$ for single cantilever tests are presented in Table 6.2 From those results it is obvious that they are of the same order for temperatures from 50-80 °C and for 90 °C the value is higher than for the other temperatures.

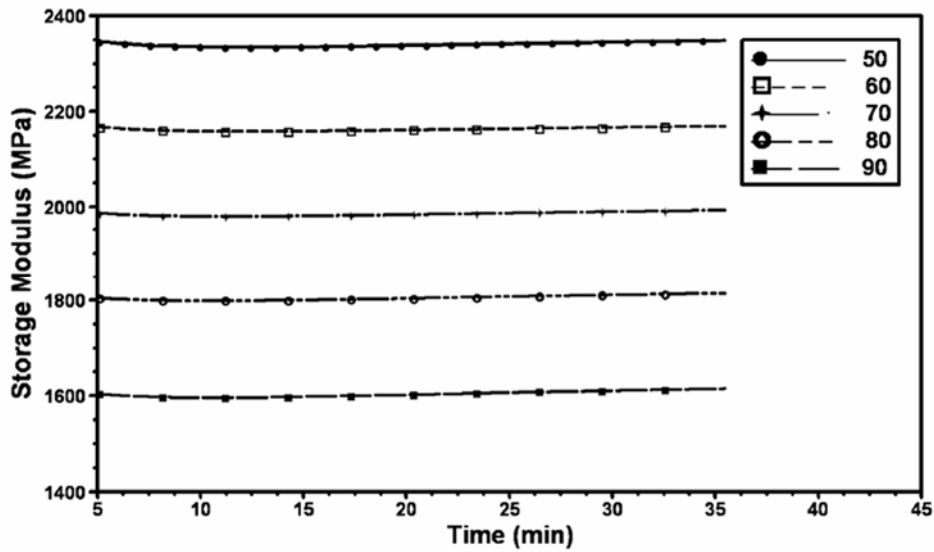


Figure 6.11. The changes E' of the rectangular specimen versus time for single cantilever tests on five constant temperatures

The dynamic temperature scan test The results of dynamic temperature scan tests for the not fatigued, and the fatigued rectangular specimen are presented in [Figure 6.12](#). The curves represent the change of E' , the loss modulus (E'') and the loss factor ($\tan\theta$) versus temperature. From these curves glass transition temperature (T_g) was derived and it is 118.7°C for fatigued and 121.6°C for not fatigued plate.

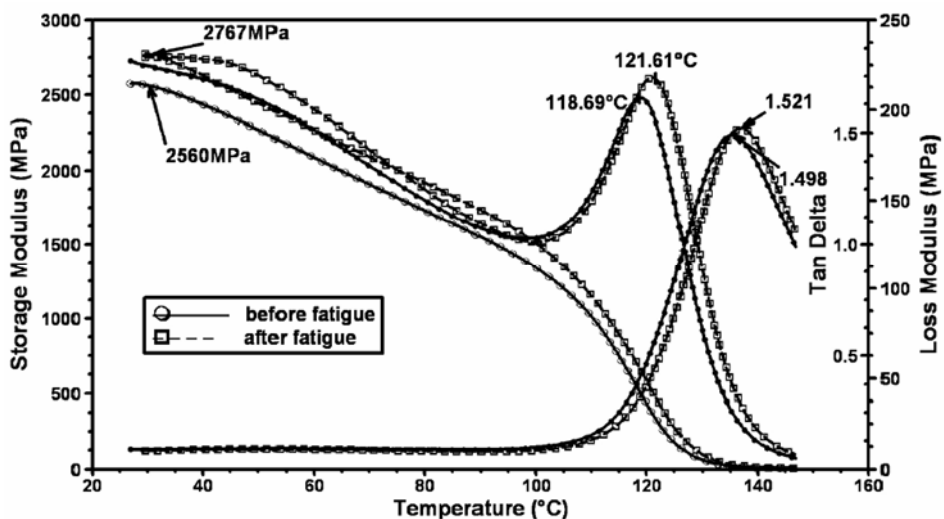


Figure 6.12. Changes of E' , E'' and $\tan\theta$ versus temperature for the rectangular specimens during single cantilever temperature scan test

The values of E' at 40, 80, 90 and 104 °C were obtained from the curves in [Figure 6. 11](#). and $\Delta E'/ E$ for fatigued and not fatigued specimen from 40-80 °C, from 40-90 °C and from 40-104 °C were calculated and presented in [Table 6.3](#).

7. OPTICAL AND MECHANICAL PROPERTIES PMMA-Y₂O₃ (Eu³⁺) NANOCOMPOSITES

7.1 INTRODUCTION

Nanocomposites are a distinct form of composite materials, which involve embedding nano- or molecular domain-sized particles into organic polymer, metal or ceramic matrix materials^{83,84}. The intimate inclusion of nanoparticles in these matrices can greatly change the mechanical, electrical, optical or magnetic properties of these materials. The reason for this is that with such small inclusions, a large amount of interfacial phase material exists in the bulk of these nanocomposites.

This paper is related to the processing and characterization of polymer–nanophosphor composites, as promising materials for the production of nanocomposite fibers. Plastic optical fibers (POF) can be used for a number of applications, such as light transmission for signs and illumination, sensors and data communication^{85,86,87}. Signal attenuation of commercial polymer fibers is much higher than that of glass fibers. In order to improve POF optical efficiency, research and processing are being developed in the direction of nanocomposite POF doped with dyes, and fluorescent or phosphorescent nanopowder⁸⁸.

The optical properties of nano-sized phosphors are significantly improved in comparison to bulk materials (stronger luminescence emission and modified radiative lifetime)^{89, 90, 91}. Poly(methyl methacrylate), PMMA, nanocomposites containing Y₂O₃ doped with rare earths (RE) ions have been investigated and it was suggested that doped Y₂O₃ nanocrystals embedded in PMMA would have potential for various photonic applications, including laser systems and optical communication devices^{92,93}. Nanocomposites PMMA-Y₂O₃:RE were successfully prepared by mixing Y₂O₃:Er³⁺, Yb³⁺ or Y₂O₃:Er³⁺ with PMMA for infrared cards. The Eu-ion doped Y₂O₃ nanophosphor is useful for nanocomposite POF light guides because the luminescence wavelength of the Eu-ion (611 nm) is in the visible range of spectrum. It is very important to preserve their optical properties for a synergetic effect in functional nanocomposites.

In this work, Eu-ion doped Y₂O₃ nanophosphor powder was dispersed in PMMA as the host. The influence of the content of nanopowder on the optical properties, dynamic mechanical properties, transition temperature, T_g, and microhardness of the nanocomposites was investigated.

When an amorphous polymer is heated, it undergoes a phase transition from the glassy state to the rubbery state at the T_g, when abrupt jumps in the thermal expansion and heat capacity occur. The temperature coefficients of the molar volume, free volume and enthalpy change of the glass–rubber transition are closely related to the cohesive energy density of the polymer. The glass transition temperature, T_g is linearly related to the cohesive energy density (CED) by the following equation⁹⁴:

$$T_g = (2E_C / mR) + C_1 \quad (7.1)$$

where EC is the CED, T_g is the glass transition temperature (in K), m a parameter that describes the internal mobility of the groups in a single chain, R is the gas constant and C₁ is a constant. The CED is also the main factor determining hardness, H, which results in an almost linear relationship between T_g and H for a number of amorphous glassy polymers^{95,96,97}

$$H = kT_g + C \quad (7.2)$$

where C and k are experimental fitting parameters.

The nanoparticles penetrate into the polymer matrix and establish cohesive forces between the polymer chains and decrease the segmental mobility thereby increasing the T_g value⁹⁸. Therefore, it is to be expected that the microhardness will also be increased. The expression for the Vickers hardness (HV) is:

$$HV = 1.854 \cdot P \cdot d^{-2} \quad (7.3)$$

where P is the applied load and d is the mean diagonal length of the diamond-shaped indent.

Dynamic mechanical analysis (DMA) is a sensitive technique that characterizes the mechanical response of materials by monitoring property change with respect to the

temperature and frequency of an applied sinusoidal stress. This technique separates the dynamic response of materials into two distinct parts: an elastic part (E') - storage modulus and a viscous component (E'') - loss modulus. The loss factor, Tan Delta ($\tan \delta$) is the ratio of the energy dissipated to the energy stored. The transition temperature (T_g) of a polymer is associated with the onset of the storage modulus - $T_g(E')$; the loss modulus peak - $T_g(E'')$ and the $\tan \delta$ peak- $T_g(\tan \delta)$. The onset of E' occurs first at the lowest temperature and relates to mechanical failure. The E'' peak occurs next and is associated with the T_g as the temperature of the onset of segmental motion. The $\tan \delta$ peak occurs at the highest temperature and represents a good measure of the “leather like” midpoint between the glassy and rubbery state^{99,100}.

7.2 EXPERIMENTAL

The nanopowder was synthesized by a complex polymer solution method (PCS), employing poly(ethylene glycol) (PEG) fuel. The particle size was about 30–40 nm¹⁰¹30

The nanocomposites were prepared by melt compounding in a Laboratory Mixing Molder (Atlas, USA), at a working temperature of 250 °C and a rotor speed of 180 rpm for 20 minutes. The polymer component of the composite was extrusion grade PMMA pellets, Acryrex® CM-205, Chi Mei Corporation, Taiwan. Samples with different contents of Y_2O_3 (Eu^{3+}) powder: 0.1 %; 0.5 %; 1.0 % and 1.5 % by weight were processed.

The infrared (IR) spectra of the powder, pure PMMA and the composites were obtained by Fourier transform infrared (FTIR) spectroscopy (Hartmann & Braun, MB-series) in KBr discs. The scanning range was between 4000 and 400 cm^{-1} with a resolution of 4 cm^{-1} .

The emission spectra of the PMMA- Y_2O_3 (Eu^{3+}) nanocomposites were collected at room temperature after excitation into the ${}^7F_0 \rightarrow {}^5D_2$ absorption band. The excitation source was an Optical Parametric Oscillator (O.P.O.) pumped by the third harmonic of an Nd:YAG laser. The emission was analyzed using an HR250 monochromator (Jobin-Yvon) and then detected by an ICCD camera (Princeton Instrument).

The microhardness measurements were performed at the room temperature using a Vickers microhardness tester Leitz, Kleinhartepuffer Durimet I. The Vickers microhardness test uses a square based pyramidal indenter with an apex of $\alpha = 136^\circ$, producing a diamond-shaped indent on the surface. A press load of 490 mN, a press time of 15 s, and a holding time of 5 s after completing the indentation were used. Individual Vickers microhardness values (HV) were calculated as the mean value of at least five indentations.

A dynamic mechanical analysis (DMA) instrument (TA Instruments Q800) was used to determine the dynamic mechanical properties of the samples. The experiments were realized in the single-cantilever mode over a temperature range from 25 °C to 160 °C at a fixed frequency of 1 Hz. The heating ramp rate was 3 °C min⁻¹. The temperature dependence of the storage modulus, loss modulus and tan δ were obtained.

7.3 RESULTS AND DISCUSSION

The FTIR transmission spectra of the powder, PMMA and composites are illustrated in [Figure 7.1](#). The peaks at 2946 cm⁻¹ and 1735 cm⁻¹ are assigned to C–H and C=O stretching vibrations in PMMA, respectively. The absorption bands of PMMA (1439, 840, 750 and 440 cm⁻¹), and the vibration bands of PMMA (3458, 1385, 1133 and 974 cm⁻¹), were observed in the spectra. In the spectrum of Y₂O₃ (Eu³⁺), the transmission band centered at 560 cm⁻¹ is attributed to Y–O lattice vibrations. This peak also appeared in all the spectra of all the composites.

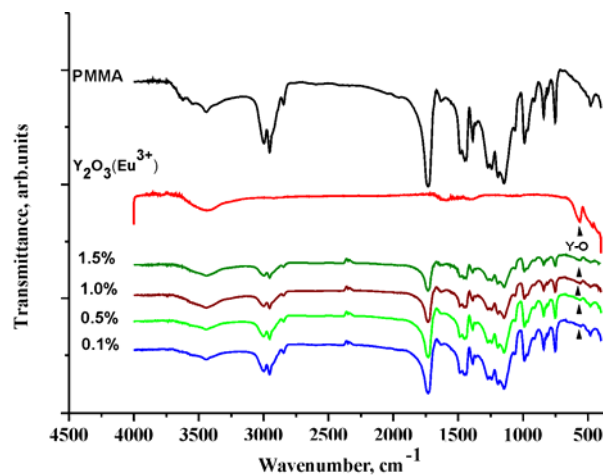


Figure 7. 1. FTIR spectra of Y_2O_3 (Eu^{3+}), PMMA and the composites with different contents of Y_2O_3 (Eu^{3+}).

The emission luminescence spectra of nanocomposite are presented in [Figure 7.2](#). The spectra exhibit groups of distinctive emission peaks in the 580–711 nm range. These emission peaks can be related to each of the $^5D_0 \rightarrow ^7F_J$ ($J = 0,1,2,3$ and 4) transitions of Eu^{3+} , which are characteristic for Eu^{3+} ions within a crystallized cubic phase. The strongest emission peak at 611 nm is caused by the electron dipole transition of Eu^{3+} ($^5D_0 \rightarrow ^7F_2$), corresponding to the red luminescence. The intensity of the emission peak increased with increasing powder content in composite. It is very important that the nano-phosphors maintain their optical properties in the composites. The strongest emission peak at 611 nm was obtained in the range of wavelengths where the maximum signal attenuation of PMMA optical fiber is expected to be found. This feature will improve the transmission properties of POF and will prolong the length of a light guide.

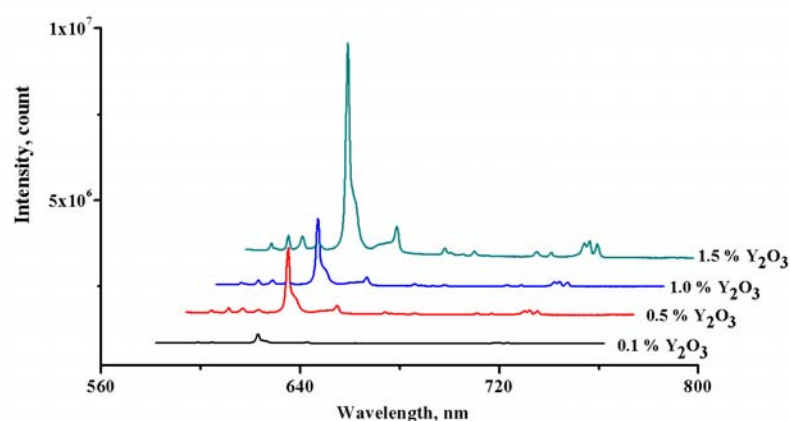
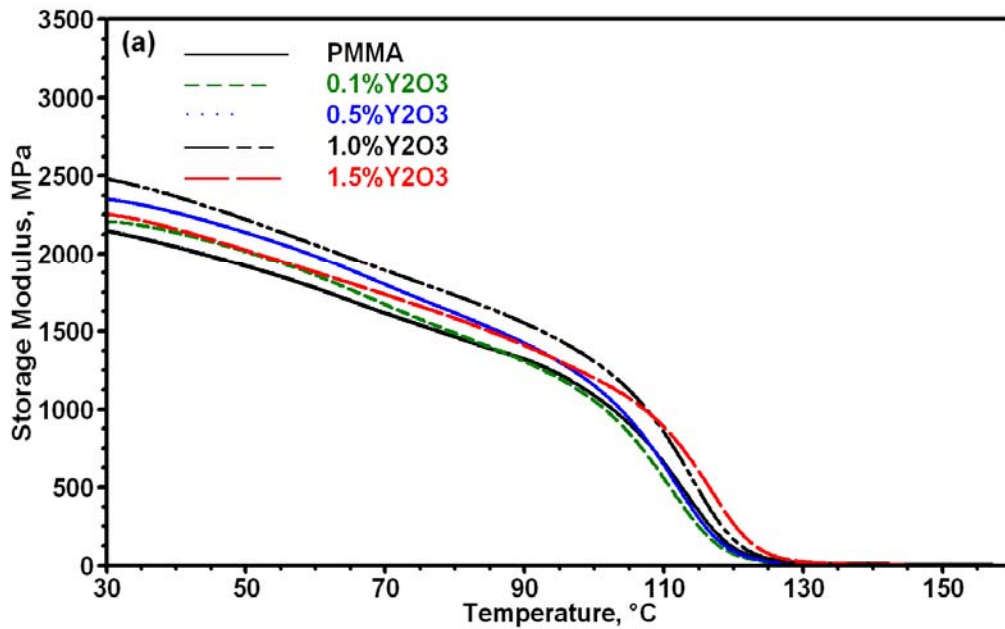


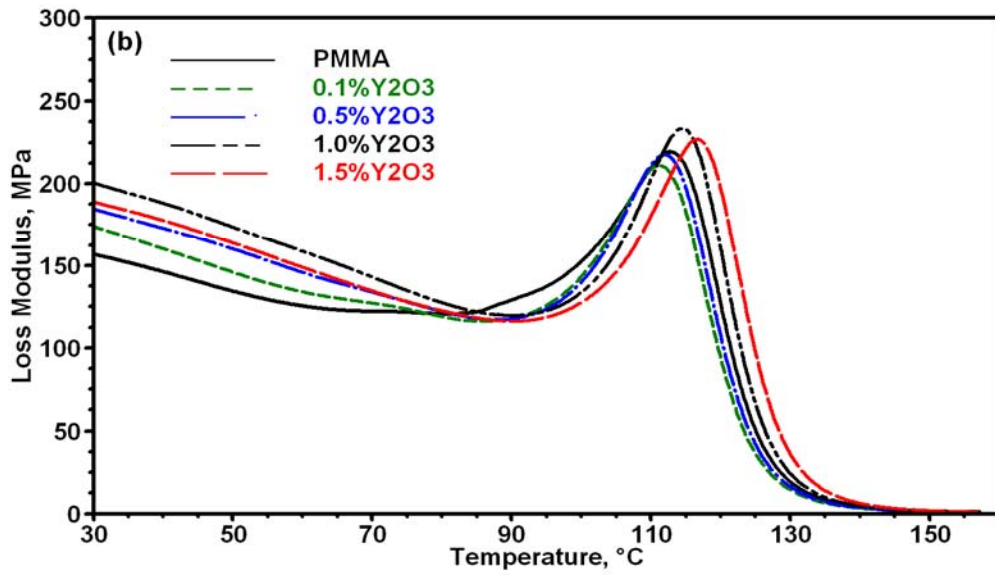
Figure 7.2. Emission spectra of the PMMA – Y_2O_3 (Eu^{3+}) nanocomposites at room temperature.

Investigations of the dynamic mechanical properties of the samples provided information on the transitions occurring in the materials ([Figure 7.3](#)). The DMA results revealed that the storage modulus of the all the composite samples were higher than that of a pure PMMA at 30 °C ([Table 7.1](#)). The increase of nanopowder content up to 1 %

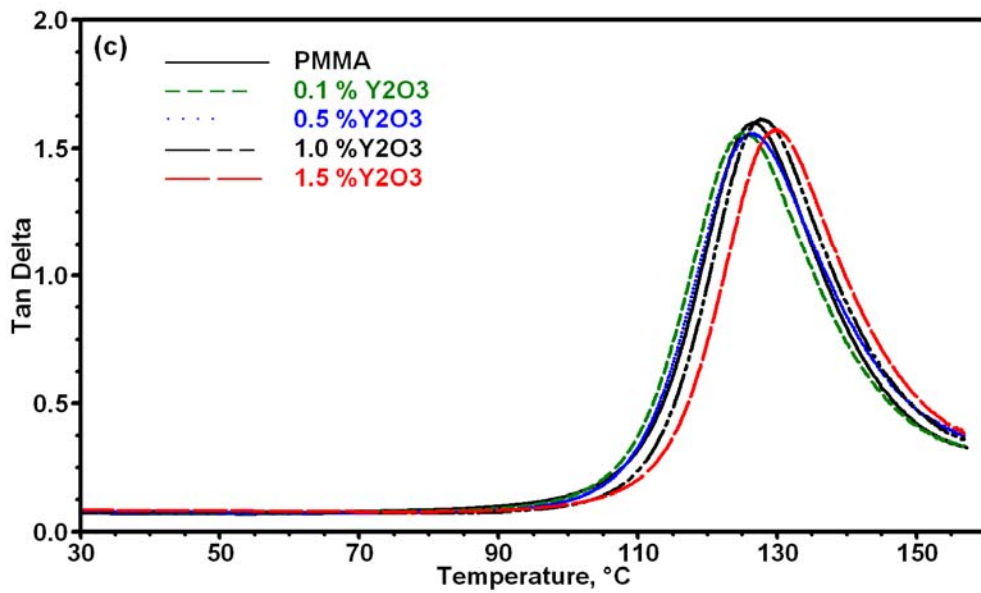
increased the storage modulus of composite by 15.5 % compared to that of pure PMMA. With 1.5 % of the nanophosphor, the storage modulus of the composite was only 5.1 % higher than that of PMMA, because of agglomeration of the nanoparticles. The corresponding loss moduli were between 175 and 200 MPa and obviously increased with increasing content of nanopowder in the same manner as the storage modulus. The T_g values of the PMMA– Y_2O_3 (Eu^{3+}) composites were also higher than that of PMMA and increased with increasing content of the nanoparticles. The results suggested that the nanoparticles did not disperse individually but as aggregates; however, notable increases in the glass transition temperature in the order of 2 to 8 °C were evidenced.



a)



b)



c)

Figure 7.3 Temperature dependence of a) the storage modulus, b) the loss modulus and c) $\tan \delta$ for composites with different contents of Y_2O_3 (Eu^{3+}).

Table 7.1 Results of DMA: E' and E'' at 30 °C, values of T_g obtained by E' onset, E'' maximum, $\tan \delta$ maximum and microhardness (HV)

$c_{Y_2O_3}/$ %	$E'/$ MPa	$\Delta E'/$ %	$E''/$ MPa	$T_{g(E')}/$ °C,	$T_{g(E'')}/$ °C,	$T_{g(\tan \delta)}/$ °C	HV/ MPa
0	2147		156.9	100.68	112.70	126.40	254.87
0.1	2199	2.4	175.0	102.05	111.33	125.48	259.256
0.5	2352	9.5	184.6	103.29	111.84	126.20	269.812
1.0	2481	15.5	200.6	105.71	114.44	127.60	276.631
1.5	2256	5.1	189.0	108.47	116.73	129.70	280.139

The hardness (H) of a material is a measure of its resistance to shear stresses under local volume compression. The hardness number increased with Y_2O_3 (Eu^{3+}) concentration in the PMMA nanocomposites. The increased resistance to surface deformation of the PMMA nanocomposites may be due to a decrease in the free volume of the matrix associated with the formation of apparent physical cross linking and entanglements. The T_g is linearly related to the microhardness according to Eq. (2). The correlations between HV and the T_g derived from the DMA curves by the E' onset, by the E'' peak and by the $\tan \delta$ peak are presented in Figure 7.4. The fitting coefficients of these correlations, C, k and R^2 are presented in Table 7.1 for all three lines. The value of R^2 of the linear correlation between HV and $T_g(E')$ is the highest. This means that the E' onset is the most sensitive to local shear stresses and it exhibits the best linearity with microhardness.

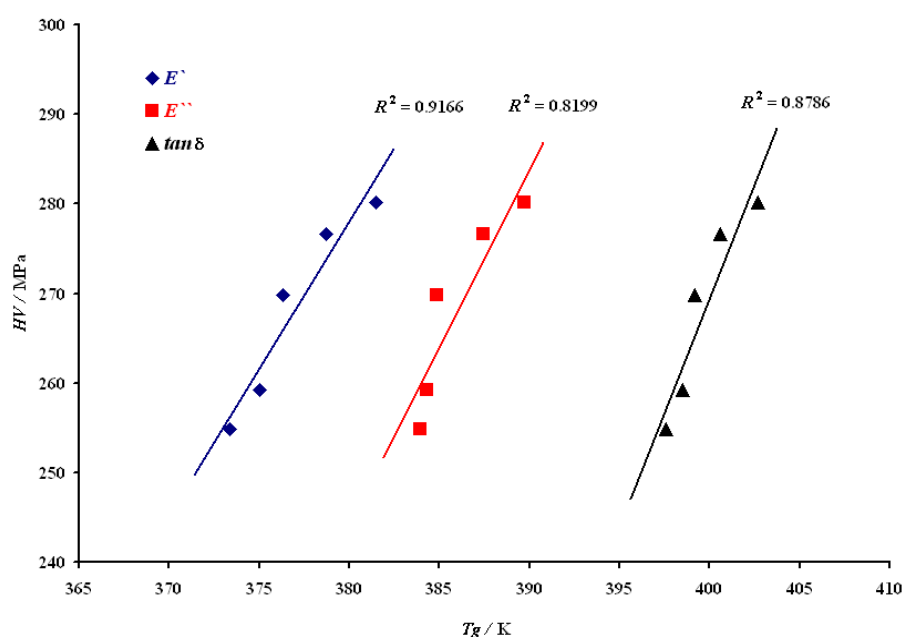


Figure 7. 4. Linear correlations of HV and T_g obtained from the DMA results - $T_g(E')$, $T_g(E'')$ and $T_g(\tan \delta)$.

Table 7.2. Fitting parameters of the T_g –HV correlations

Fitting parameters	HV – $T_{g(E')}$	HV – $T_{g(E'')}$	HV – $T_{g(\tan \delta)}$
C / MPa	–969.28	–1272.6	–1773.6
$k / \text{MPa K}^{-1}$	3.2825	3.9911	5.108
R^2	0.9166	0.8199	0.8786

The optical and mechanical properties of PMMA- Y_2O_3 (Eu^{3+}) nanocomposites were investigated. The luminescence spectra of the nanocomposites revealed that the phosphorescence of the powder remained on compositing and the emission intensity was enhanced as the content of the powder in the composites increased. The results obtained from the DMA showed that on the addition of nanopowder, the T_g of the PMMA increased, but only by a few degrees; this also suggests that the nanoparticles

did not disperse individually but as aggregates. The microhardness number increased with increasing Y_2O_3 (Eu^{3+}) content in the PMMA nanocomposites. A nearly linear correlation between T_g and microhardness was obtained, because both properties are closely related to the cohesive energy density. This result is in accordance with previously reported results for amorphous glassy polymers, and now this linear correlation is applicable to similar composite configurations.

8. OPTICAL AND MECHANICAL PROPERTIES PMMA-Gd₂O₃ (Eu³⁺) NANOCOMPOSITES

8.1 INTRODUCTION

Rare-earth-based nanoparticles are highly photostable and exhibit long luminescence lifetimes and narrow emission bands with similar properties as those of quantum dots¹⁰². They possess excellent luminescent properties of inorganic phosphors which lead to promising applications of polymer–nanophosphor composites. Among the inorganic oxides, Gd₂O₃^{103,104,105,106} was widely employed as ideal host materials for the rare earth ions (RE) ion down- or up-conversion emission because of their low-phonon energy, high chemical- and photo stability, and efficient sensitization (host-to- RE energy transfer).

Thermoplastic polymer nanocomposites doped with the rare earth ions such as Tb, Eu, Yb and Er have attracted considerable interest due to energy transfer, up-conversion effects and broad application possibilities. They have a wide range of applications in photonic devices, signal links in medical devices, illuminating systems, fiber optic sensors and amplifiers^{107,108,109,110,111}. Recently, polymer optical fibers have found new applications in bio-sensors, bio-analytics and even clinical imaging diagnostics.

Poly (methyl methacrylate) (PMMA) is known as an optical plastic with excellent transparency and good processability, but with relatively poor mechanical properties. For improvement of mechanical properties of the transparent PMMA, techniques are used such as polymer blending and nanoparticles or continuous fiber reinforcement^{112,113,114,115}. As a consequence, the transmittance of the composites decreased significantly due to the difference between refractive indices of the PMMA and the reinforcement materials. An imperfect interface also contributes to the composite opacity. To resolve these problems, a potential method is to reduce the diameter of the reinforcing fibers to a size smaller than the wave-length of a visible light, so that the visible light does not reflect or refract while travelling through the composite¹¹⁶. Selected nanophosphors satisfy the prerequisites for presented hypothesis

in that the size of particles in optical composites should be less than the wavelength of light because of light scattering and the appropriate deagglomeration of nanoparticles in composite preparation could lead to the increase of mechanical properties. The optical effectiveness of the Gd_2O_3 (Eu^{3+}) in PMMA has already been reported^{117, 118}.

The melt mixing molding is quite extensive composite processing technique, with the pros and cons in that there is no need for other chemicals as for solution methods, but the deagglomeration and dispersion degree, especially in nano dimension, is rather low in comparison to other processing routes.

Solution casting method is usually utilized for processing of polymer nanocomposites because of the wide possibilities in mixing and deagglomeration of nanoparticles in solution. Potential drawbacks emerge with forming films after casting, with their thickness and particle distribution uniformity. Some of them could be resolved using the spin coating method.

Electrospinning is a versatile and effective technique to produce long, continuous fibers, and it is applicable to a diversity of materials, including not only polymers^{119,120}, but also bio-molecules^{121,122}, as well as inorganic/polymer composites^{123,124,125}. It is an electrostatically induced assembly process for generating ultrathin fibers with nanoscale diameters.

Thermo-mechanical properties of nanocomposites in form of bulk, films or nanofibers were measured by DMA because this technique is able to detect short range motion before the glass transition range is attained and thus identify the onset of main chain motion. Thus, the DMA method is more sensitive to detection of temperature transition than DSC because the mechanical changes are more dramatic than changes in the heat capacity^{126,127}. In addition, the nanomechanical properties of composite films were measured in order to point the effects of silanization of nanoparticles.

8.2 EXPERIMENTAL

Commercially available PMMA Acryrex[®] CM205 (Chi Mei Corp.) pellets were used as a matrix for preparing samples ($M_w \approx 90400$ g/mol). The Gd_2O_3 doped with 3 at. % Eu^{3+} nanopowder was synthesized using the combustion reaction based on polyethylene

glycol (PEG) fuel. The particle size of the Gd_2O_3 (Eu^{3+}) sample was determined by transmission electron microscopy-TEM (Phillips CM100 instrument operating at 60 kV). The silane coupling agent used for modification of particles was γ -Aminopropyltriethoxysilane- AMEO, Dynasylan[®] Evonik-Degussa¹²⁸. In the present study, the grafting reaction was carried out in a 95 wt% ethanol - 5 wt% water mixture to yield a 2 wt% final concentration of silane. The required amount of AMEO silane was calculated assuming 1 mol of AMEO per mol of Gd_2O_3 (Eu^{3+}). After silane addition the dispersion was refluxed with intensive stirring for 48 h at 80 °C, centrifuged and washed with ethanol in order to remove the residual silane and dried at 110 °C in a vacuum oven. Bulk nanocomposites were produced using Laboratory mixing molder, Dynisco. The sample contents were processed with different Gd_2O_3 (Eu^{3+}) powder: 0.5 wt%; 1.0 wt%; and 3 wt%. Nanocomposite films and nanofibers were processed with content of 3 wt% of unmodified and modified particles. Three solutions with fixed polymer concentration at 22 wt% were made using dimethylformamide (DMF, Uvasol[®] for spectroscopy, Merck-Alkaloid, Skopje) as solvent. The first solution was used for preparation of film and electrospun nanofibers of pure PMMA. The second solution consisted of polymer and Gd_2O_3 (Eu^{3+}) particles and the third contained polymer and AMEO modified Gd_2O_3 (Eu^{3+}) particles. Concentration of particles was set as 3 wt% related to polymer. One part of solution was used for electrospinning and the other was for solution casting. Electrospinning process (Electrospinner CH-01, Linari Engineering, Italy.) was setup: a 20 ml plastic syringe with a metallic needle of 1 mm inner diameter was set vertically on the syringe pump (R-100E, RAZEL Scientific Instruments); the high-voltage power supply (Spellman High Voltage Electronics Corporation, Model: PCM50P120) was set to the voltage of 28 kV. The flow rate of polymer solution was constant at 0.5 ml/h. Distance from the needle tip and collector was 14 cm. For the solution casting the solutions were poured into flat-bottomed Petri dishes to form film with a thickness of 500 μm . The infrared (IR) spectra of samples in KBr discs were obtained by transmission Fourier transform infrared (FTIR) spectroscopy (Hartmann & Braun, MB-series). The FTIR spectra were recorded between 4000 and 400 cm^{-1} with a resolution of 4 cm^{-1} . An insight of dispersion and deagglomeration of nanoparticles was performed using FESEM (TESCAN MIRA 3) with fracture surfaces sputtered with gold. The measuring of

electrospun nanofibers diameter was performed by Image Pro Plus 4.0. A dynamic mechanical analyzer DMA Q800 (TA Instruments) was used in the dual cantilever mode over a temperature range from 25 °C to 160 °C at a fixed frequency of 1 Hz. The heating ramp rate was 3 °C/min. DMA of fibers and thin films was established with the stainless steel sample holder loaded in the DMA Q800 (TA Instruments) using a dual cantilever mode, with temperature ramp 3 °C/min from 30 °C to 160 °C, and at a fixed frequency of 1 Hz. Because of the architecture of electrospun nanofibers, the modified DMA tests were performed with specific stainless steel sample holder with the 60 mm×13 mm×1 mm dimensions.

Nanoindentation tests on the polymer and composite film samples were done using the Hysitron Triboindenter with a Berkovich diamond tip and in-situ imaging scan mode. The hardness and reduced elastic modulus were calculated from the curves using the Oliver and Pharr method¹²⁹. The indentation maximum load was set to be 2 mN for all tested samples. The loading and unloading times as well as the hold time at the peak force were set to 25 s each.

8.3 RESULTS AND DISCUSSION

Morphology and particle sizes of powder were checked with TEM. It is revealed that Gd_2O_3 (Eu^{3+}) nanopowders in the form of particle agglomerates with dimensions of individual particles of about 40 nm, as shown in [Figure 8.1](#).

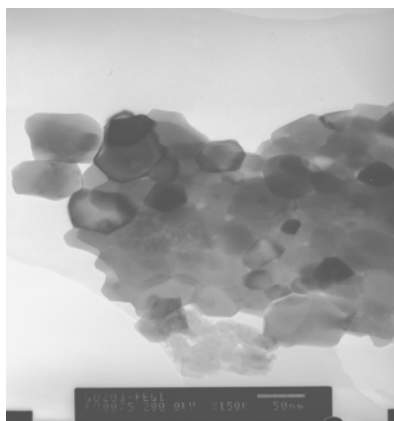


Figure 8.1. TEM image of Gd_2O_3 (Eu^{3+}) powder

FESEM photos of the composite fracture surfaces of bulk samples and films with unmodified (a) and modified (b) particles are presented in Figures 8.2 and 8.3. FESEM analysis reveals that the better dispersion of nanoparticles is achieved with modified particles. The silanization of particles leads to better deagglomeration of particles.

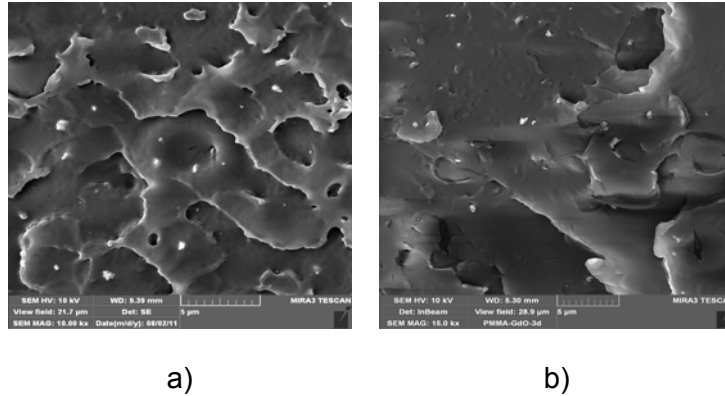


Figure 8.2. FESEM of bulk samples: a) PMMA- Gd_2O_3 (Eu^{3+}) (3 wt %); b) PMMA- Gd_2O_3 (Eu^{3+})-AMEO (3 wt %)

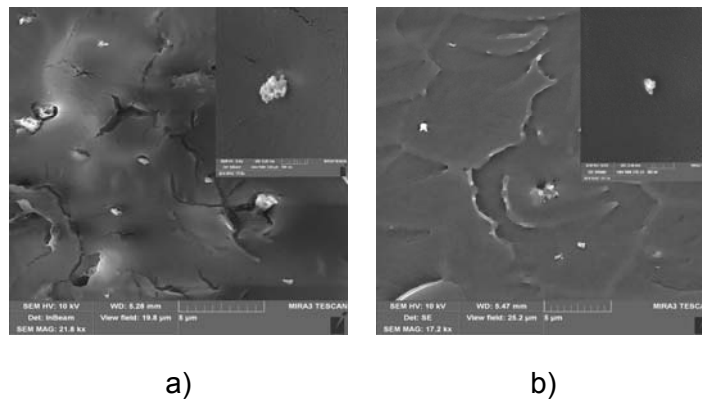


Figure 8.3 FESEM of films: a) PMMA- Gd_2O_3 (Eu^{3+}) (3 wt %); b) PMMA- Gd_2O_3 (Eu^{3+}) AMEO (3 wt %)

SEM photos of the electrospun nanofibers are presented in Figure 8.4. Image analysis revealed that nanofibers were in mean diameter of 200-500 nm of PMMA, 400-600 nm of PMMA- Gd_2O_3 (Eu^{3+}) and 300-550 nm of PMMA- Gd_2O_3 (Eu^{3+})-AMEO nanocomposites, respectively. A favorable dispersion of particles in nanofibers was achieved and a better deagglomeration of modified particles was obtained.

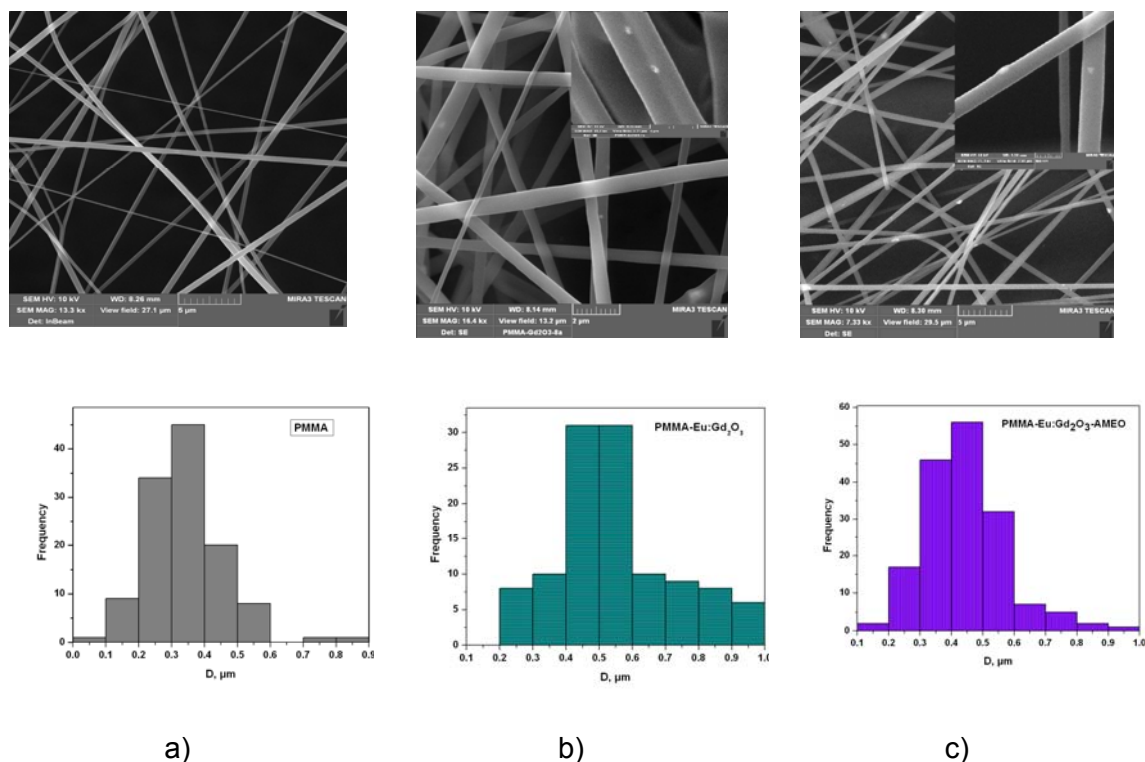


Figure 8. 4. FESEM photo of electrospun nanofibers: a) PMMA; b) PMMA- Gd_2O_3 (Eu^{3+}) (3 wt%); c) PMMA- Gd_2O_3 (Eu^{3+})-AMEO (3 wt %)

The FTIR spectrum of unmodified, modified Gd_2O_3 (Eu^{3+}) nanoparticles and AMEO silane is presented in Figure 8.5. The IR spectrum of unmodified Gd_2O_3 (Eu^{3+}) shows the characteristic bands observed at 1017, 1397 and 1506 cm^{-1} of nitrate and carbonate as consequence of combustion method¹³⁰. The presence of adsorbed water molecules was assigned to the bands $\delta(H_2O)$ at 1635 cm^{-1} and $\nu(H_2O)$ at 3434 cm^{-1} . The characteristic band for Gd-O bond was observed at 542 cm^{-1} . The FTIR spectrum of the amino modified gadolinium particles (Figure 8.5 (b)), shows the band originating from Si-O-Si vibrations at 1064 cm^{-1} , and the weak bands at 2924 cm^{-1} and 2846 cm^{-1} , which were assigned to the asymmetric, ν_{as} , and symmetric, ν_s , stretching modes of CH_2 groups. In the FTIR spectrum of the amino modified gadolinium particles, Figure 8.5 (b), can be seen the band originating from Si-O-Si vibrations at 1064 cm^{-1} , the weak bands at 2924 cm^{-1} and 2846 cm^{-1} were assigned to the asymmetric, ν_{as} , and symmetric, ν_s , stretching modes of CH_2 groups. The band at 1128 cm^{-1} could also be due to Si-O-Gd groups, the weak band at 1541 cm^{-1} may be attributed to $\delta(NH_2)$ deformation vibrations of the NH_2 groups, respectively, which is in agreement with the data reported in the literature¹²⁸. The broadening of the signal centered at about 3434 cm^{-1} was also

assigned to the presence of adsorbed water molecules and overlapped with signals of $\nu(\text{H}_2\text{O})$ of the adsorbed water, silanol and $\nu(\text{NH}_2)$ group vibrations. This indicates that the chemical modification on $\text{Gd}_2\text{O}_3 (\text{Eu}^{3+})$ surface was achieved.

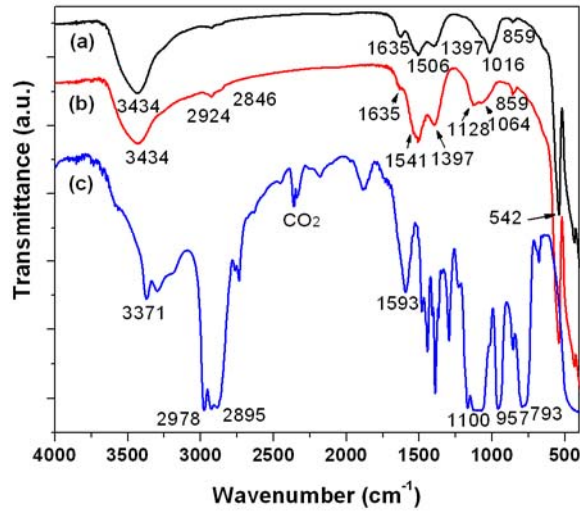


Figure 8.5 The FTIR spectrum of a) neat $\text{Gd}_2\text{O}_3 (\text{Eu}^{3+})$, b) modified $\text{Gd}_2\text{O}_3 (\text{Eu}^{3+})$ and c) AMEO silane

Further investigation on the optimal composite configuration for appropriate mechanical properties was undertaken by DMA, as presented in Figure 8.6. The results of DMA for bulk samples with different nanophosphors are presented in Figure 8.6 (a). The glass transition temperature (T_g) of a polymer increased after the addition of inorganic fillers and the storage modulus composites are changed correspondingly¹³¹. It is obvious that even in the absence of specific interactions with the polymer, the particles behaved as functional physical crosslink and thus reducing the overall mobility of the polymer chains, as was already reported^{132,133}. After adding the modified particles, the storage modulus increased considerably and T_g increased slightly (Figure 8.6 (b)). So, the modification of interface particle-matrix improved the mechanical properties of nanocomposite.

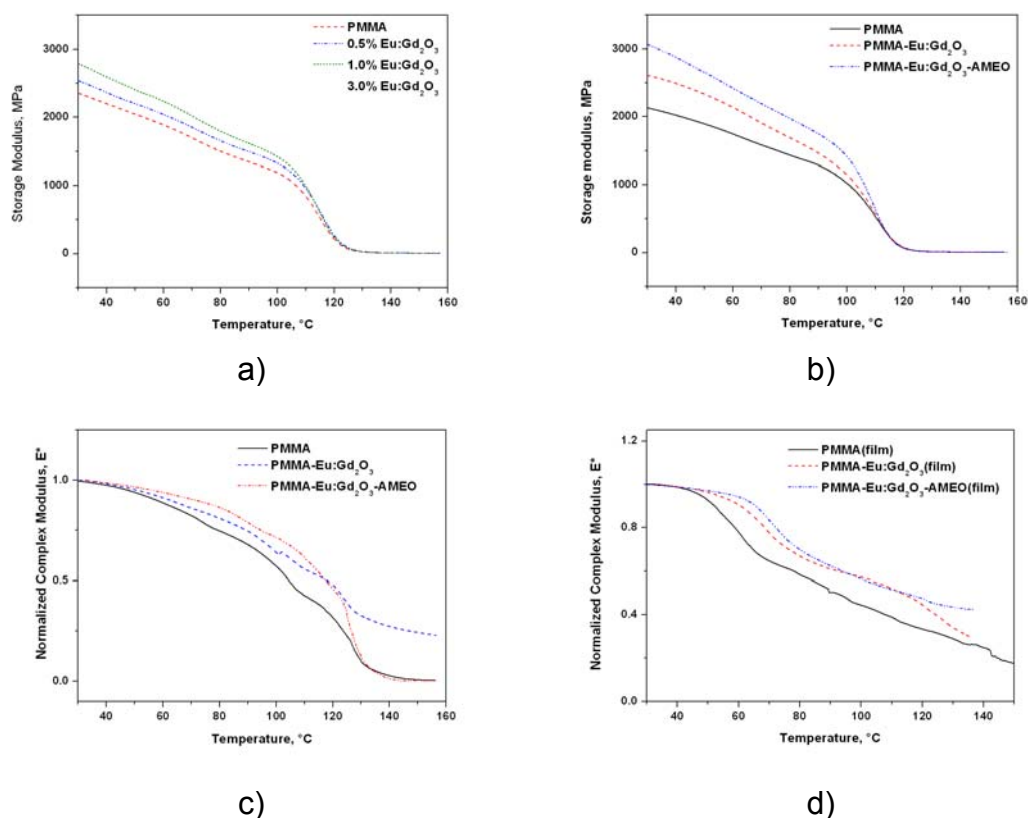


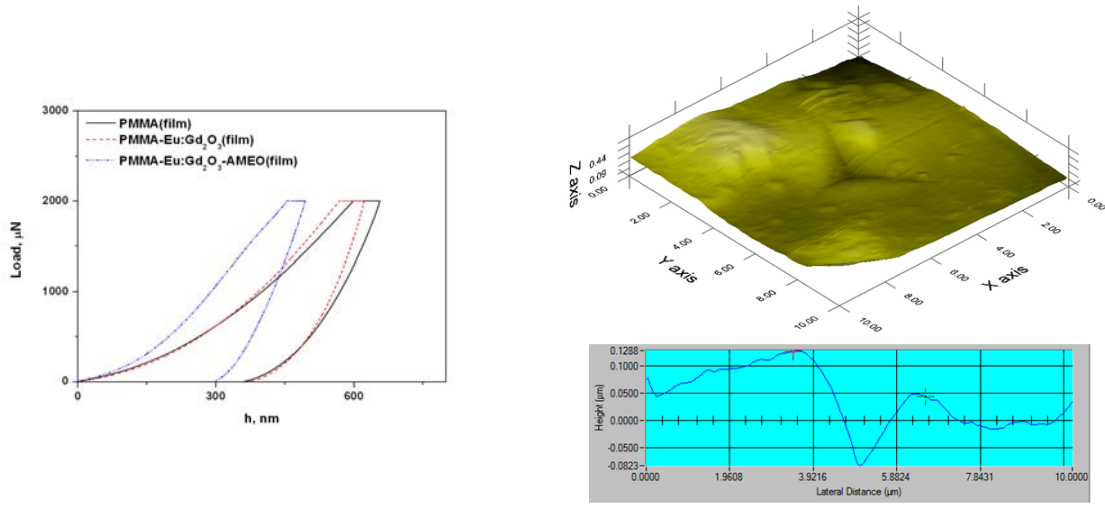
Figure 8.6. DMA- a) Storage modulus of pure PMMA and nanocomposites - Bulk samples; b) Storage modulus of pure PMMA and nanocomposites with 3 wt% unmodified and 3 wt% modified nanoparticles; c) Complex modulus, E^* , of electrospun nanofibers; d) Complex modulus, E^* , of different films

Table 8.1. The glass transition temperature (T_g)

Sample	$T_g/^\circ\text{C}$	$T_g/^\circ\text{C}$	$T_g/^\circ\text{C}$
	Bulk samples	Nanofibers	Films
PMMA	101.18	97.47	60.02 °C
PMMA- Gd ₂ O ₃ (Eu ³⁺)	101.76	102.89	62.31 °C
PMMA- Gd ₂ O ₃ (Eu ³⁺) -AMEO	102.12	107.68	64.12 °C

The using of stainless steel holder enabled the characterization of the T_g with temperature change by observing the signal change of the calculated normalized complex modulus, E^* ^{134,135,136}. The magnitudes of the storage modulus and the loss modulus are only qualitative. This complex modulus, E^* , presents the ratio of the complex modulus within a sample set to the value of the maximum modulus in the same data set. The DMA results for nanofibers (Figure 8.6 (c)) clearly display that the glass transition temperature is accompanied by significant loss (onset point) of the normalized complex modulus, E^* . Better thermal stability was achieved for nanocomposite with modified particles with respect to nanocomposite with unmodified particles and pure PMMA. The shift of T_g for nanofibers is more remarkable than that for bulk samples. This indicates that the distribution of nanoparticles is much better in electrospun nanofibers. DMA results for films with modified and unmodified particles obtained by steel sample holder are presented in Figure 8.6 (d). The results show that the onset point, corresponding to the α -transition (glass transition), is shifted towards the lower temperatures, as compared with the bulk polymer obtained by molding, without any solvent. The effect of the solvent contained in the film decreases the glass transition temperature (T_g) of the polymer and composites^{137,138}. But the results show the same trend as a bulk and nanofibers in that the value of T_g raised in the order PMMA, PMMA- Gd₂O₃ (Eu³⁺) and PMMA- Gd₂O₃ (Eu³⁺) -AMEO.

Figure 8.7 (a) shows typical force–depth curves obtained in the nanoindentation tests for neat PMMA film and composites with Gd₂O₃ (Eu³⁺) and AMEO silane treated Gd₂O₃ (Eu³⁺). The curves appear to be with continuity and without pop in or pop out in both loading and unloading phases. Figure 8.7 (b) displays the plastic imprint of the indent for the sample with AMEO silane treated particles with the scan trace in the vicinity of the indent.



a)

b)

Figure 8.7 a) Load–displacement curves of neat PMMA and nanocomposite films; b) Indent plastic imprint with scan trace of the PMMA- $Gd_2O_3(Eu^{3+})$ -AMEO sample

In-situ imaging mode used for scanning the surface trace reveals the absence of cracks and fractures around the indent. Line trace shows small piling-up along the edges but in addition to the film surface roughness (adequate but not ideal); these scans (only one is displayed) raise the confidence that nanoindentation tests captured actual material properties¹³⁹. The results of reduced elastic modulus and hardness for neat polymer and composites with 3 wt% of nanoparticles are presented in [Table 8.2](#).

Table 8.2. The results of reduced elastic modulus and hardness for neat polymer and composites

Sample	E_r /GPa	Standard deviation/GPa	H /GPa	Standard deviation/GPa
PMMA	4.278	± 0.3	0.263	± 0.2
PMMA- $Gd_2O_3(Eu^{3+})$	4.817	± 1.6	0.268	± 0.15
PMMA- $Gd_2O_3(Eu^{3+})$ AMEO	5.597	± 1.0	0.293	± 0.15

The reduced modulus for composite with untreated particles increases for 12.6% while the hardness remains similar in comparison to the neat PMMA films. For composites with AMEO silane treated particles the modulus increases for about 30% and hardness increase is about 11%. For composites with silane treated particles, results are comparable to those with other nanoparticle composites which achieved favorable dispersion and particle matrix bonding^{140, 141}. Previous work reported the use of PEG silane, TEOS or grafting method for the silanization of Gd₂O₃ and RE:Gd₂O₃ nanoparticles^{142,143} this study presents the first report on the modification of Gd₂O₃ (Eu³⁺) with AMEO silane adhesion promoter. The modification routes using PEG silane, TEOS or grafting methods leads to the appropriate nanoparticle deagglomeration in solvents (but not in polymer composites), as proven by electron microscopy and optical characterization of modified particles. This study presents the first attempt of establishing relations between the modification methods of Gd₂O₃ (Eu³⁺) particles with the nanocomposite mechanical properties.

9. CONCLUSIONS

Single cantilever tests on POFs at constant frequency and amplitude and on five constant temperatures showed that E' slightly increased with number of performed oscillations at each temperature. Relative changes of E' are similar for temperatures from 50-80 °C and significantly bigger at 90 °C. During those tests considered as kind of fatigue tests the values of I/I_0 was decreasing and $\Delta I/I_0$ are similar at both wavelengths of the optical signal. The biggest relative decreasing of optical transmission is at 90 °C which corresponded to the most significant change in E' .

For dynamic temperature scan test two kinds of comparison were done: one between not fatigued and fatigued POFs, and second for the same measurements at two wavelengths 840 and 650 nm. In general the storage modulus of POF is decreasing significantly with rising temperature from 40-110 °C. From 40-80 °C the decrease of storage modulus is linear versus temperature, and for higher temperature the behavior is nonlinear. The optical signals are almost constant from 40-50 °C, and in the temperature interval from 50-80 °C the transmission of POF is increasing linearly versus temperature. At higher temperatures the optical signal is ascending, reaching its maximum and then descending on both wavelengths. Optical transmission change versus temperature at 840 nm is significantly higher for not fatigued fiber than for fatigued. Measurements at 650 nm showed that transmission changes versus temperatures for fatigued and not fatigued POFs are less different.

The maximum intensity of optical signals are almost at same temperatures at both wavelengths (88-89 °C for not fatigued and 104 °C for fatigued POF).

Comparing the dependence of E' and E'' versus temperature of rectangular specimens with the optical signals of POF during temperature scan tests it is obvious that maximums in optical signals transmission of POFs are at temperatures close to loss modulus minimums. They are lower than T_g , both for fatigued and not fatigued POF. So, optical signal changes in POF could indicate the beginning of glass transition process, but not the T_g .

It is showed that simultaneous DMA and optical signal intensity measurements could be done on POF. In the temperature interval from 40-80 °C the relative changes in storage modulus are opposite to the change of the intensity of optical signal, i.e. its transmission. It is possible to choose optical wavelengths with higher and lower sensitivity to temperature, and in general fatigue of the POF decrease its temperature sensitivity. The measuring modes for rectangular specimens could be used for POF, but the calculations should be multiplied with appropriate factor.

The DMA of POF is potentially useful for fiber optic sensors development, especially for their temperature sensitivity investigations during various types of mechanical measurements.

The optical and mechanical properties of PMMA-Y₂O₃ (Eu³⁺) nanocomposites were investigated. The luminescence spectra of the nanocomposites revealed that the phosphorescence of the powder remained on compositing and the emission intensity was enhanced as the content of the powder in the composites increased. The results obtained from the DMA showed that on the addition of nanopowder, the T_g of the PMMA increased, but only by a few degrees; this also suggests that the nanoparticles did not disperse individually but as aggregates. The microhardness number increased with increasing Y₂O₃ (Eu³⁺) content in the PMMA nanocomposites. A nearly linear correlation between T_g and microhardness was obtained, because both properties are closely related to the cohesive energy density. This result is in accordance with previously reported results for amorphous glassy polymers, and now this linear correlation is applicable to similar composite configurations.

This study reports the preparation of composites with PMMA matrix reinforced with Gd₂O₃ (Eu³⁺) nanophosphor powder with enhanced mechanical properties utilizing the quasi-industrial melt-mixing technique (bulk nanocomposite), solution casting (thin films) and electrospinnig (nanofiber). The three processing methods have different possibilities for the particle dispersion efficiency. The modification of the nanoparticles with the silane adhesion promotor enabled their dispersion and deagglomeration in all three cases (bulk, film and nanofibers) and yielded enhanced mechanical properties of

the composite materials. The DMA results revealed that electrospinning could be used for increased uniformity of nanoparticle distribution in polymer composites and that the relaxation temperatures associated with the glass transition (T_g) of the nanofibers were greater than those of the bulk and films nanocomposite samples. As shown by nanoindentation tests, incorporation of 3 wt% of silanized nanoparticles increased the reduced modulus and hardness of PMMA composite for 30% and 11% , respectively.

REFERENCES

- ¹ D. R. Paul, L. M. Robeson, *Polymer*, **49** (2008) 3187
- ² S. C. Tjong, *Mater. Sci. Eng., R*, **53** (2006) 73
- ³ Y. Osada, D. E. D. Rossi, *Polymer Sensors and Actuators*, Springer-Verlag, Berlin Heidelberg, Germany, 2000
- ⁴ S. M. Vaezi-Nejad, *Selected Topics in Advanced Solid State and Fiber Optic Sensors*, IEE, London, UK, 2000
- ⁵ R. J. Bartlett, R. Philip-Chandy, P. Eldridge, D. F. Merchant, R. Morgan, P. J. Scully, *Trans. Inst. Meas. Control* **22** (2000) 431
- ⁶ K. Mohamed, T. G. Gerasimov, H. Abourahma, M. J. Zaworotko, J. P. Harmon, *Mater. Sci. Eng., A* **409** (2005) 227
- ⁷ H. Eilers, B. M. Tissue, *Chem. Phys. Lett.* **251** (1996) 74
- ⁸ B. Bihari, H. Eilers, B. M. Tissue, *J. Lumin.* **75** (1997) 1
- ⁹ E. Ritzhaupt-Kleissl, J. Boehm, J. Hausselt, T. Hanemann, *Mater. Sci. Eng., C* **26** (2006) 1067
- ¹⁰ T. K. Anh, N. Vu, M. H. Nam, L. Q. Minh, *Adv. Nat. Sci.* **7** (2006) 63
- ¹¹ Z. Antic, R. Krsmanovic, M. Marinovic-Cincovic, M. D. Dramicanin, *Acta Phys. Pol. A*, **117** (2010) 831-836.
- ¹² M. Nichkova, D. Dosev, S. J. Gee, B. D. Hammock, I. M. Kennedy, *Anal. Chem.*, **77** (2005) 6864-6873
- ¹³ K. S. Dhiraj, S. Chandra, J. B. Gruber, W. Gorski, M. Zhang, J. H. Shim, *J. Appl. Phys.* **105** (2009) 093105
- ¹⁴ K. S. Dhiraj, S. Chandra, J. B. Gruber, W. Gorski, M. Zhang, J. H. Shim, *J. Appl. Phys.* **105** (2009) 093105
- ¹⁵ C. Sonnichsen, A. P. Alivisatos, *Nano Lett.*, **5** (2005), 301.
- ¹⁶ L. M. Liz-Marzan, P. Mulvaney, *J. Phys. Chem. B.*, **107** (2003), 7312.
- ¹⁷ Z. Liu, D. Zhang, S. Han, C. Li, B. Lei, W. Lu, J. Fang, C. Zhou, *J. Am. Chem. Soc.*, **127** (2005), 6.
- ¹⁸ P. Yang, C. L. Li, N. Murase, *Langmuir.*, **21** (2005), 8913.
- ¹⁹ J. Riegler, P. Nick, U. Kielmann, T. Nann, *J. Nanosci. Nanotechnol.*, **3** (2003), 380.

-
- ²⁰ H. H. Yang, S. Q. Zhang, X. L. Chen, Z. X. Zhuang, J. G. Xu, X. R. Wang, *Anal. Chem.*, **77** (2005), 354.
- ²¹ C. B. Murray, D.J. Norris, M.G. Bawendi, *J. Am. Chem. Soc.*, , **115**(1993), 8706.
- ²² M. Lee, J.K. Kuno, B.O. Dabbousi, F.V. Mikulec, M.G. Bawendi, *J. Chem. Phys.*, , **106**(1997), 9869.
- ²³ B.M. Tissue, *Chem. Mater.* **10** (1998) 2837-2845.
- ²⁴ T. K. Anh, P. Benalloul, C. Barthou, L. T. K. Giang, N. Vu, L. Q. Minh, *J. Nanomaterials* **2**, (2007).
- ²⁵ Wang, Y.; Archambault, N.; Marold, A.; Weng, L.; Lucht, B. L.; Euler, W. B. *Macromolecules*, **37** (2004), 5415.
- ²⁶ Balamurugan, S. S.; Bantchev, G. B.; Yang, Y. M.; McCarley, R. L. *Angew. Chem. Int. Ed.*, **44** (2005), 4872.
- ²⁷ Lawrence, J. R.; Shim, G. H.; Jiang, P.; Han, M. G.; Ying, Y. R.; Foulger, S. H. *Adv. Mater.*, **17** (2005), 2344.
- ²⁸ Lee, S. B.; Koepsel, R. R.; Russell, A. J. *Nano Lett.*, **5** (2005), 2202.
- ²⁹ Albert, K. J.; Lewis, N. S.; Schauer, C. L.; Sotzing, G. A.; Stitzel, S. E.; Vaid, T. P.; Walt, D. R. *Chem. Rev.*, **100**, (2000), 2595.
- ³⁰ Potyrailo, R. A. *Angew. Chem. Int. Ed.*, **45**, (2006), 702.
- ³¹ Shibaev, V.; Bobrovsky, A.; Boiko, N. *J. Photochem. Photobiol., A*, **155** (2003), 3.
- ³² Wigglesworth, T. J.; Myles, A. J.; Branda, N. R. *Eur. J. Org. Chem.*, 1233, (2005)
- ³³ Argun, A. A.; Aubert, P. H.; Thompson, B. C.; Schwendeman, I.; Gaupp, C. L.; Hwang, J.; Pinto, N. J.; Tanner, D. B.; MacDiarmid, A. G.; Reynolds, J. R. *Chem. Mater.*, **16** (2004), 4401.
- ³⁴ Mortimer, R. J.; Dyer, A. L.; Reynolds, J. R. *Displays*, **27** (2006), 2
- ³⁵ Bamfield, P. *Chromic Phenomena*, RSC: Cambridge, 1991.
- ³⁶ Jenekhe, S. A.; Kiserow, D. J., *Chromogenic Phenomena in Polymers: Tunable Optical Properties*; ACS Symposium Series 888; American Chemical Society: Washington, DC, 2005; pp 2-15.
- ³⁷ Shionoya, S. and Yen, W.M. *Phosphor Handbook*. New York: CRC Press. p. 608. (1998).

-
- ³⁸ Kitai A., *Luminescent Materials and Applications*. John Wiley & Sons, Ltd ISBN: 978-0-470-05818-3 2008.
- ³⁹ Lee, J.D. *Concise Inorganic Chemistry*. Noida, India: Blackwell Science. p. 1032. (2005).
- ⁴⁰ Round, H.J., *Elect. World* **49**(9) (1907): 309.
- ⁴¹ Bera, D., Kuiry, S.C. and Seal, S., *Jom.* **56**(1) (2004): 49–53.
- ⁴² Alivisatos, A.P., *J. Phys. Chem.* **100**(31) (1996): 3226–39.
- ⁴³ Yang, H.S., et al., *Adv. Mat.* **18**(21) (2006): 2890.
- ⁴⁴ Santra, S., et al., *Adv. Mat.* **17**(18) (2005): 2165–9.
- ⁴⁵ G.S. Ofelt, *J. Chem. Phys.* **37**(3) (1962) 511-520.
- ⁴⁶ R.D. Shannon, *Acta Cryst.* **A32** (1976) 751-767.
- ⁴⁷ C. Görller-Walrand and K. Binnemans, Spectral Intensities of f-f Transitions, in K.A. Gschneider, Jr. and L. Eyring (Eds.) *Handbook on the Physics and Chemistry of Rare Earths*, Vol. 25, Chap. 167, 101-264. Elsevier, Amsterdam (1998).
- ⁴⁸ S. Shionoya and W.M. Yen, *Phosphor Handbook*, CRC Press, Boca Raton, Florida 1999.
- ⁴⁹ G.S. Ofelt, *J. Chem. Phys.* **37**(3) (1962) 511-520.
- ⁵⁰ M. H. V. Werts, *Science Prog.* **88**(2) (2005) 101-131.
- ⁵¹ G. Blasse, Chemistry and physics of R-activated phosphors, in: L.R. Eyring (Ed.), *Handbook on the Physics and Chemistry of Rare Earths*, (1979) Vol. 4, Chap. 34, pp. 237–274. North-Holland Publishing Company, Amsterdam.
- ⁵² E. Antic-Fidancev, et al., *J. Phys.: Condens. Mater.* **15** (2003) 863-876.
- ⁵³ C. Liu and J. Liu, *J. Phys. Chem. B* **110** (2006) 20277-20281.
- ⁵⁴ M. Buijs, A. Meyerink and G. Blasse, *J. Lumin.* **37** (1987) 9-20.
- ⁵⁵ Ch.-Ch. Lin, K.-M. Lin and Y.-Y. Li, *J. Lumin.* **126** (2007) 795-799.
- ⁵⁶ A.M. Pires, et al., *J. Alloys Comp.* **344** (2002) 276-279
- ⁵⁷ G. Liu, et al., *J. Alloys Comp.* **432** (2007) 200-204.
- ⁵⁸ Ch.-S. Park, et al., *J. Lumin.* **118** (2006) 199-204.
- ⁵⁹ Y.C. Kang et al., *J. Phys. Chem. Solids* **60** (1999) 379-384.
- ⁶⁰ H. Guo, et al., *Appl. Surf. Sci.* **230** (2004) 215-221.
- ⁶¹ A. Garcia-Murillo, et al., *Opt. Mater.* **19** (2002) 161-168.

-
- ⁶² J. Zubia, J. Arrue, *Opt. Fiber Tech.*, **7** (2001), 101-140.
- ⁶³ T. Nyu, S. Yamazaki, A. K. Dutta, *Proc. 4th Int. Conf. POF & Appl. '95*, Boston, 119-121 (1995).
- ⁶⁴ K. Numata, S. Furusawa, S. Mirikura, *Proc. 8th Int. Conf. POF & Appl. '99*, Chiba (Japan), 74-77 (1999).
- ⁶⁵ Y. Koike, T. Ishigure, E. Nihei, **13**(1995), 1475-1489.
- ⁶⁶ M. Naritomi, *POF Asia-Pacific Forum '96*, Tokyo (1996).
- ⁶⁷ W. Daum et al, *Polymer Optical Fibers for Data Communication* (1st Ed.), Springer, Ch.3.
- ⁶⁸ IGI Consulting, "POF-Market & Technology Assessment Study 2002 Update", IGI Consulting, Alston (2002). (b) W. Daum, J. Krauser, P. E., Zamzow, O. Ziemann, *POF-Polymer Optical Fibers for Data Communication*, Springer, Berlin (2002).
- ⁶⁹ H. Murofushi, *Proc. 5th Int. Conf. POF & Appl. '96*, Paris, France, 17-23 (1996).
- ⁷⁰ Y. Koike, S. Matsuoka, H. E. Bair, *Macromolecules*, **25**(1992), 4807-4815.
- ⁷¹ B. G. Shin, J. H. Park, J. J. Kim, *Appl. Phys. Lett.*, **82**(2003), 4645-4647.
- ⁷² Y. Koike, Y. Ohtsuka, , *Appl. Opt.*, **22**(1983), 418-423
- ⁷³ Y. Koike, T. Ishigure, E. Nihei, *J. Lightwave Technol.*, **13**(1995), 1475-1489.
- ⁷⁴ J. Zubia, J. Arrue, *Opt. Fiber Technol.* **7** (2001) 101-140.
- ⁷⁵ W. Jones, *Organic Molecular Solids: properties and applications*, W. Jones Ed. CRC Press LLC, Boca Raton (1997), pp. 202-223.
- ⁷⁶ R. J. Bartlett, R. Phylip-Chandy, P. Eldridge, D. F. Merchant, R. Morgan, P. J. Scully, *Trans. Ins. Meas. Control* **22** (2000) 431-457.
- ⁷⁷ A. Appajaiah, *Climatic Stability of Polymer Optical Fibers*, PhD Thesis, Potsdam University, Berlin (2004), pp.11-20.
- ⁷⁸ K. S. C. Kuang, S. T. Quek, C. G. Koh, W. J. Cantwell, P. J. Scully, *J. Sensors* 2009, Article ID 312053, 13 pages, 2009. doi:10.1155/2009/312053
- ⁷⁹ H. Asanuma, O. Haga, K. Kimura, J. Ohira, H. Kurihara, A. Paolozzi, *J. Thermoplast. Compos. Mater.* **19** (2006) 277-292.
- ⁸⁰ D. Stojanovic, A. Orlovic, S. Markovic, V. Radmilovic, P. S. Uskokovic, R. Aleksic, *J. Mater. Sci.* **44** (2009) 6223-6232.

-
- ⁸¹ D. Aitken, S. M. Burkinshaw, R. Cox, J. Cantherall, R. E. Litchfield, D. M. Price N. G. Todd, *J. Appl. Polym. Sci.* **47** (1991), 263-269.
- ⁸² G. Swaminathan, K. Shivakumar, *J. Reinf. Plast. Compos.* **28** (2009) 979-944.
- ⁸³ D. R. Paul, L. M. Robeson, *Polymer*, **49** (2008) 3187
- ⁸⁴ S. C. Tjong, *Mater. Sci. Eng., R*, **53** (2006) 73
- ⁸⁵ Y. Osada, D. E. D. Rossi, *Polymer Sensors and Actuators*, Springer-Verlag, Berlin Heidelberg, Germany, 2000.
- ⁸⁶ S. M. Vaezi-Nejad, *Selected Topics in Advanced Solid State and Fiber Optic Sensors*, IEE, London, UK, 2000.
- ⁸⁷ R. J. Bartlett, R. Philip-Chandy, P. Eldridge, D. F. Merchant, R. Morgan, P. J. Scully, *Trans. Inst. Meas. Control* **22** (2000) 431.
- ⁸⁸ K. Mohamed, T. G. Gerasimov, H. Abourahma, M. J. Zaworotko, J. P. Harmon, *Mater. Sci. Eng., A* **409** (2005) 227.
- ⁸⁹ H. Eilers, B. M. Tissue, *Chem. Phys. Lett.* **251** (1996) 74.
- ⁹⁰ 19. E. Ritzhaupt-Kleissl, J. Boehm, J. Hausselt, T. Hanemann, *Mater. Sci. Eng., C* **26** (2006) 1067.
- ⁹¹ T. K. Anh, N. Vu, M. H. Nam, L. Q. Minh, *Adv. Nat. Sci.* **7** (2006) 63.
- ⁹² K. S. Dhiraj, S. Chandra, J. B. Gruber, W. Gorski, M. Zhang, J. H. Shim, *J. Appl. Phys.* **105** (2009) 093105.
- ⁹³ T. K. Anh, P. Benalloul, C. Barthou, L. T. K. Giang, N. Vu, L. Q. Minh, *J. Nanomaterials* (2007) 2
- ⁹⁴ B. Crist, in *Materials Science and Technology*, Vol. 1, E. L. Thomas, Ed., VCH, Weinheim, Germany, 1993, p. 427.
- ⁹⁵ F. J. Baltá-Calleja, A. Flores, F. Ania, in *Mechanical properties of polymers based on nanostructure and morphology*, G. H. Michler, F. J. Baltá-Calleja, Eds., Taylor and Francis, London, UK, 2005, p. 285.
- ⁹⁶ A. Flores, F. Ania, F. J. Baltá-Calleja, *Polymer* **50** (2009) 729.
- ⁹⁷ S. Fakirov, F. J. Balta-Calleja, M. Krumova, *J. Polym. Sci., Part B: Polym. Phys.* **37** (1999) 1413.
- ⁹⁸ A. K. Adiyodi, X. Joseph, P. V. Jyithy, G. Jose, N. V. Unnikrishnan, *Materials Science-Poland* **27** (2009) 297.

-
- ⁹⁹ E. A. Turi, *Thermal Characterization of Polymeric Materials*, Vol. I, 2nd ed., Academic Press, Brooklyn, New York, 1997, p. 980.
- ¹⁰⁰ M. Dixit, S. Gupta, V. Mathur, K. S. Rathore, K. Sharma, N. S. Saxena, *Chalcogenide Lett.* **6**, (2009) 131.
- ¹⁰¹ Z. Antic, R. Krsmanovic, I. Zekovic, M. D. Dramicanin in *Proceeding of Electroceramics XI*, (2008), University of Manchester, Manchester, UK, Abstracts and CD proceedings, C-038-P.
- ¹⁰² W. O. Gordon, J. A. Carter, B. M. Tissue, *J. Lumin.*, 108 (2004) 339-342.
- ¹⁰³ Y. C. Kang, S. B. Park, I. W. Lenggoro, K. Okuyama, *J. Phys. Chem. Solids*, **60** (2000) 379-384.
- ¹⁰⁴ G. Xia, S. Wang, S. Zhou, J. Xu, *Nanotechnology*, **21** (2010) 345601.
- ¹⁰⁵ E. Ritzhaupt-Kleissl, J. Boehm, J. Hausselt, T. Hanemann. *Mater. Sci. Eng. C*, **26** (2006) 1067-1071.
- ¹⁰⁶ X. Ye, W. Gao, L. Xia, H. Nie, W. Zhuang, *J. Rare Earth.*, **28** (3) (2010) 345-350.
- ¹⁰⁷ R. M. Pectoral, Jr., F. Söderlind, A. Klasson, A. Suska, M. A. Fortin, N. Abrikossova, L. Selegård, P. O. Käll, M. Engström, K. Uvdal, *J. Phys. Chem. C*, **113** (2009) 6913-6920.
- ¹⁰⁸ R. J. Bartlett, R. Philip-Chandy, P. Eldridge, D. F. Merchant, R. Morgan, P. Scully, T. I. Meas. *Control*, **22** (5) (2000) 431-457.
- ¹⁰⁹ T. K. Anh, P. Benalloul, C. Barthou, L. K. Giang, N. Vu, Le Quoc Minh., *J. Nanomater.*, 2007 (2007) Article ID 48247, 10 pages, doi:10.1155/2007/48247
- ¹¹⁰ V. Radojević, T. Serbez, R. Aleksić, D. Nedeljković, Lj. Brajović *J. Min. Metall. Sect. B-Metall.*, **41 B** (1) (2005) 103-112.
- ¹¹¹ A. Grujić, N. Talijan, D. Stojanović, J. Stajić-Trošić, Z. Burzić, Lj. Balanović, R. Aleksić, *J. Min. Metall. Sect. B-Metall* **46 B** (1) (2010) 125-132.
- ¹¹² X. Wang, Z. Huang, L. Chen, *Fiber. Polym.*, **12** (3) (2011) 359-365.
- ¹¹³ S. K. Cheng, C. Y. Chen, *Eur. Polym. J.*, **40** (2004) 1239-1248.
- ¹¹⁴ E. Schauer, L. Berglund, G. Pena, *Polymer*, **43** (2002) 1241-1248.
- ¹¹⁵ L. Q. Liu, D. Tasis, M. Prato, H. D. Wagner, *Adv. Mater.*, **19** (2007) 1228-1233.
- ¹¹⁶ G. F. Chen, H. Q. Liu, *J. Appl. Polym. Sci.*, **110** (2008) 641-646.

-
- ¹¹⁷ Z. Antic, R. Krsmanovic, M. Marinovic-Cincovic, M. D. Dramicanin, *Acta Phys. Pol. A*, 117 (2010) 831-836.
- ¹¹⁸ M. Nichkova, D. Dosev, S. J. Gee, B. D. Hammock, I. M. Kennedy, *Anal. Chem.*, 77 (2005) 6864-6873
- ¹¹⁹ C. L. Casper, J. S. Stephens, N. G. Tassi, D. B. Chase, J. F. Rabolt, *Macromolecules*, 37 (2004) 573-578.
- ¹²⁰ K. P. Matabola, A. R. de Vries, A. S. Luyt, R. Kumar, *Express Polym. Lett.*, 5 (7) (2011) 635-642.
- ¹²¹ S. Piperno, L. Lozzi, R. Rastelli, M. Passacantando, S. Santucci, *App. Surf. Sci.*, 252 (2006) 5583-5586.
- ¹²² Y. You, B. Min, S. J. Lee, T. S. Lee, W. H. Park, *J. Appl. Polym. Sci.*, 95 (2005) 193-200.
- ¹²³ C. Hoffmann, A. C. Faure, C. Vancaeyzeele, S. Roux, O. Tillement, E. Pauthe, F. Goubard, *Anal. Bioanal. Chem.*, 399 (2011) 1653-1663.
- ¹²⁴ D. Li, Y. Xia, *Adv. Mater.*, 16 (2004) 1151-1170.
- ¹²⁵ J. Macossay, J. H. Leal, A. Kuang, R. E. Jones, *Polym. Adv. Technol.*, 17 (2006) 391-394.
- ¹²⁶ M. Li, Z. Zhang, T. Cao, Y. Sun, P. Liang, C. Shao, Y. Liu, *Mater. Res. Bull.*, 47 (2012) 321-327.
- ¹²⁷ D. Mahlin, J. Wood, N. Hawkins, J. Mahey, P. G. Royall, *Int. J. Pharm.* 371 (2009) 120-125.
- ¹²⁸ M. G. Abiad, O. H. Campanella, M. T. Carvajal, *Pharmaceutics*, 2 (2010) 78-90.
- ¹²⁹ A. M. Torki, D. B. Stojanović , I. D. Živković , A. Marinković, S. D. Škapin, P. S. Uskoković, R. R. Aleksić, *Polym. Compos.*, 33 (1) (2012) 22-34.
- ¹³⁰ W. C. Oliver, G. M. Pharr, *J. Mater. Res.*, 7 (1992) 1564-1583.
- ¹³¹ F. Söderlind, H. Pedersen, R.M. Petoral Jr. , P. O. Käll , K. Uvdal, *J. Collid Interf. Sci.*, 288 (2005) 140-148.
- ¹³² S. S. Musbah, V. Radojević, N. Borna, D. Stojanović, M. Dramićanin, A. Marinković, R. Aleksić, *J. Serb. Chem. Soc.*, 76 (8) (2011) 1153-1161.
- ¹³³ S. C. Tjong, *Mater. Sci. Eng. R*, 53 (2006) 73-197.

-
- ¹³⁴ S. Y. Fu, X. Q. Feng, B. Lauke, Y. W. Mai, *Compos. Part B-Eng*, 39 (6) (2008) 933-961.
- ¹³⁵ J. Gearing, K. P. Malik., P. Matejtschuk, *Cryobiology*, 61 (2010) 27-32.
- ¹³⁶ P. Alves, J. F. Coelho, J. Haack, A. Rota, A. Bruinink, M. H. Gil, *Eur. Polym. J.*, 45 (2009) 1412-1419.
- ¹³⁷ S. D. Clas, K. Lalonde, K. Khougaz, C. R. Dalton, R. Bilbeisi, *J. Pharm. Sci.*, 101 (2) (2012) 558-565.
- ¹³⁸ S. Bistac, J. Schultz, *Prog. Org. Coat.*, 31 (4) (1997) 347-350.
- ¹³⁹ C. Gourgon, J. H. Tortai, F. Lazzarino, C. Perret, G. Micouin, O. Joubert, S. Landis, *J. Vac. Sci. Technol.*, B 22 (2004) 602-606.
- ¹⁴⁰ Y.Y. Sun, M. Song, *J. Min. Metall. Sect. B-Metall.* 48 (1) B (2012) 45 – 51.
- ¹⁴¹ D. Stojanovic, A. Orlovic, S. Markovic, V. Radmilovic, P. S. Uskokovic, R. Aleksic, *J. Mater. Sci.*, 44 (2009) 6223-6232.
- ¹⁴² E. Tang, G. Cheng, X. Ma, *Powder Technol.*, 161 (2006) 209-214.
- ¹⁴³ M. A. Fortin, R. M. Petoral Jr, F. Söderlind, A. Klasson, M. Engström, T. Veres, P. O. Käll, K. Uvdal, *Nanotechnology*, 18 (2007) 395501

APPENDIX I/III

Прилог 1.

Изјава о ауторству

Потписани-а: Salah Salem Musbah

број индекса _____

Изјављујем

да је докторска дисертација под насловом

ОПТИЧКА И МЕХАНИЧКА СВОЈСТВА ХИБРИДНИХ КОМПОЗИТНИХ
СВЕТЛОВОДНИХ ВЛАКАНА

- резултат сопственог истраживачког рада,
- да предложена дисертација у целини ни у деловима није била предложена за добијање било које дипломе према студијским програмима других високошколских установа,
- да су резултати коректно наведени и
- да нисам кршио/ла ауторска права и користио интелектуалну својину других лица.

Потпис докторанда

У Београду, 20.01.2013.



Прилог 2.

Изјава о истоветности штампане и електронске верзије докторског рада

Име и презиме аутора Salah Salem Musbah

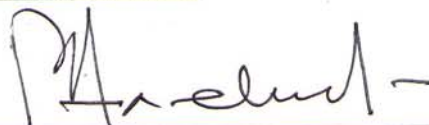
Број индекса:

Студијски програм Инжењерство материјала

Наслов рада: ОПТИЧКА И МЕХАНИЧКА СВОЈСТВА ХИБРИДНИХ
КОМПОЗИТНИХ СВЕТЛОВОДНИХ ВЛАКАНА

Ментор: Др Радослав Алексић, ред. проф

Потписани/а



Изјављујем да је штампана верзија мог докторског рада истоветна електронској верзији коју сам предао/ла за објављивање на порталу **Дигиталног репозиторијума Универзитета у Београду**.

Дозвољавам да се објаве моји лични подаци везани за добијање академског звања доктора наука, као што су име и презиме, година и место рођења и датум одбране рада.

Ови лични подаци могу се објавити на мрежним страницама дигиталне библиотеке, у електронском каталогу и у публикацијама Универзитета у Београду.

Потпис докторанда

У Београду, 20.01.2013.



Прилог 3.

Изјава о коришћењу

Овлашћујем Универзитетску Библиотеку „Светозар Марковић“ да у Дигитални репозиторијум Универзитета у Београду унесе моју докторску дисертацију под насловом:

ОПТИЧКА И МЕХАНИЧКА СВОЈСТВА ХИБРИДНИХ КОМПОЗИТНИХ
СВЕТЛОВОДНИХ ВПАКАНА

која је моје ауторско дело.

Дисертацију са свим прилозима предао/ла сам у електронском формату погодном за трајно архивирање.

Моју докторску дисертацију похрањену у Дигитални репозиторијум Универзитета у Београду могу да користе сви који поштују одредбе садржане у одбраном типу лиценце Креативне заједнице (Creative Commons) за коју сам се одлучио/ла.

1. Ауторство

2. Ауторство - некомерцијално

3. Ауторство – некомерцијално – без прераде

4. Ауторство – некомерцијално – делити под истим условима

5. Ауторство – без прераде

6. Ауторство – делити под истим условима

(Молимо да заокружите само једну од шест понуђених лиценци, кратак опис лиценци дат је на полеђини листа)

Потпис докторанда

У Београду, 20.01.2013.

